

Supporting information

Highly sensitive mechano-controlled luminescence in polymer films modified by dynamic Cu^I-based cross-linkers

Ayumu Karimata,^{a†} Pradnya H. Patil,^{a†} Eugene Khaskin,^a Sébastien Lapointe,^a Robert R. Fayzullin,^b Pavlos Stampoulis,^c and Julia R. Khusnutdinova*^a

^aOkinawa Institute of Science and Technology Graduate University, Coordination Chemistry and Catalysis Unit, 1919-1 Tancha, Onna-son, Okinawa, Japan, 904-0495

^bArbuzov Institute of Organic and Physical Chemistry, FCR Kazan Scientific Center, Russian Academy of Sciences, 8 Arbuzov Street, Kazan 420088, Russian Federation

^cJEOL RESONANCE Inc., Musashino, Akishima, Tokyo, 196-8558, Japan

Email: juliak@oist.jp

Table of Contents

I. General specifications	S2
II. Synthesis of ligands, metal complexes and polymers	S3
III. FT-IR spectra.....	S14
IV. UV-vis spectra.....	S16
V. EXSY and VT NMR experiments.....	S17
VI. Cyclic voltammetry.....	S23
VII. Photophysical properties of complexes and polymer films	S25
VIII. Photoluminescence intensity measurements in response to mechanical stress	S27
IX. Air stability	S30
X. Mechanical properties	S31
XI. DSC analysis	S32
XII. Imaging analysis	S33
XIII. NMR spectra.....	S34
XIV. X-ray structure determination details.....	S52
XV. References	S59

[†] These authors contributed equally to this work

I. General specifications

Materials

All manipulations unless stated otherwise were performed using Schlenk or glovebox techniques under a dry argon atmosphere. Sodium hydride was washed with hexane, dried under vacuum, and stored in a glove box. Pyridine-2,6-dialdehyde,¹ 3-aminopropyl (*tert*-butyl)dimethylsilyl ether,² N,N'-dimethyl-2,11-diaza[3,3](2,6)pyridinophane,³ N,N'-di-*iso*-propyl-2,11-diaza[3,3](2,6)pyridinophane³, N,N'-di-*tert*-butyl-2,11-diaza[3,3](2,6)pyridinophane,⁴ (1,3-dibenzylbenzimidazol-2-ylidene)copper(I) chloride⁵ were synthesized by the previously reported procedures.

NMR spectroscopy

NMR spectra were measured on JEOL ECZ600R or JEOL ECZ400S NMR spectrometers.

Luminescent properties

Luminescence spectra and luminescence quantum yields were recorded by Hamamatsu Quantaaurus-QY Plus (excitation wavelength is 380 nm). For PLQY measurements, a solid sample placed on a quartz dish was purged with nitrogen gas for 30 min and measured in nitrogen gas flow. Luminescence lifetime was measured with second harmonics of a Spectra-Physics Mai Tai pulsed laser and a Hamamatsu Photonics Streak scope camera (excitation wavelength is 380 nm). Fitting curves of emission decay were obtained as biexponential fits and emission lifetimes were obtained as intensity-weighted average estimated by $(A_1\tau_1^2 + A_2\tau_2^2)/(A_1\tau_1 + A_2\tau_2)$. Integrated luminescence intensities were obtained by dividing the integrated luminescence spectrum in 450 -760 nm range with the area of reflection of excitation.

Mechanical properties

All tensile tests were performed inside a glove box. Films with 25 mm [L] × 10 mm [W] × 0.6 mm [T] were used. Strain-Stress curves were recorded with a compact uniaxial tensile testing machine manufactured by Acroedge Co with speed of 1 mm per second. Stress and strain at break were estimated as an average of measurements of 3 samples ± deviation. Strain was defined as $100 \times (L - L_0)/L_0$ (L_0 is initial length) and stress (MPa) was calculated as dividing load (N) with cross-section area of the film (m^2).

Thermal properties

Differential scanning calorimetry (DSC) was performed using a Perkin Elmer DSC 8500 with heating rate of 10 °C/min under nitrogen gas flow at 20 mL/min.

Luminescence spectra during stretching

Luminescence spectra of the films during stretching were obtained by monitoring emission of the central area of the film using a Reflection/Backscattering Probe R600-7 manufactured by Ocean optics Co. during stretching from both edge sides of the film using a compact uniaxial tensile testing machine.

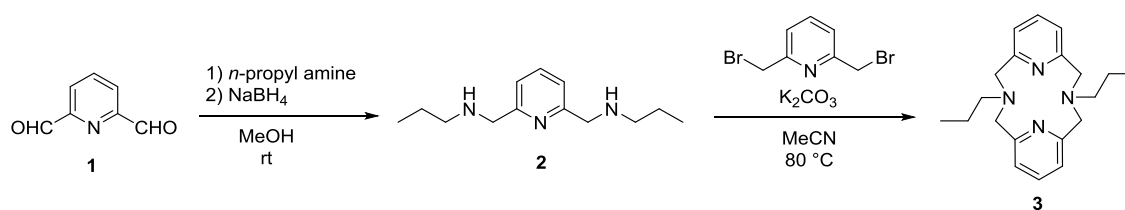
Luminescence imaging and luminescence time profile of film during stretching

The photographs and movies of luminescence imaging were taken by a CCD camera manufactured by Thorlabs attached with a UV cut filter. The taken photographs and movies were analyzed by free software Image J.

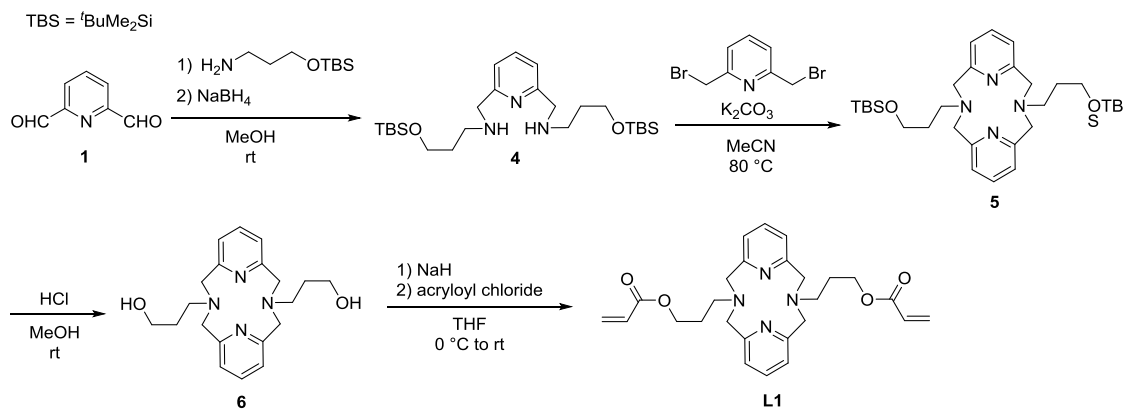
Cyclic voltammetry

Cyclic voltammetry was performed inside glovebox, using ALS/CHI electrochemical analyzers 660E. 0.1 M solution of ${}^n\text{Bu}_4\text{NPF}_6$ as a supporting electrolyte in CH_2Cl_2 was used. Pt disk electrode ($d = 1.6$ mm) as the working electrode, a platinum wire as the auxiliary electrode, and non-aqueous silver wire reference electrode assembly filled with a 0.01 M $\text{AgNO}_3/0.1$ M ${}^n\text{Bu}_4\text{NClO}_4/\text{MeCN}$ solution were used. All potentials were referenced against ferrocene (Fc/Fc^+).

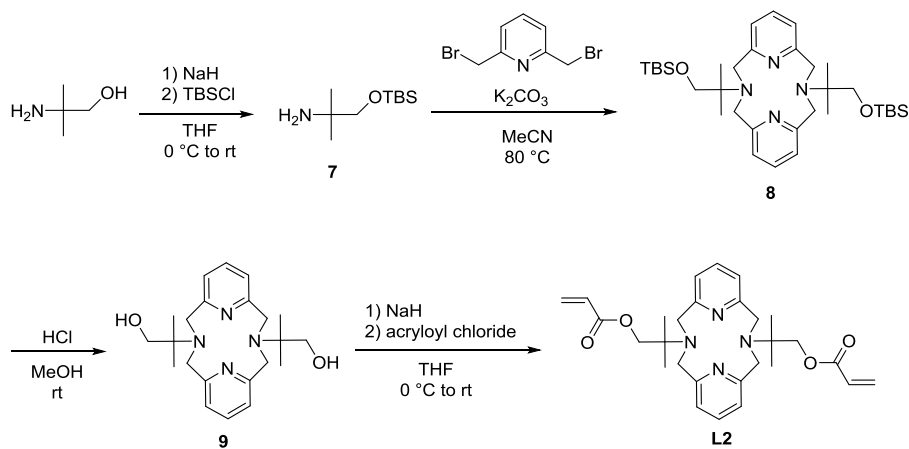
II. Synthesis of ligands, metal complexes and polymers



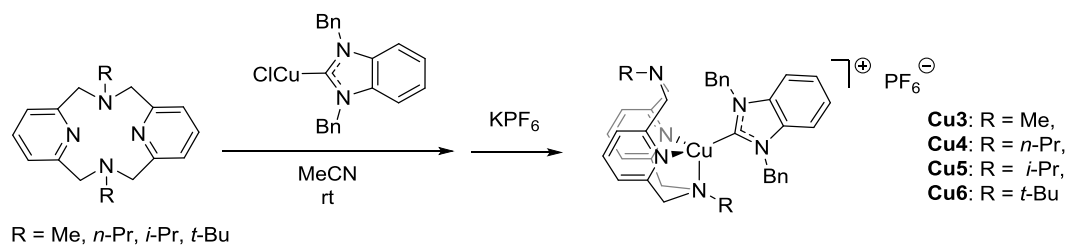
Scheme S1. Synthesis of compound **3**.



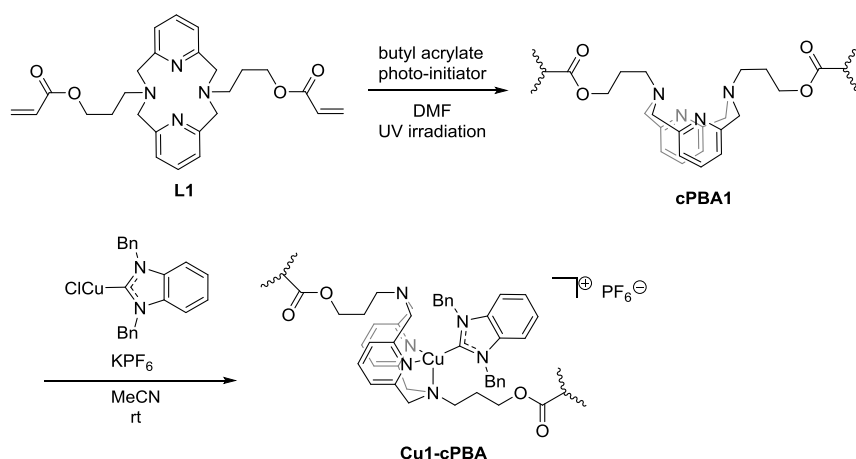
Scheme S2. Synthesis of **L1**.



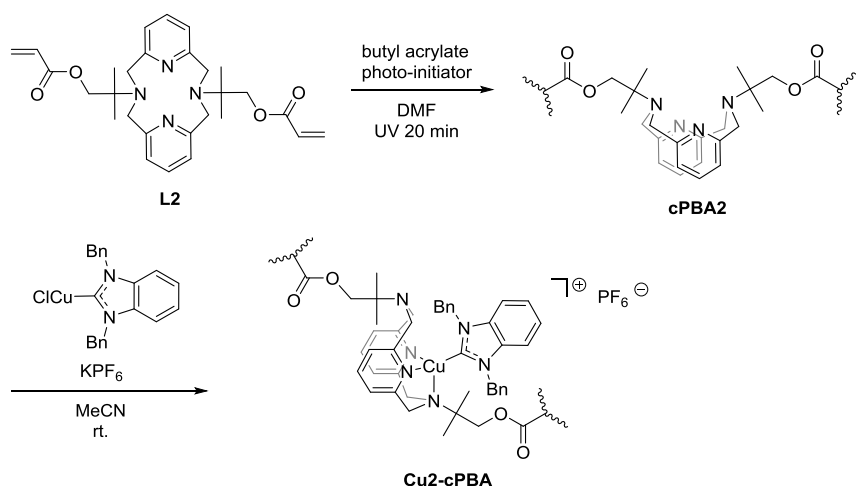
Scheme S3. Synthesis of **L2**.



Scheme S4. Synthesis of model complex **Cu3-6**.

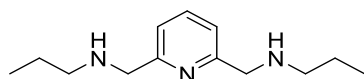


Scheme S5. Synthesis of **Cu1-cPBA**.



Scheme S6. Synthesis of **Cu2-cPBA**.

2,6-Bis(*n*-propylaminomethyl)pyridine (**2**)



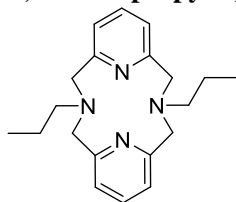
2,6-Bis(*n*-propylaminomethyl)pyridine (**2**) was prepared according to the previously reported procedure⁶. A mixture of pyridine-2,6-dialdehyde **1** (500 mg, 3.70 mmol), propylamine (438 mg, 7.41 mmol), 3 Å molecular sieves (0.50 g) in dry MeOH (5.0 mL) was stirred at room temperature under an argon atmosphere for 3 h. Sodium borohydride (310 mg, 8.19 mmol) was added slowly over 5 min at 0 °C under argon gas flow. After stirring at room temperature for 3 h, the mixture was filtered through Celite and concentrated under reduced pressure. The saturated aqueous solution of NH₄Cl (1 mL) was added, and the mixture was stirred for 10 min. After addition of a saturated aqueous solution of potassium carbonate (3 mL), the aqueous layer was extracted with diethyl ether (20 mL × 3). The combined organic layers were washed with water (10 mL × 2), dried over magnesium sulfate, filtered, and concentrated under reduced pressure to give a colorless oil, 810 mg, yield 99%. The product was used for the next reaction without further purification.

¹H NMR (400 MHz, 23 °C, CDCl₃): δ 7.58 (t, ³J_{HH} = 7.8 Hz, *p*-H_{Py}, 1H), 7.14 (d, ³J_{HH} = 7.8 Hz, *m*-H_{Py}, 2H), 3.88 (s, Py-CH₂-N, 4H), 2.63 (t, *J* = 7.3 Hz, N-CH₂-C, 4H), 2.02 (s, NH, 2H), 1.56 (sext, ³J_{HH} = 7.3 Hz, C-CH₂-C, 4H), 0.92 (t, ³J_{HH} = 7.3 Hz, C-CH₃, 6H).

¹³C NMR (100 MHz, 23 °C, CDCl₃): δ 159.5 (*o*-C_{Py}), 136.9 (*p*-C_{Py}), 120.5 (*m*-C_{Py}), 55.3 (-Py-C-N-), 51.7 (-N-C-C), 23.4 (-C-C-C), 11.9 (C-CH₃).

ESI-HRMS *m/z* calcd for C₁₃H₂₄N₃ [M+H⁺]: 222.1965, found: 222.1956.

N,N'-Di-*n*-propyl-2,11-diaza[3,3](2,6)-pyridinophane (3)



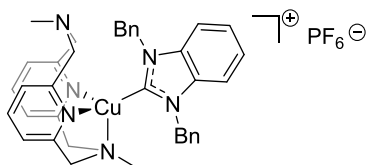
A solution of 2,6-bis(bromomethyl)pyridine (978 mg, 3.69 mmol) in MeCN (50 mL) was added dropwise using a dropping funnel to a mixture of compound **2** (810 mg, 3.66 mmol), potassium carbonate (3.06 g, 22.1 mmol), and MeCN (400 mL) with stirring at 80 °C for over 4 h. After stirring at 80 °C for 2 days, the hot mixture was filtered off and concentrated under reduced pressure. The crude mixture was suspended in CH₂Cl₂ (30 mL) and washed with water (10 mL × 3), dried over MgSO₄, filtered off, and concentrated under reduced pressure. The mixture was suspended in MeCN (8 mL) by sonication, filtered off to remove insoluble precipitate, and concentrated under reduced pressure. The mixture was suspended in hexane (20 mL) and stirred at room temperature for 30 min, then filtered through Celite to remove insoluble sticky solid. The filtrate was concentrated under reduced pressure to give a white powder. The crude product was purified by basic alumina column chromatography using hexane : AcOEt (2:1/v:v) as an eluent. The solid was dissolved in a solution of hexane-diethyl ether (1:1/v:v) (2 mL) and evaporated slowly at room temperature to give a colorless crystalline product, 370 mg, yield 31%.

¹H NMR (400 MHz, 23 °C, CDCl₃): δ 7.10 (t, ³J_{HH} = 7.7 Hz, *p*-H_{py}, 2H), 6.76 (d, ³J_{HH} = 7.6 Hz, *m*-H_{py}, 4H), 3.89 (s, Py-CH₂-N, 8H), 2.82 (t, ³J_{HH} = 7.4 Hz, -N-CH₂-, 4H), 1.72 (sext, ³J_{HH} = 7.4 Hz, C-CH₂-CH₃, 4H), 1.04 (t, ³J_{HH} = 7.4 Hz, -CH₂-CH₃, 6H).

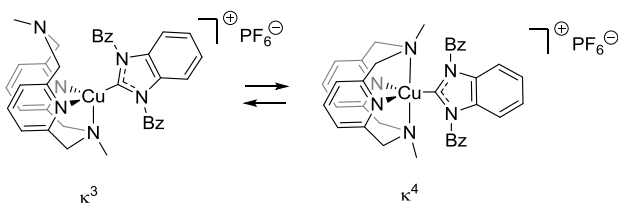
¹³C NMR (100 MHz, 23 °C, CDCl₃): δ 158.1 (*o*-C_{py}), 135.5 (*p*-C_{py}), 122.6 (*m*-C_{py}), 64.0 5-(Py-C-N-), 62.7 (-N-C-C), 20.9 (-C-C-C), 12.1 (C-CH₃).

ESI-HRMS *m/z* calcd for C₂₀H₂₉N₄ [M+H⁺]: 325.2387, found: 325.2378.

Synthesis of Cu3



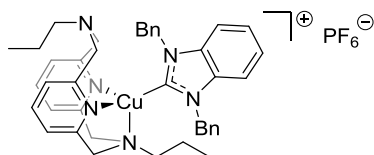
In a glovebox, (1,3-dibenzylbenzimidazol-2-ylidene)copper(I) chloride (44.5 mg, 0.112 mmol) was added to a solution of N,N'-dimethyl-2,11-diaza[3,3](2,6)-pyridinophane (30.0 mg, 0.112 mmol) in MeCN (2 mL). After stirring at room temperature for 3 h (consumption of ligand was confirmed by NMR), KPF₆ (206 mg, 1.12 mmol) was added to the reaction mixture, and the mixture was stirred at room temperature. After removing solvent under reduced pressure, dichloromethane (2 mL) was added and the reaction mixture was filtered through Celite pad. The filtrate was concentrated under vacuum and purified by crystallization via vapor diffusion with dichloromethane-diethyl ether repeatedly to give yellow crystals. (66.5 mg, 74%) These crystals were used for X-ray crystallography analysis.



At -30 °C, κ^3 and κ^4 isomers were present in CD₂Cl₂ solution in a 40.8 : 59.2 ratio according to NMR integration.

κ^4 , major isomer. $^1\text{H NMR}$ (600 MHz, $-30\text{ }^\circ\text{C}$, CD_2Cl_2): δ 7.42-7.24 (m, $p\text{-H}_{\text{py}}$, Ar- H_{benz} , 12H), 7.15 (d, $^3J_{\text{HH}} = 5.5\text{ Hz}$, Ar- H_{benz} , 4H), 6.68 (d, $^3J_{\text{HH}} = 7.8\text{ Hz}$, $m\text{-H}_{\text{py}}$, 4H), 5.80 (s, $\text{CH}_{2\text{benz}}$, 4H), 3.76 (d, $^2J_{\text{HH}} = 14.8\text{ Hz}$, -Py- $\text{CH}_2\text{-N-}$, 4H), 3.39 (d, $^2J_{\text{HH}} = 15.5\text{ Hz}$, -Py- $\text{CH}_2\text{-N-}$, 4H), 2.40 (s, -N- CH_3 , 6H). $^{13}\text{C NMR}$ (151 MHz, $-30\text{ }^\circ\text{C}$, CD_2Cl_2): δ 192.65 (quat, C_{Imd}), 156.3 (quat, C_{Py}), 137.0 (Ar- CH_{benz}), 136.96 (Ar- C_{benz}), 134.3 (Ar- C_{benz}), 128.8 (Ar- CH_{benz}), 128.0 (Ar- C_{benz}), 126.7 (Ar- CH_{benz}), 123.4 (Ar- CH_{benz}), 122.2 ($m\text{-C}_{\text{py}}$), 111.5 (Ar- CH_{benz}), 64.2 (-Py- $\text{CH}_2\text{-N-}$), 52.0 ($\text{CH}_{2\text{benz}}$), 48.8 (-N- CH_3). κ^3 : minor isomer: $^1\text{H NMR}$ (600 MHz, $-30\text{ }^\circ\text{C}$, CD_2Cl_2): δ 7.42-7.24 (m, $p\text{-H}_{\text{py}}$, Ar- H_{benz} , 12H), 7.06 (d, $^3J_{\text{HH}} = 5.1\text{ Hz}$, Ar- H_{benz} , 4H), 6.91 (d, $^3J_{\text{HH}} = 7.4\text{ Hz}$, $m\text{-H}_{\text{py}}$, 2H), 6.83 (d, $^3J_{\text{HH}} = 8.2\text{ Hz}$, $m\text{-H}_{\text{py}}$, 2H), 5.73 (s, $\text{CH}_{2\text{benz}}$, 4H), 4.27 (d, $^2J_{\text{HH}} = 13.1\text{ Hz}$, -Py- $\text{CH}_2\text{-N-}$, 2H), 3.92 (dd, $^2J_{\text{HH}} = 14.4, 13.8\text{ Hz}$, -Py- $\text{CH}_2\text{-N-}$, 4H), 3.57 (d, $^2J_{\text{HH}} = 15.1\text{ Hz}$, -Py- $\text{CH}_2\text{-N-}$, 2H), 2.37 (s, -N- CH_3 , 3H), 2.32 (s, -N- CH_3 , 3H). $^{13}\text{C NMR}$ (151 MHz, $-30\text{ }^\circ\text{C}$, CD_2Cl_2): δ 191.34 (quat, C_{Imd}), 155.0 (quat, C_{Py}), 154.9 (quat, C_{Py}), 137.4 (Ar- CH_{benz}), 136.96 (Ar- C_{benz}), 134.4 (Ar- C_{benz}), 128.95 (Ar- CH_{benz}), 128.03 (Ar- C_{benz}), 126.4 (Ar- CH_{benz}), 124.4 ($m\text{-C}_{\text{py}}$), 123.7 (Ar- CH_{benz}), 121.6 ($m\text{-C}_{\text{py}}$), 111.4 (Ar- CH_{benz}), 66.4 (-Py- $\text{CH}_2\text{-N-}$), 65.2 (-Py- $\text{CH}_2\text{-N-}$), 51.8 ($\text{CH}_{2\text{benz}}$), 50.8 (-N- CH_3), 42.9 (-N- CH_3). Anal. Found (calcd for $\text{C}_{37}\text{H}_{38}\text{CuF}_6\text{N}_6\text{P}$): C, 57.17, (57.32); H, 4.74, (4.94); N, 11.07, (10.84).

Synthesis of Cu4



Cu4 was prepared by the same procedure as **Cu3** using (1,3-dibenzylbenzimidazolyl-2-ylidene)copper(I) chloride (30.6 mg, 0.0770 mmol), compound **3** (25.0 mg, 0.0770 mmol), MeCN (5 mL), and KPF_6 (285 mg, 1.55 mmol) to provide yellow crystal (55.8 mg, 84%). Crystals suitable for X-ray crystallography were obtained by the vapor diffusion method with dichloromethane-diethyl ether.

At $-30\text{ }^\circ\text{C}$, κ^3 and κ^4 isomers were present in CD_2Cl_2 solution in a 66.7 : 33.3 ratio according to NMR integration.

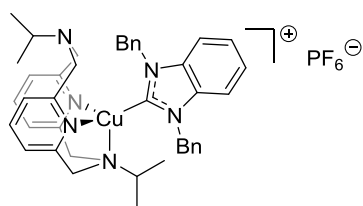
κ^3 , major isomer:

$^1\text{H NMR}$ (600 MHz, $-30\text{ }^\circ\text{C}$, CD_2Cl_2): δ 7.44-7.33 (m, $p\text{-H}_{\text{py}}$, Ar- H_{benz} , 6H), 7.29-7.23 (m, Ar- H_{benz} , 6H), 7.07-7.04 (m, Ar- H_{benz} , 4H), 6.90 (d, $^3J_{\text{HH}} = 7.8\text{ Hz}$, $m\text{-H}_{\text{py}}$, 2H), 6.81 (d, $^3J_{\text{HH}} = 7.6\text{ Hz}$, $m\text{-H}_{\text{py}}$, 2H), 5.82 (d, $^2J_{\text{HH}} = 16.4\text{ Hz}$, $\text{CH}_{2\text{benz}}$, 2H), 5.70 (d, $^2J_{\text{HH}} = 16.4\text{ Hz}$, $\text{CH}_{2\text{benz}}$, 2H), 4.13 (d, $^2J_{\text{HH}} = 13.1\text{ Hz}$, -Py- $\text{CH}_2\text{-N-}$, 2H), 3.96 (d, $^2J_{\text{HH}} = 13.1\text{ Hz}$, -Py- $\text{CH}_2\text{-N-}$, 2H), 3.71 (d, $^2J_{\text{HH}} = 15.3\text{ Hz}$, -Py- $\text{CH}_2\text{-N-}$, 2H), 3.53 (d, $^2J_{\text{HH}} = 14.8\text{ Hz}$, -Py- $\text{CH}_2\text{-N-}$, 2H), 2.42-2.39 (m, -N- $\text{CH}_2\text{-CH}_2\text{-}$, 2H), 2.34-2.31 (m, -N- $\text{CH}_2\text{-CH}_2\text{-}$, 2H), 1.44-1.36 (m, - $\text{CH}_2\text{-CH}_2\text{-CH}_3$, 4H), 0.64 (t, $^3J_{\text{HH}} = 7.3\text{ Hz}$, - $\text{CH}_2\text{-CH}_3$, 3H), 0.63 (t, $^3J_{\text{HH}} = 7.4\text{ Hz}$, - $\text{CH}_2\text{-CH}_3$, 3H). $^{13}\text{C NMR}$ (151 MHz, $-30\text{ }^\circ\text{C}$, CD_2Cl_2): δ 191.72 (quat, C_{Imd}), 156.62 (quat, C_{py}), 154.88 (quat, C_{py}), 137.51 ($p\text{-C}_{\text{py}}$), 136.85 (Ar- C_{benz}), 134.44 (Ar- C_{benz}), 128.96 (Ar- CH_{benz}), 127.99 (Ar- C_{benz}), 126.34 (Ar- CH_{benz}), 124.31 ($m\text{-C}_{\text{py}}$), 123.70 (Ar- CH_{benz}), 121.70 ($m\text{-C}_{\text{py}}$), 111.54 (Ar- CH_{benz}), 64.25 (-N- $\text{CH}_2\text{-CH}_2\text{-}$), 63.90 (-Py- $\text{CH}_2\text{-N-}$), 63.72 (-N- $\text{CH}_2\text{-CH}_2\text{-}$), 63.56 (-Py- $\text{CH}_2\text{-N-}$), 61.20 (-Py- $\text{CH}_2\text{-N-}$), 52.0 ($\text{CH}_{2\text{benz}}$), 51.74 ($\text{CH}_{2\text{benz}}$), 19.41 (- $\text{CH}_2\text{-CH}_2\text{-CH}_3$), 17.23 (- $\text{CH}_2\text{-CH}_2\text{-CH}_3$), 11.53 (- $\text{CH}_2\text{-CH}_3$), 11.24 (- $\text{CH}_2\text{-CH}_3$).

κ^4 , minor isomer:

$^1\text{H NMR}$ (600 MHz, $-30\text{ }^\circ\text{C}$, CD_2Cl_2): δ 7.44-7.33 (m, Ar- H_{benz} , 4H), 7.29-7.23 (m, $p\text{-H}_{\text{py}}$, Ar- H_{benz} , 8H), 7.07-7.04 (m, Ar- H_{benz} , 4H), 6.69 (d, $^3J_{\text{HH}} = 7.6\text{ Hz}$, $m\text{-H}_{\text{py}}$, 4H), 5.79 (s, $\text{CH}_{2\text{benz}}$, 4H), 3.99 (d, $^2J_{\text{HH}} = 15.3\text{ Hz}$, -Py- $\text{CH}_2\text{-N-}$, 4H), 3.61 (d, $^2J_{\text{HH}} = 15.3\text{ Hz}$, -Py- $\text{CH}_2\text{-N-}$, 4H), 2.51 (t, $^3J_{\text{HH}} = 7.1\text{ Hz}$, -N- $\text{CH}_2\text{-CH}_2\text{-}$, 4H), 1.60-1.54 (m, - $\text{CH}_2\text{-CH}_2\text{-CH}_3$, 4H), 0.93 (t, $^3J_{\text{HH}} = 7.13\text{ Hz}$, - $\text{CH}_2\text{-CH}_3$, 6H). $^{13}\text{C NMR}$ (151 MHz, $-30\text{ }^\circ\text{C}$, CD_2Cl_2): δ 193.11 (quat, C_{Imd}), 156.67 (quat, C_{py}), 137.04 ($p\text{-C}_{\text{py}}$), 136.92 (Ar- C_{benz}), 134.41 (Ar- C_{benz}), 128.80 (Ar- CH_{benz}), 126.66 (Ar- CH_{benz}), 123.46 (Ar- C_{benz}), 122.27 ($m\text{-C}_{\text{py}}$), 111.64 (Ar- CH_{benz}), 63.72 (-Py- $\text{CH}_2\text{-N-}$), 57.92 (-N- $\text{CH}_2\text{-CH}_2\text{-}$), 52.0 ($\text{CH}_{2\text{benz}}$), 20.65 (- $\text{CH}_2\text{-CH}_2\text{-CH}_3$), 11.50 (- $\text{CH}_2\text{-CH}_3$). Anal. Found (calcd for $\text{C}_{41}\text{H}_{46}\text{N}_6\text{CuF}_6\text{P}$): C, 58.96 (59.23), H, 5.58 (5.58), N, 9.88 (10.11).

Synthesis of Cu5



Cu5 was prepared by the same procedure as **Cu3** using (1,3-dibenzylbenzimidazol-2-ylidene)copper(I) chloride (25.0 mg, 0.0629 mmol), N,N'-diisopropyl-2,11-diaza[3,3](2,6)-pyridinophane (20.5 mg, 0.0632 mmol), MeCN (0.5 mL), THF (0.5 mL), and KPF₆ (233 mg, 1.27 mmol), and vapor diffusion with dichloromethane-ether provided yellow crystal (38.5 mg, 71%). Crystals suitable for X-ray crystallography were obtained by vapor diffusion method with dichloromethane-diethyl ether.

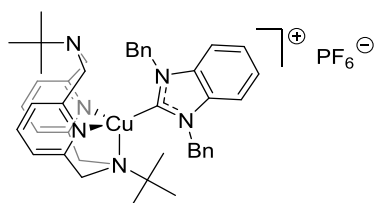
Cu5 exists as a single isomer [κ^3 -¹⁹PtN4(Benz)Cu]PF₆ in a CD₂Cl₂ solution.

κ^3 -**3**:

¹H NMR (600 MHz, -30 °C, CD₂Cl₂): δ 7.35 (t, ³J_{HH} = 7.7 Hz, *p*-H_{py}, 2H), 7.31-7.30 (m, Ar-H_{benz}, 10H), 7.06 (t, ³J_{HH} = 3.6 Hz, Ar-H_{benz}, 4H), 6.88 (d, ³J_{HH} = 7.7 Hz, *m*-H_{py}, 2H), 6.80 (d, ³J_{HH} = 7.5 Hz, *m*-H_{py}, 2H), 5.93 (d, ²J_{HH} = 16.2 Hz, CH_{2benz}, 2H), 5.74 (d, ²J_{HH} = 16.2 Hz, CH_{2benz}, 2H), 4.15 (d, ²J_{HH} = 14.8 Hz, -Py-CH₂-N-, 2H), 3.83 (d, ²J_{HH} = 13.0 Hz, -Py-CH₂-N-, 2H), 3.69 (d, ²J_{HH} = 12.7 Hz, -Py-CH₂-N-, 2H), 3.61 (d, ²J_{HH} = 15.2 Hz, -Py-CH₂-N-, 2H), 3.06 (septet, ³J_{HH} = 6.4 Hz, -N-CH(CH₃)₂, 1H), 2.70-2.65 (m, -N-CH(CH₃)₂, 1H), 1.12 (d, ³J_{HH} = 6.4 Hz, -N-CH(CH₃)₂, 6H), 1.00 (d, ³J_{HH} = 6.4 Hz, -N-CH(CH₃)₂, 6H).
¹³C NMR (101 MHz, -30 °C, CD₂Cl₂): δ 192.3 (quat. C_{Imd}), 159.4 (quat. C_{Py}), 154.8 (quat. C_{Py}), 137.8 (*p*-C_{Py}), 136.6 (Ar-C_{benz}), 134.5 (Ar-C_{benz}), 129.1 (Ar-CH_{benz}), 128.1 (Ar-C_{benz}), 126.3 (Ar-CH_{benz}), 124.7 (*m*-C_{Py}), 123.8 (Ar-CH_{benz}), 121.9 (*m*-C_{Py}), 111.97 (Ar-CH_{benz}), 61.8 (-Py-CH₂-N-), 60.4 (-Py-CH₂-N-), 59.4 (-N-CH(CH₃)₂), 59.1 (-N-CH(CH₃)₂) and (-Py-CH₂-N-), 52.1 (CH_{2benz}), 19.1 (-N-CH(CH₃)₂), 18.9 (-N-CH(CH₃)₂).

Anal. Found (calcd for C₄₁H₄₆N₆CuF₆P): C, 59.56 (59.23), H, 5.70 (5.58), N, 10.24 (10.11).

Synthesis of Cu6



Cu6 was prepared by the same procedure as **Cu3** using (1,3-dibenzylbenzimidazol-2-ylidene)copper(I) chloride (28.3 mg, 0.0712 mmol), N,N'-di-*t*-butyl-2,11-diaza[3,3](2,6)-pyridinophane (25.0 mg, 0.0709 mmol), MeCN (1 mL), THF (1 mL), and KPF₆ (264 mg, 1.43 mmol) to provide yellow crystalline solid (50.7 mg, 81%). Crystals suitable for X-ray crystallography were obtained by the vapor diffusion method with dichloromethane-diethyl ether.

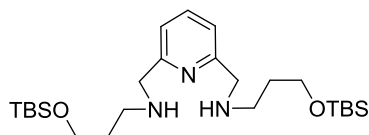
In CD₂Cl₂ **Cu6** features a tetragonal geometry with a κ^3 coordinated ligand and exists in solution as a single isomer.

¹H NMR (600 MHz, 20 °C, CD₂Cl₂) (κ^3): Single conformer: δ 7.31-7.25 (m, *p*-H_{py} and Ar-H_{benz}, 12H), 7.06-7.04 (m, Ar-H_{benz}, 4H), 6.78 (d, ³J_{HH} = 7.8 Hz, *m*-H_{py}, 2H), 6.75 (d, ³J_{HH} = 7.5 Hz, *m*-H_{py}, 2H), 6.12 (d, ²J_{HH} = 16.1 Hz, CH_{2benz}, 2H), 5.62 (d, ²J_{HH} = 16.1 Hz, CH_{2benz}, 2H), 4.75 (d, ²J_{HH} = 15.0 Hz, -Py-CH₂-N-, 2H), 3.70 (d, ²J_{HH} = 13.1 Hz, -Py-CH₂-N-, 2H), 3.57 (d, ²J_{HH} = 14.8 Hz, -Py-CH₂-N-, 2H), 3.46 (d, ²J_{HH} = 13.0 Hz, -Py-CH₂-N-, 2H), 1.37 (s, -N-C(CH₃)₃, 9H), 1.00 (s, -N-C(CH₃)₃, 9H).

¹³C NMR (101 MHz, 20 °C, CD₂Cl₂) (κ^3): Single conformer: δ 192.5 (quat. C_{Imd}), 159.9 (quat. C_{Py}), 155.2 (quat. C_{Py}), 137.6 (*p*-C_{Py}), 136.1 (Ar-C_{benz}), 134.4 (Ar-C_{benz}), 129.0 (Ar-CH_{benz}), 128.0 (Ar-C_{benz}), 126.2 (Ar-CH_{benz}), 124.2 (*m*-C_{Py}), 123.7 (Ar-CH_{benz}), 121.5 (*m*-C_{Py}), 112.2 (Ar-CH_{benz}), 59.6 (-Py-CH₂-N-), 59.2 (-Py-CH₂-N-), 59.1 (-Py-CH₂-N-), 56.3 (-N-C(CH₃)₂), 52.2 (CH_{2benz}), 27.5 (-N-C(CH₃)₃).

Anal. Found (calcd for C₄₃H₅₀CuF₆N₆P): C, 60.11, (60.10); H, 5.88, (5.86); N, 10.43, (9.78).

Synthesis of 4



Compound **4** was prepared according to the previously reported procedure.⁶

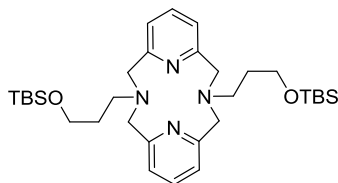
A mixture of pyridine-2,6-dialdehyde (**1**) (2.16 g, 16.0 mmol) and 3 Å molecular sieves (6.0 g) in dry MeOH (30 mL) was stirred at room temperature in a three-necked flask under an argon atmosphere. After addition of 3-aminopropyl (*tert*-butyl)dimethylsilyl ether (6.06 g, 32.0 mmol), the mixture was stirred at room temperature for 3 h. Sodium borohydride (1.33 g, 35.2 mmol) was added slowly at 0 °C under argon gas flow. After stirring at room temperature for 3 h, the mixture was filtered through Celite, and concentrated under reduced pressure. Saturated NH₄Cl aqueous solution (5 mL) was added slowly to the mixture at 0 °C, and the mixture was stirred at room temperature for 10 min. Saturated aqueous solution of potassium carbonate (10 mL) was added and extracted with dichloromethane (20 mL × 5). The dichloromethane solution was dried over magnesium sulfate, filtered, and concentrated under reduced pressure. The crude mixture was purified by basic alumina column chromatography with hexane : AcOEt (2:1/v:v) as an eluent to give an oil, 4.60 g, yield 60%.

¹H NMR (400 MHz, 23 °C, CDCl₃): δ 7.56 (t, ³J_{HH} = 7.6 Hz, *p*-**H**_{Py}, 1H), 7.14 (d, ³J_{HH} = 7.6 Hz, *m*-**H**_{Py}, 2H), 3.86 (s, Py-**CH**₂-N, 4H), 3.68 (t, ³J_{HH} = 6.2 Hz, N-**CH**₂-C, 4H), 2.73 (t, ³J_{HH} = 6.9 Hz, C-**CH**₂-C, 4H), 1.85 (br s, **NH**), 1.74 (quint, ³J_{HH} = 6.6 Hz, C-**CH**₃, 6H), 0.86 (s, Si-C-C(**CH**₃)₃, 18H), 0.023 (s, Si-**CH**₃, 12H).

¹³C NMR (100 MHz, 23 °C, CDCl₃): δ 159.4 (*o*-C_{Py}), 136.9 (*p*-C_{Py}), 120.5 (*m*-C_{Py}), 61.8 (-N-C-C), 55.5 (Py-C-N-), 47.0 (-C-C-O), 33.1 (-C-C-C), 26.1 (Si-C(**CH**₃)₃), 18.4 (Si-C(**CH**₃)₃), -5.2 (-Si-**CH**₃).

ESI-HRMS *m/z* calcd for C₂₅H₅₂O₂N₃Si₂ [M+H⁺]: 482.3593, found: 482.3574.

Synthesis of **5**



A solution of 2,6-bis(bromomethyl) pyridine (2.54 g, 9.59 mmol) in MeCN (50 mL) was added dropwise using a dropping funnel to a mixture of compound **4** (4.60 g, 9.55 mmol), potassium carbonate (7.97 g, 57.7 mmol), and MeCN (500 mL) with stirring at 80 °C for over 4 h. After stirring at 80 °C for 2 days, the hot mixture was filtered off and concentrated under reduced pressure. The crude mixture was purified by silica gel column chromatography using CHCl₃ : MeOH : 28% NH₃ aqueous solution (50 : 1 : 0.1) as an eluent to give a white solid. The solid was recrystallized from MeCN to give a colorless solid product, 2.20 g, yield 39%.

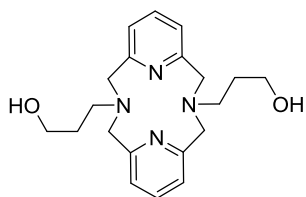
The crude mixture also can be purified by basic alumina column chromatography with hexane : AcOEt (4:1/v:v).

¹H NMR (400 MHz, 23 °C, CDCl₃): δ 7.10 (t, ³J_{HH} = 7.5 Hz, *p*-**H**_{Py}, 2H), 6.75 (d, ³J_{HH} = 7.5 Hz, *m*-**H**_{Py}, 4H), 3.89 (s, Py-**CH**₂-N, 8H), 3.82 (t, ³J_{HH} = 6.9 Hz, N-**CH**₂-C, 4H), 2.94 (t, ³J_{HH} = 6.9 Hz, C-**CH**₂-O, 4H), 1.92 (quint, ³J_{HH} = 6.9 Hz, C-**CH**₂-C, 4H), 0.93 (s, Si-C(**CH**₃)₃, 18H), 0.10 (s, Si-**CH**₃, 12H).

¹³C NMR (100 MHz, 23 °C, CDCl₃): δ 158.0 (*o*-C_{Py}), 135.6 (*p*-C_{Py}), 122.6 (*m*-C_{Py}), 64.0 (-N-C-C), 61.5 (-Py-C-N-), 57.1 (C-C-O), 30.9 (-C-C-C), 26.1 (Si-C(**CH**₃)₃), 18.5 (Si-C(**CH**₃)₃), -5.1 (Si-**CH**₃).

ESI-HRMS *m/z* calcd for C₃₂H₅₇N₄O₂Si₂ [M+H⁺]: 585.4004, found: 585.3992.

Synthesis of 6



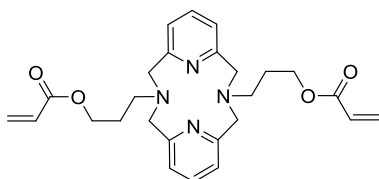
Compound **5** (2.20 g, 3.76 mmol) was dissolved in MeOH (10 mL). After the addition of 35% hydrochloric acid (1.0 mL), the mixture was stirred at room temperature for 1 day. The solvents were removed under reduced pressure. Potassium carbonate (2.60 g, 18.8 mmol) and water (10 mL) were added to the mixture. The mixture was extracted with CH₂Cl₂ (10 mL × 5), dried over a mixture of magnesium sulfate and potassium carbonate, filtered off, and concentrated under reduced pressure. The mixture was recrystallized from MeCN to give a colorless solid product, 1.23 g, yield 92%.

¹H NMR (400 MHz, 23 °C, CDCl₃): δ 7.10 (t, ³J_{HH} = 7.8 Hz, *p*-H_{Py}, 2H), 6.75 (d, ³J_{HH} = 7.8 Hz, *m*-H_{Py}, 4H), 6.03 (br, 2H, OH), 4.04 (t, ³J_{HH} = 5.0 Hz, N-CH₂-C, 4H), 3.95 (s, Py-CH₂-N, 8H), 3.08 (t, ³J_{HH} = 5.5 Hz, C-CH₂-O, 4H), 1.93 (quint, ³J_{HH} = 5.0 Hz, C-CH₂-C, 4H).

¹³C NMR (100 MHz, 23 °C, CDCl₃): δ 157.2 (*o*-C_{Py}), 136.3 (*p*-C_{Py}), 122.3 (*m*-C_{Py}), 65.0 (-N-C-C), 64.6 (-Py-C-N-), 61.2 (C-C-O), 29.0 (-C-C-C).

ESI-HRMS *m/z* calcd for C₂₀H₂₉N₄O₂ [M+H⁺]: 357.2285, found: 357.2289.

Synthesis of L1



Method A

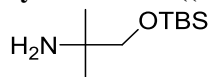
In a glove box, sodium hydride (20.3 mg, 0.846 mmol) and anhydrous THF (5 mL) were placed in 25 mL Schlenk tube. The Schlenk tube was taken out from the glove box. After the addition of compound **6** (101 mg, 0.283 mmol) under argon gas flow at 0 °C, the mixture was stirred at room temperature for 1 h. Acryloyl chloride (112 mg, 1.24 mmol) was added slowly at 0 °C under argon gas flow. The reaction mixture was allowed to warm to room temperature, and stirred for 16 h. After the addition of MeOH (1 mL) at 0 °C, the reaction mixture was concentrated under vacuum at room temperature. Acetonitrile (3 mL) and 10 wt% potassium carbonate aqueous solution (3 mL) was added, and extracted with a solution of hexane-diethyl ether (10:1 v:v) (30 mL × 5). The extracted solution was dried over a mixture of magnesium sulfate and potassium carbonate, filtered, and concentrated under reduced pressure at room temperature to give the product as a white powder (84.0 mg, 64%). This ligand was used for polymerization immediately.

Method B

A solution of compound **6** (100 mg, 0.281 mmol), triethylamine (290 mg, 2.87 mmol), and 2,6-di-*tert*-butyl-*p*-cresol (5.0 mg, 0.0227 mmol) in dry dichloromethane (5 mL) was stirred at 0 °C in 25 mL Schlenk tube under an argon atmosphere. Acryloyl chloride (67.2 mg, 0.742 mmol) was added to the solution slowly over 5 min. under argon gas flow, and the reaction mixture was stirred at room temperature for 18 h. After addition of methanol (1 mL), the mixture was concentrated at room temperature under reduced pressure. The crude mixture was purified by basic alumina column chromatography using ethyl acetate : hexane (2:1 v/v), then ethyl acetate as an eluent to give a white powder (88.3 mg, 67%). (TLC plate was stained by iodine) This ligand was used for polymerization immediately. CDCl₃ solution for NMR analysis was passed through K₂CO₃ before measurement because the product can be easily protonated.

^1H NMR (400 MHz, 23 °C, CDCl_3): δ 7.12 (t, $^3J_{\text{HH}} = 7.78$ Hz, $p\text{-H}_{\text{Py}}$, 2H), 6.75 (d, $^3J_{\text{HH}} = 7.8$ Hz, $m\text{-H}_{\text{Py}}$, 4H), 6.45 (d, $^2J_{\text{HH}} = 17.4$ Hz, -C=CH , 2H), 6.18 (dd, $^3J_{\text{HH}} = 17.4$ and 10.1 Hz, -CH=CH , 2H), 5.85 (d, $^2J_{\text{HH}} = 10.1$ Hz, -C=CH , 2H), 4.43 (t, $^3J_{\text{HH}} = 6.4$ Hz, $\text{C-CH}_2\text{-O}$, 4H), 3.89 (s, $\text{Py-CH}_2\text{-N}$, 8H), 2.95 (t, $^3J_{\text{HH}} = 6.4$ Hz, $\text{C-CH}_2\text{-N}$, 4H), 2.08 (quint, $^3J_{\text{HH}} = 6.4$ Hz, $\text{C-CH}_2\text{-C}$, 4H).
 ^{13}C NMR (100 MHz, 23 °C, CDCl_3): δ 166.5 (C=O), 157.8 ($o\text{-C}_{\text{Py}}$), 135.8 ($p\text{-C}_{\text{Py}}$), 131.0 (O=C-C=C), 128.6 (O=O-C=C), 122.8 ($m\text{-C}_{\text{Py}}$), 64.1 (C-C-O), 63.0 (-Py-C-N-), 56.7 (N-C-C), 27.2 (C-C-C).
 ESI-HRMS m/z calcd for $\text{C}_{26}\text{H}_{33}\text{N}_4\text{O}_4$ [$\text{M}+\text{H}^+$]: 465.2496, found: 465.2482.

Synthesis of 1-((*tert*-butyldimethylsilyloxy)-2-methylpropan-2-amine (7)



1-((*tert*-butyldimethylsilyloxy)-2-methylpropan-2-amine (7) was prepared by following the previously reported procedure with some modifications.

In a glove box, sodium hydride (3.19 g, 133 mmol) and dry THF (300 mL) were placed in 500 mL Schlenk flask. The flask was capped and taken out of glovebox and cooled with an ice bath.

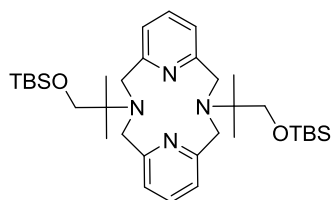
2-Amino-2-methylpropanol (11.9 g, 133 mmol) was added slowly over 5 min. under argon gas flow with stirring. The reaction mixture was stirred at room temperature for 1 h. A solution of *tert*-butyldimethyl chloride (20.0 g, 133 mmol) in dry THF (50 mL) was added to the mixture slowly over 5 min at 0 °C, then the mixture was stirred at room temperature for 3 h. After addition of methanol (10 mL), the reaction mixture was concentrated to *ca.* 50 mL volume under reduced pressure. After addition of hexane (100 mL), the mixture was washed with water (20 mL \times 3) and brine (20 mL), dried over magnesium sulfate, filtered off, and concentrated under reduced pressure to give the product as a colorless oil (25.3 g, yield 93%). This compound was used for the next reaction without further purification.

^1H NMR (400 MHz, 23 °C, CDCl_3): δ 3.25 (s, 2H, C- $\text{CH}_2\text{-O}$), 1.03 (s, 6H, C- CH_3), 0.89 (s, 9H, Si-C(CH_3) $_3$), 0.028 (s, 6H, Si- CH_3). The peaks of NH $_2$ could not be assigned unambiguously due to possible exchange with water (broad singlet at 1.60 ppm).

^{13}C NMR (100 MHz, 23 °C, CDCl_3): δ 73.2 (C-C-O), 50.8 (-N-C-C), 26.9 (-C- CH_3), 26.0 (Si-C(CH_3) $_3$), 18.4 (Si-C(CH_3) $_3$), -5.3 (Si- CH_3).

ESI-HRMS m/z calcd for $\text{C}_{10}\text{H}_{26}\text{NOSi}$ [$\text{M}+\text{H}^+$]: 204.1778, found: 204.1777.

Synthesis of 8



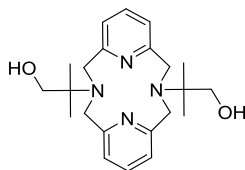
A solution of 2,6-bis(bromomethyl) pyridine (6.36 g, 24.0 mmol) in MeCN (50 mL) was added dropwise over 4 h using a dropping funnel to a mixture of compound 7 (4.88 g, 24.0 mmol), potassium carbonate (20.0 g, 145 mmol), and MeCN (1.2 L) with stirring at 80 °C. After stirring at 80 °C for 2 days, the hot mixture was filtered off and concentrated under reduced pressure. The mixture was suspended in dichloromethane (100 mL) and washed with water (20 mL \times 2), dried over a mixture of potassium carbonate and magnesium sulfate, filtered off and concentrated under reduced pressure. The mixture was suspended in hexane (30 mL) and stirred at 60 °C, then cooled to room temperature slowly. After cooling further with an ice bath, the mixture was filtered off to remove precipitate. The mixture was purified by silica gel column chromatography using CHCl_3 : MeOH : 28% NH_3 aqueous solution (50 : 1 : 0.1/v) to give a white powder, 1.99 g, yield 27%.

^1H NMR (400 MHz, 23 °C, CDCl_3): δ 7.04 (t, $J = 7.3$ Hz, $p\text{-H}_{\text{Py}}$, 2H), 6.72 (d, $J = 7.3$ Hz, $m\text{-H}_{\text{Py}}$, 4H), 4.04 (s, $\text{Py-CH}_2\text{-N}$, 8H), 3.67 (s, C- $\text{CH}_2\text{-O}$, 4H), 1.28 (s, N-C-(CH_3) $_2$, 12H), 0.93 (s, Si-C(CH_3) $_3$, 18H), 0.09 (s, Si- CH_3 , 12H).

^{13}C NMR (100 MHz, 23 °C, CDCl_3): δ 159.6 ($o\text{-C}_{\text{Py}}$), 135.3 ($p\text{-C}_{\text{Py}}$), 122.1 ($m\text{-C}_{\text{Py}}$), 69.6 (C-C-O), 59.6 (C- CH_3), 58.1 (-Py-C-N-), 26.1 (-C- CH_3), 23.7 (Si-C(CH_3) $_3$), 18.5 (Si-C(CH_3) $_3$), -5.3 (Si- CH_3).

ESI-HRMS m/z calcd for $\text{C}_{34}\text{H}_{61}\text{O}_2\text{N}_4\text{Si}_2$ [$\text{M}+\text{H}^+$]: 613.4328, found: 613.4315.

Synthesis of 9



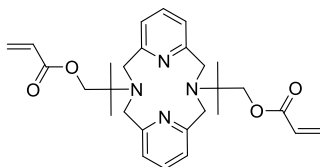
Compound **8** (1.98 g, 3.23 mmol) was suspended in MeOH (10 mL). After the addition of 35% hydrochloric acid (1.0 mL), the mixture was stirred at room temperature for 1 day. The solvents were removed under reduced pressure. Potassium carbonate (16.2 g, 117 mmol) and water (10 mL) were added to the mixture. The mixture was extracted with CH₂Cl₂ (20 mL × 8) (the target compound only slightly dissolves in water). The combined organic layers were dried over a mixture of potassium carbonate and magnesium sulfate, filtered off, and concentrated under reduced pressure. Toluene (20 mL) was added to the mixture and stirred at 110 °C for 5 min. The hot mixture was filtered off to remove viscous solid and concentrated under reduced pressure. Recrystallization from MeCN (5 mL) provided target product as a colorless crystalline solid, 1.01 g, yield 81%.

¹H NMR (400 MHz, 23 °C, CDCl₃): δ 7.04 (t, *J* = 7.3 Hz, *p*-H_{Py}, 2H), 6.50 (d, *J* = 7.3 Hz, *m*-H_{Py}, 4H), 3.92 (s, Py-CH₂-N, 8H), 3.54 (s, C-CH₂-O, 4H), 2.14 (s, 2H, OH), 1.29 (s, N-C-(CH₃)₂, 12H).

¹³C NMR (100 MHz, 23 °C, CDCl₃): δ 159.8 (*o*-C_{Py}), 135.5 (*p*-C_{Py}), 120.4 (*m*-C_{Py}), 69.9 (C-C-O), 59.1 (C-CH₃), 55.7 (-Py-C-N-), 23.0 (C-CH₃).

ESI-HRMS *m/z* calcd for C₂₂H₃₃N₄O₂ [M+ H⁺]: 385.2598, found: 385.2587.

Synthesis of L2



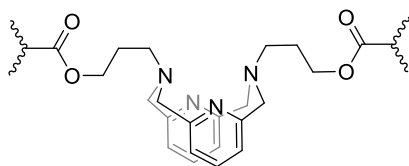
L2 was prepared by the same procedure with **L1** using compound **8** (100 mg, 0.260 mmol), sodium hydride (20.0 mg, 0.834 mmol), dry THF (5 mL) and acryloyl chloride (112 mg, 1.24 mmol) to give the product as a white powder (82.5 mg, yield 64%).

¹H NMR (400 MHz, 23 °C, CDCl₃): δ 7.07 (t, ³*J*_{HH} = 7.8 Hz, *p*-H_{Py}, 2H), 6.71 (d, ³*J*_{HH} = 7.8 Hz, *m*-H_{Py}, 4H), 6.47 (d, ²*J*_{HH} = 17.4 Hz, -C=CH, 2H), 6.21 (dd, ³*J*_{HH} = 17.4 and 10.52 Hz, -CH=CH, 2H), 5.88 (d, ²*J*_{HH} = 10.52 Hz, -C=CH, 2H), 4.30 (s, C-CH₂-O, 4H), 4.07 (s, Py-CH₂-N, 8H), 1.34 (s, C-CH₃, 12H).

¹³C NMR (100 MHz, 23 °C, CDCl₃): δ 166.3 (C=O), 159.1 (*o*-C_{Py}), 135.6 (*p*-C_{Py}), 131.2 (CO-C=C), 128.6 (CO-C=C), 122.2 (*m*-C_{Py}), 69.8 (C-C-O), 58.1 (C_q-CH₃), 58.0 (-Py-CH₂-N-), 24.4 (C-CH₃).

ESI-HRMS *m/z* calcd for C₂₈H₃₇O₄N₄ [M+ H⁺]: 493.2809, found: 493.2785.

Synthesis of cPBA1



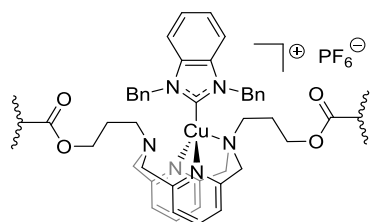
In a glove box, 2-methyl-4'-(methylthio)-2-morpholinopropiophenone (39.5 mg, 0.141 mmol) was dissolved in a solution of **L1** (65.1 mg, 0.140 mmol) and butyl acrylate (1.79 g, 14.0 mmol) in dry DMF (6 mL). The reaction mixture was split into two Teflon molds [40 mm [W] × 70 mm [L] × 5 mm [D]]. The molds were covered with thin glass plate [50 mm [W] × 80 mm [L] × 0.15 mm [T]] and sealed with

silicone grease. After irradiation with UV lamp for 20 min, the molds were left in a glove box for 24 h, then taken out of the glove box. The formed films were taken from mold and put in a solution of hexane-diethyl ether in a capped glass bottle. After 4-10 h, the solvent was replaced. This washing process was repeated five times.

The washing solvents were concentrated and analyzed by ^1H NMR, which gave no peak of pyridinophane ligand, indicating the ligand with acryloyloxy was incorporated completely. The films were further dried under vacuum for 2 days on Teflon sheet to give transparent films (1.52 g, 82%).

FT-IR (ATR, solid): ν 738, 840, 940, 1021, 1062, 1116, 1156, 1241, 1449, 1727, 2873, 2957 cm^{-1} .

Synthesis of Cu1-cPBA



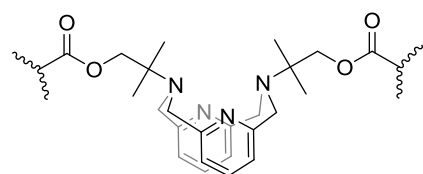
Cut films [25 mm \times 10 mm] were used for the reaction. In a glove box, cross-linked poly(butyl acrylate) films [0.09 mmol/g of **L1** incorporated in **cPBA**] (2.39 g) were placed in dry MeCN (30 mL) in a capped metal container for 1 h. (1,3-Dibenzylbenzimidazol-2-ylidene)copper(I) chloride (23.9 mg, 0.0471 mmol) was dissolved in dry MeCN (20 mL) by stirring and added to the swollen films in solution. The mixture was left at room temperature for 24 h. The solvent was replaced with fresh MeCN, then left for 4-10 h. This washing process was repeated three times.

The washing solvents were concentrated and analyzed by ^1H NMR, which gave no peak of (1,3-dibenzylbenzimidazol-2-ylidene)copper(I) chloride.

After the addition of KPF_6 (174 mg, 0.945 mmol), the films in MeCN were left for 6 h. After replacing the MeCN solution, the films were left for 4-10 h to wash the films, then taken out from solution and dried under vacuum for 2 days on Teflon sheet.

FT-IR (ATR, solid): ν 741, 841, 943, 1025, 1063, 1116, 1156, 1244, 1377, 1452, 1728, 2334, 2871, 2957 cm^{-1} .

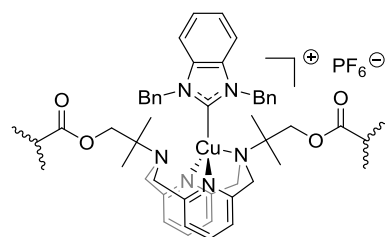
Synthesis of cPBA2



cPBA2 was prepared by the same procedure as **cPBA1** by using **L2** (69.0 mg, 0.140 mmol), 2-methyl-4'-(methylthio)-2-morpholinopropiophenone (39.1 mg, 0.140 mmol), butyl acrylate (1.79 g, 14.0 mmol) and dry DMF (6 mL) to provide films (1.54 g, 83%)

FT-IR (ATR, solid): ν 738, 806, 840, 941, 1020, 1062, 1116, 1156, 1242, 1450, 1540, 1576, 1727, 2873, 2958 cm^{-1} .

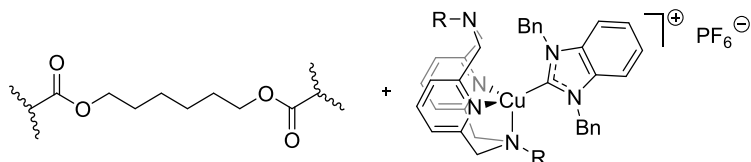
Synthesis of Cu2-cPBA



Cu2-cPBA was prepared by the same procedure as **Cu1-cPBA** by using films of **cPBA2** [0.09 mmol/g of **L2** incorporated in **cPBA**] (1.98 g) and (1,3-dibenzylbenzimidazol-2-ylidene)copper(I) chloride (19.8 mg, 0.0391 mmol), and potassium hexafluorophosphate (145 mg, 0.788 mmol). ¹H NMR analysis of concentrated washing solvent confirmed no peaks of (1,3-dibenzylbenzimidazol-2-ylidene)copper(I) chloride.

FT-IR (ATR, solid): ν 737, 841, 940, 1021, 1062, 1116, 1156, 1241, 1449, 1589, 1727, 2873, 2932, 2957 cm^{-1} .

Preparation of reference film for control experiments



The films for the control experiment were prepared as the same method as described above by using 1,6-bis(acryloyloxy)hexane (31.8 mg, 0.141 mmol), butyl acrylate (1.79 g, 14.0 mmol), 2-methyl-4'-(methylthio)-2-morpholinopropiophenone (39.2 mg, 0.140 mmol), and DMF (6 mL) to give transparent films (1.41 g, 77%)

Cut films [25 mm × 10 mm] were used for further experiments. In a glove box, reference cross-linked poly(butyl acrylate) films were placed on Teflon sheet and each film was swollen in MeCN (0.2 mL). Then, the swollen films were further swollen by a solution of MeCN (0.3 mL) including 1 wt% of **Cu4** or **Cu6**. After leaving for 3 h, the films were dried under vacuum for 2 days on a Teflon sheet.

III. FT-IR spectra

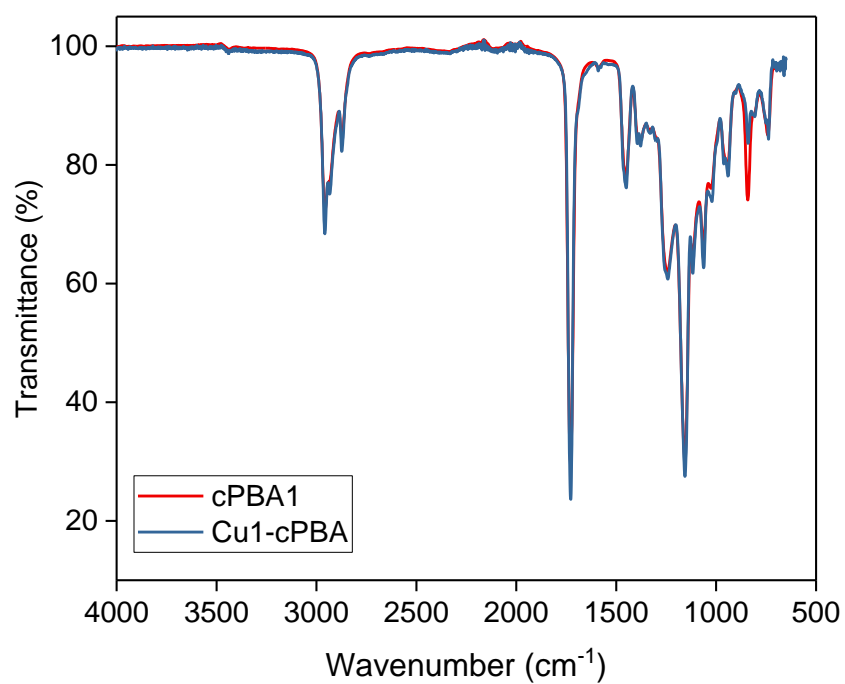


Figure S1. FT-IR spectra of **cPBA1** and **Cu1-cPBA**.

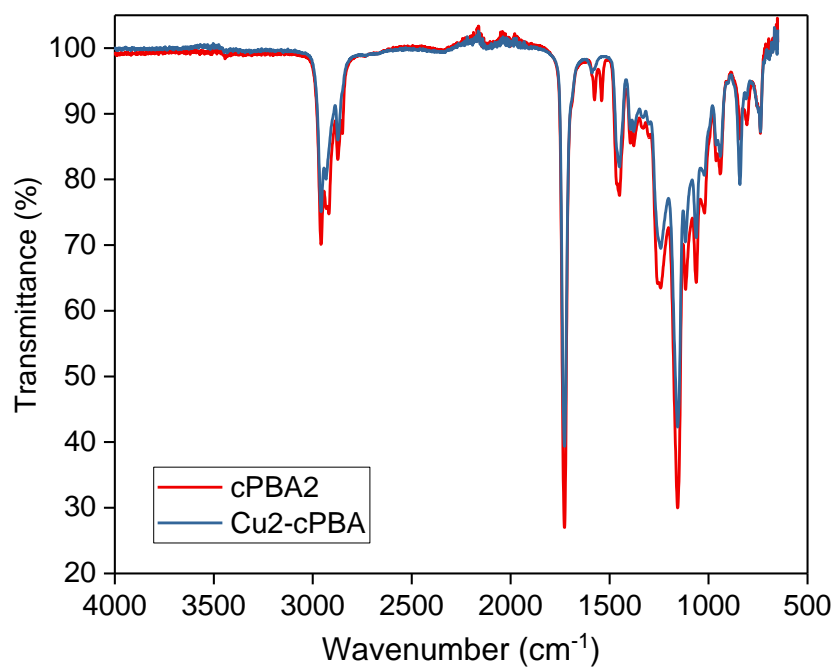


Figure S2. FT-IR spectra of **cPBA2** and **Cu2-cPBA**.

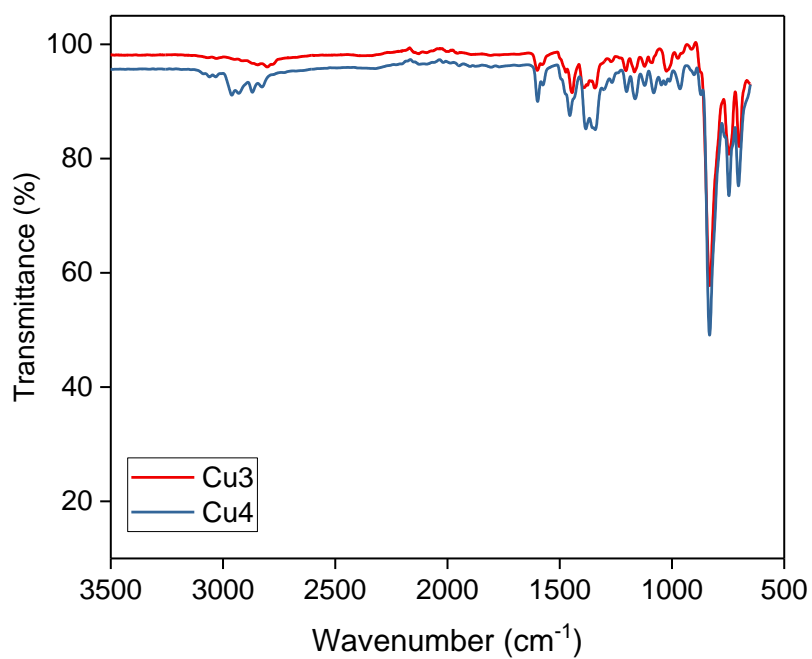


Figure S3. FT-IR spectra of **Cu3** and **Cu4**.

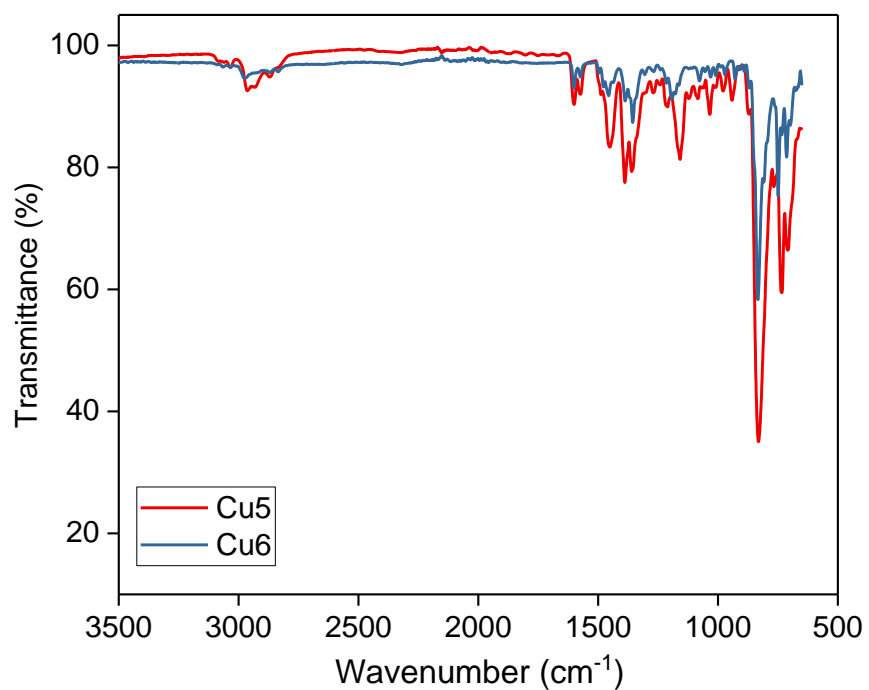


Figure S4. FT-IR spectra of **Cu5** and **Cu6**.

IV. UV-vis spectra

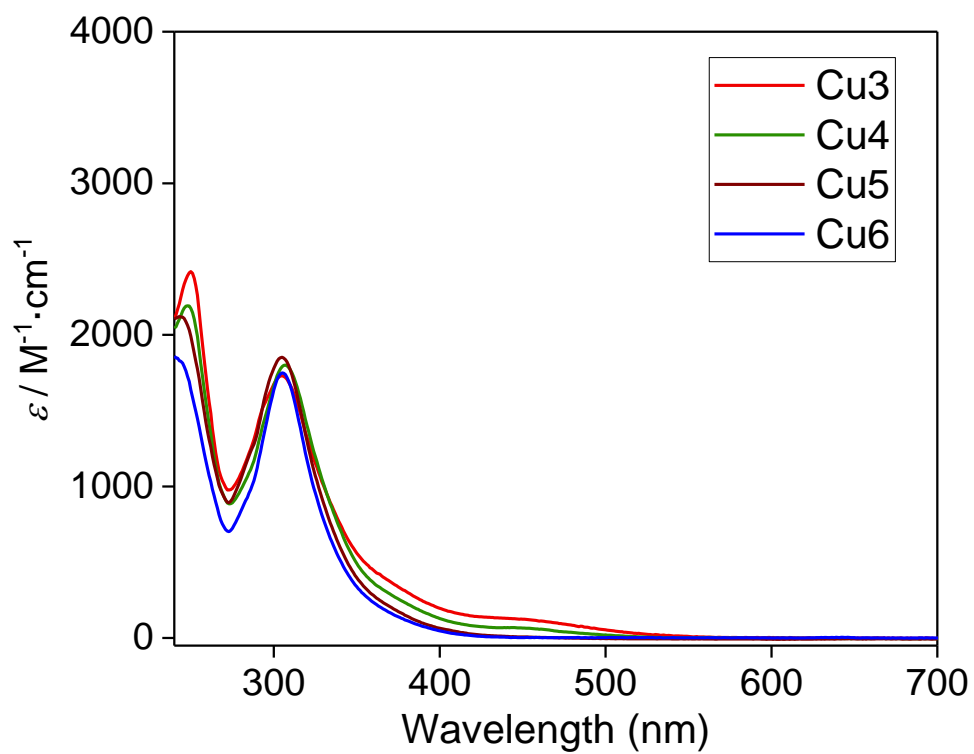
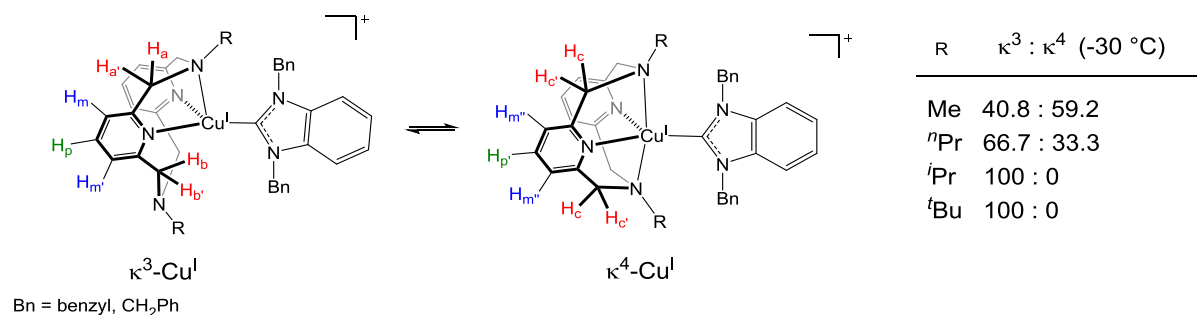


Figure S5. UV-vis absorption spectra of **Cu3-6** in dichloromethane.

V. EXSY and VT NMR experiments

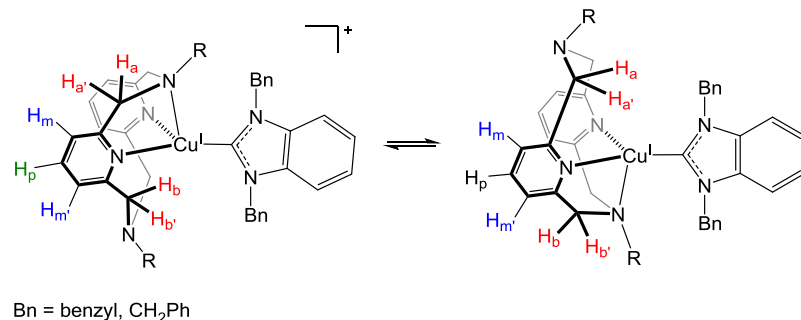
To study conformational flexibility of the ligand in complexes **Cu3-6**, NOESY (EXSY) NMR experiments at VT experiments were performed. The isomerization in complexes **Cu3-6** is similar to that observed in previously reported copper(I) iodide complexes.⁸ Mixing time of 0.5 s and relaxation delay of 1.5 s were used.

Two isomers were present in solution of complexes **Cu3** and **Cu4**, assigned as complexes with κ^4 - and κ^3 -bound ligands based on symmetry considerations.⁸ EXSY experiment shows an exchange between two isomers with κ^4 - and κ^3 -bound ligands (Scheme S8). For example, exchange cross-peaks are observed between methylene protons $H_{a/a'}$, $H_{b/b'}$ and $H_{c/c'}$.



Scheme S7. Isomer interconversion involving $(\kappa^3\text{-}^R\text{N4})\text{Cu}^{\text{I}}(\text{BnNHC})^+$ and $(\kappa^4\text{-}^R\text{N4})\text{Cu}^{\text{I}}(\text{BnNHC})^+$ (R = Me, ⁿPr).

In addition, degenerative exchange was also observed in complexes **Cu5** and **Cu6** where only one isomer, $(\kappa^3\text{-}^R\text{N4})\text{Cu}^{\text{I}}(\text{BnNHC})^+$, was present involving an exchange between pendant and coordinated amines (Scheme S8).⁸



Scheme S8. Exchange process in solution of $(\kappa^3\text{-}^R\text{N4})\text{Cu}^{\text{I}}(\text{BnNHC})^+$ involving coordinated and non-coordinated amines (R = ^tBu, ⁱPr).

Such degenerative exchange is evident from EXSY spectrum showing exchange peaks between H_m and $H_{m'}$ protons and methylene protons $H_{a/a'}$ and $H_{b/b'}$.

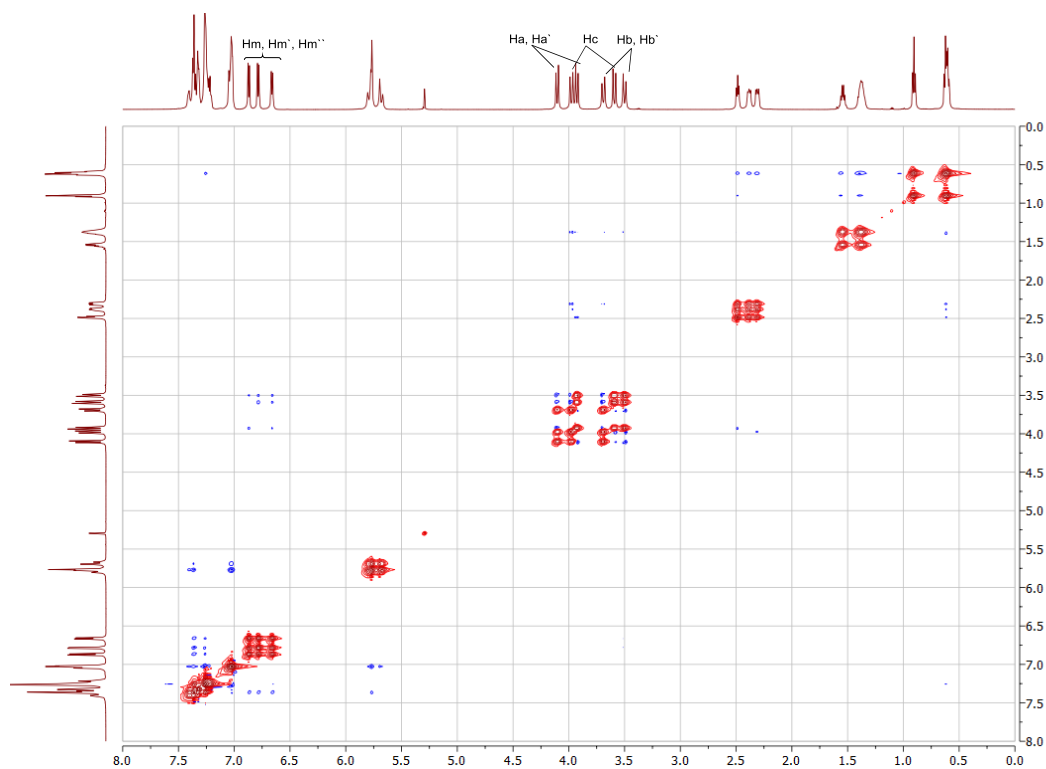


Figure S6. EXSY spectrum of **Cu4** in CD_2Cl_2 at $-20\text{ }^\circ\text{C}$. Exchange cross-peaks are shown in red color (same phase with diagonal peaks) and NOE peaks are shown in blue color (opposite phase to diagonal peaks).

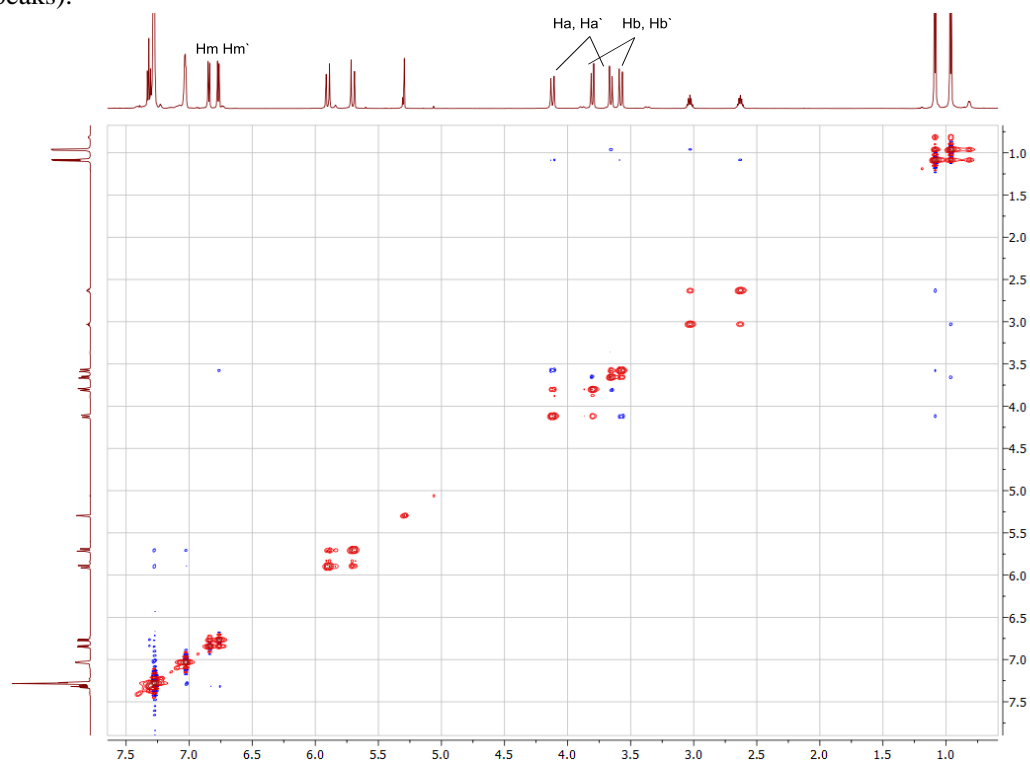


Figure S7. EXSY spectrum of **Cu5** in CD_2Cl_2 at $-20\text{ }^\circ\text{C}$. Exchange cross-peaks are shown in red color (same phase with diagonal peaks) and NOE peaks are shown in blue color (opposite phase to diagonal peaks).

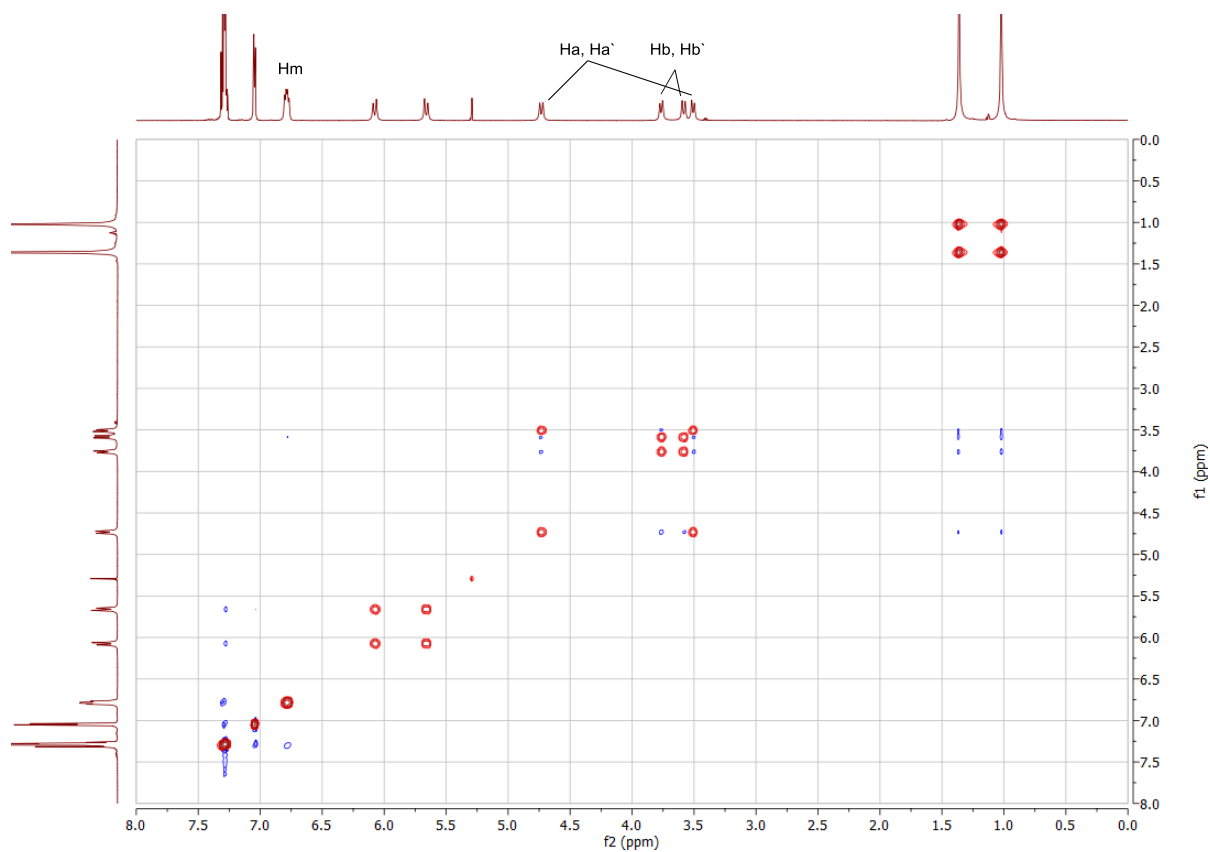


Figure S8. EXSY spectrum of **Cu6** in CD_2Cl_2 at $27\text{ }^\circ\text{C}$. Exchange cross-peaks are shown in red color (same phase with diagonal peaks) and NOE peaks are shown in blue color (opposite phase to diagonal peaks).

According to VT NMR experiments, for complexes **Cu3** and **Cu4**, coalescence temperature for aromatic *meta*-protons of pyridine H_{meta} is *ca.* $20\text{ }^\circ\text{C}$, and for **Cu5** and **Cu6**, the coalescence temperature is above $27\text{ }^\circ\text{C}$ (the sample could not be heated at high temperature due to low boiling point of CD_2Cl_2 solvent). Complex **Cu6** shows sharp peaks already at room temperature, although the exchange is evident from EXSY spectra (see above).

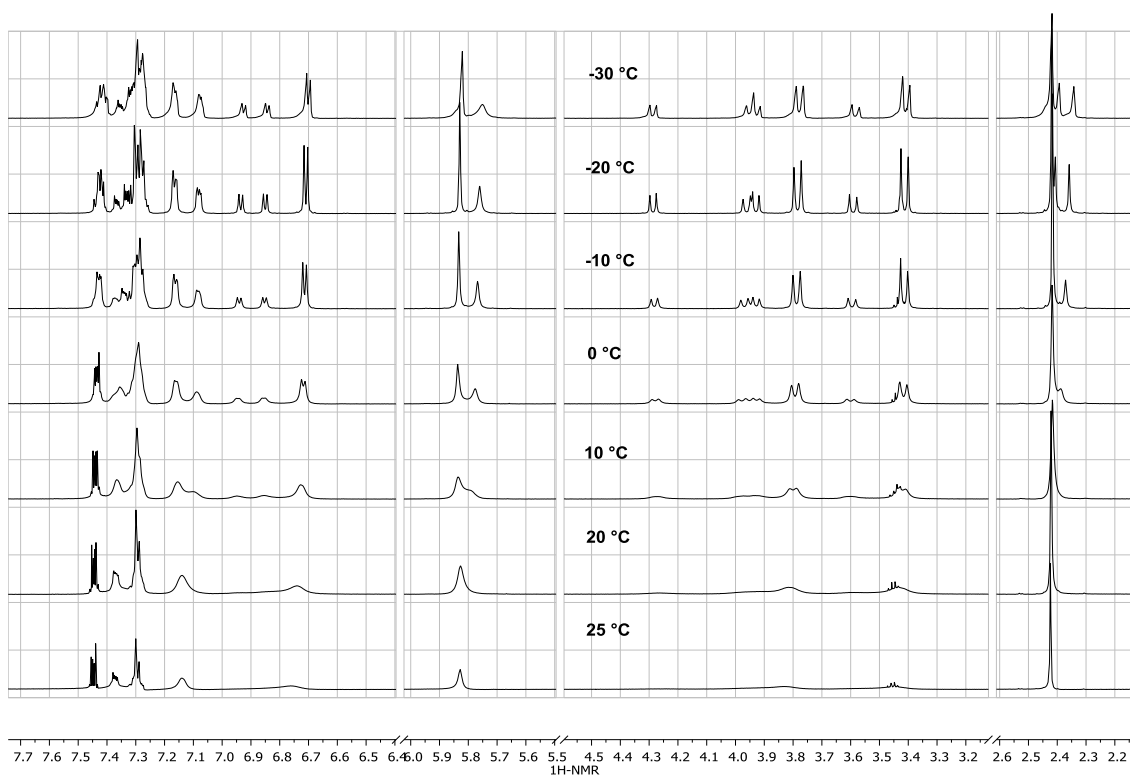


Figure S9. VT $^1\text{H-NMR}$ spectra of **Cu3** in CD_2Cl_2 .

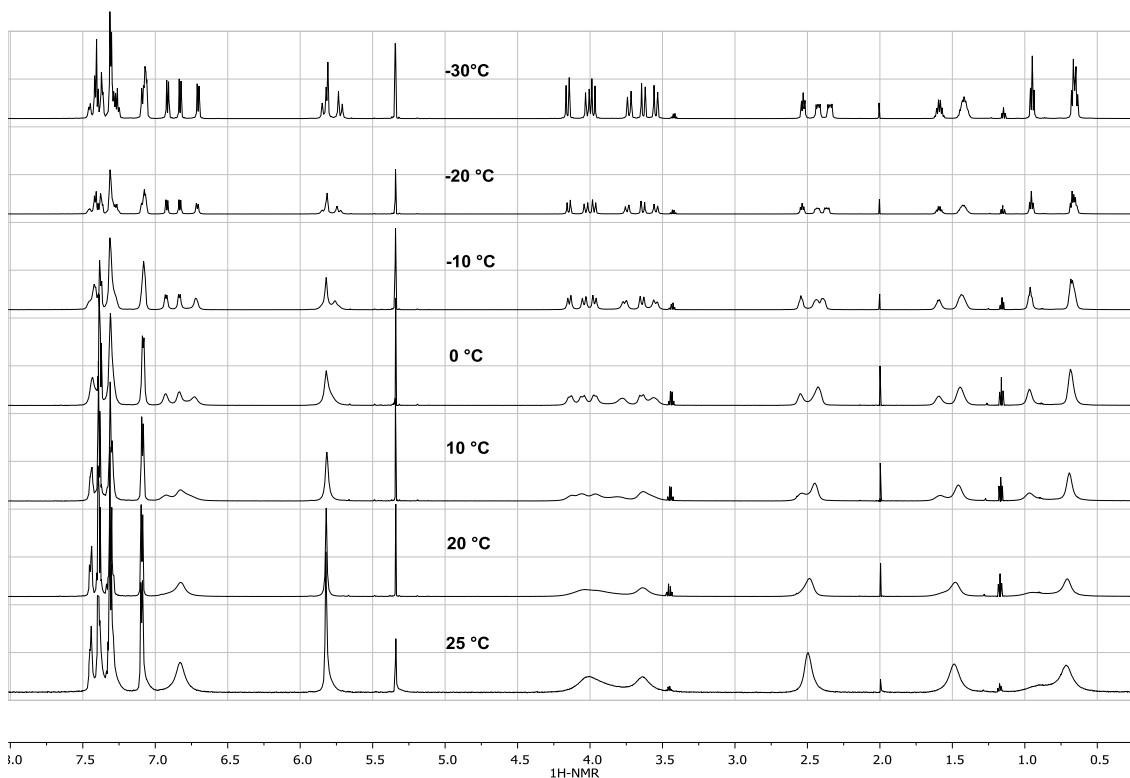


Figure S10. VT $^1\text{H-NMR}$ spectra of **Cu4** in CD_2Cl_2 .

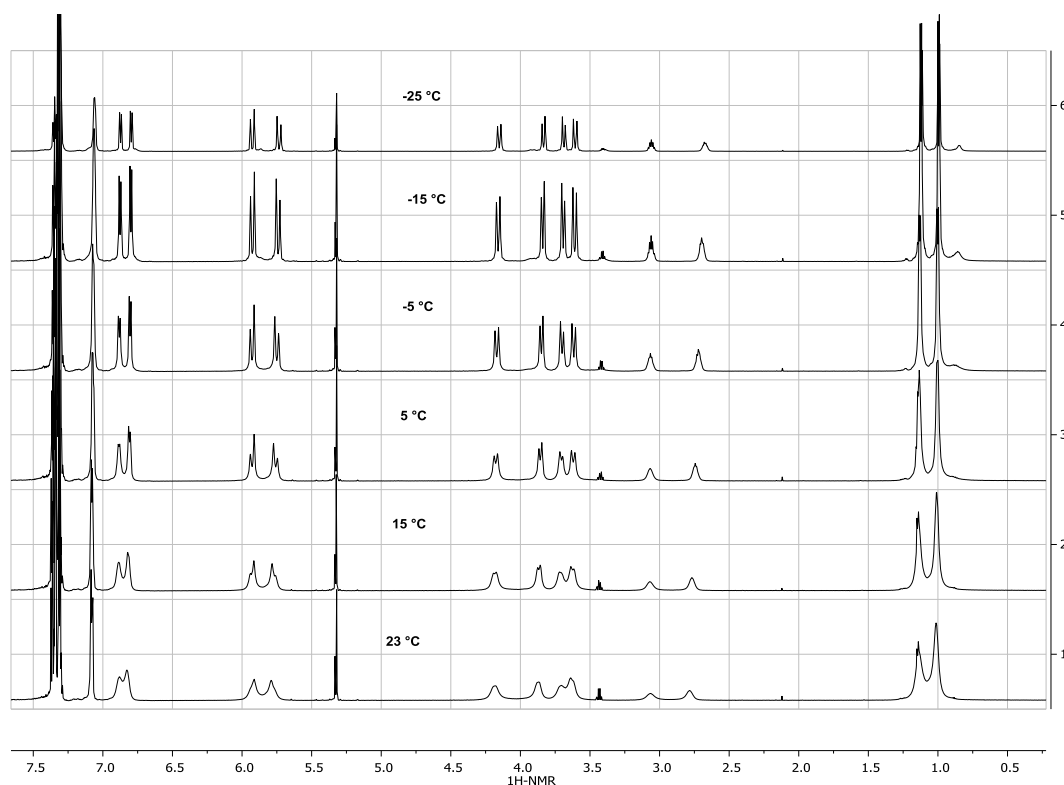
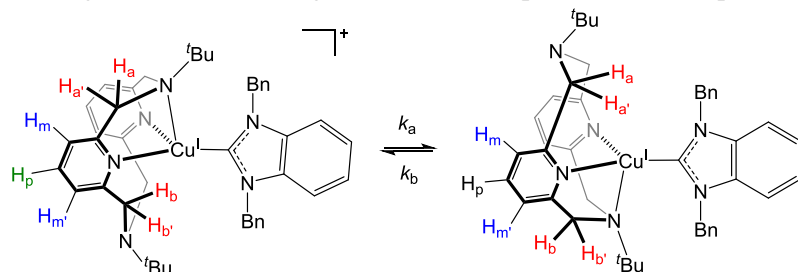


Figure S11. VT ^1H NMR spectrum of **Cu5** in CD_2Cl_2 .

The preliminary study of the kinetics of the exchange in complex **Cu6** was performed using soft pulse transfer experiment (SPT).⁹ A solution of **Cu6** in CD_2Cl_2 was used for the measurements at a constant temperature of 27 °C, and double pulse shape experiment implemented on JEOL EXZ600R was used. Soft pulse length of 15 ms and relaxation delay of 7 s were used.

The signal of the ^tBu group at 1.02 ppm (signal **A**) was irradiated, and the intensity of signal **A** and the signal of another ^tBu group at 1.36 ppm (signal **B**) were monitored. The intensity change conforms to the theoretical equations confirming both signals are in a state of slow mutual exchange. The fitting was done according to the general equations given in the reported method⁹ with a nonlinear least squares minimization iterative procedure based on Levenberg-Marquardt algorithm without enforcing equal rate of degenerative exchange between two chemically equivalent isomers; nevertheless, similar values of k_a and k_b were obtained, 19.6 s^{-1} and 15.9 s^{-1} , respectively, thus giving an estimate that the rate of exchange between isomers is *ca.* 16 s^{-1} (the difference between two values might be within experimental error). This can be used as an estimate of the order of the exchange rate, rather than exact values, as these results are not free from error due to NOE effects. This value is of the same order of magnitude, as determined for structurally similar ($^{\text{R}}\text{N4}$) Cu^{I} complexes.⁸ As expected for slow exchange, the exchange rate k_{ex} ($k_{\text{ex}} = k_a + k_b$), 35.5 Hz, is smaller than the difference of chemical shifts of signals **A** and **B** (205 Hz). More detailed investigation of the exchange kinetics will be performed in a separate study.



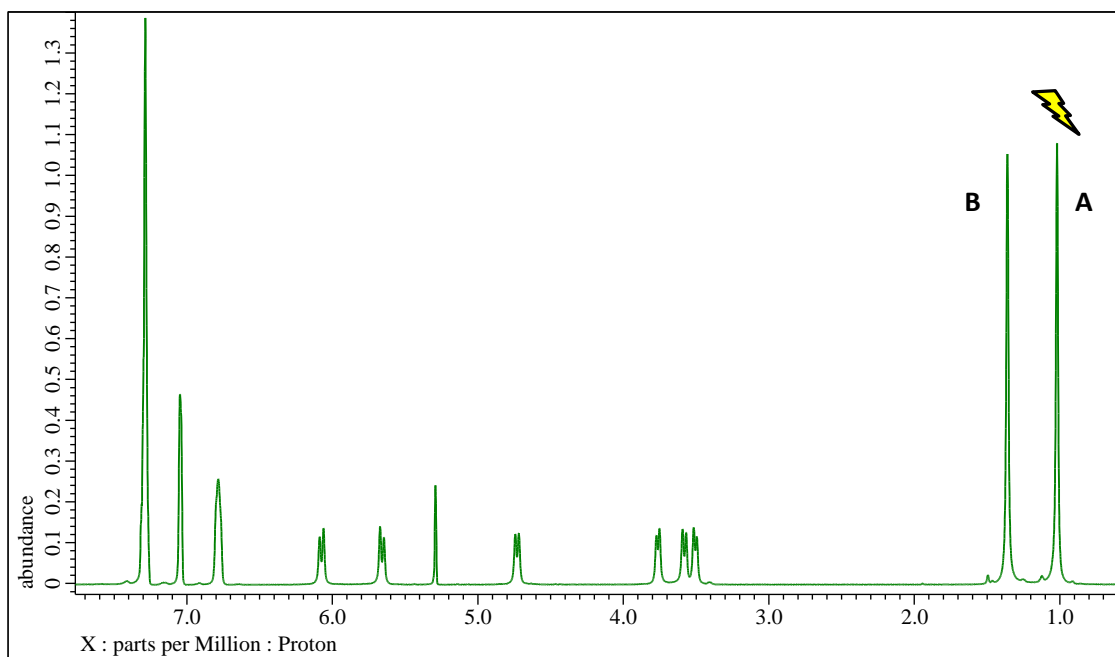


Figure S12. ^1H NMR spectrum showing ^tBu signals **A** and **B** of **Cu6** monitored in the following experiment.

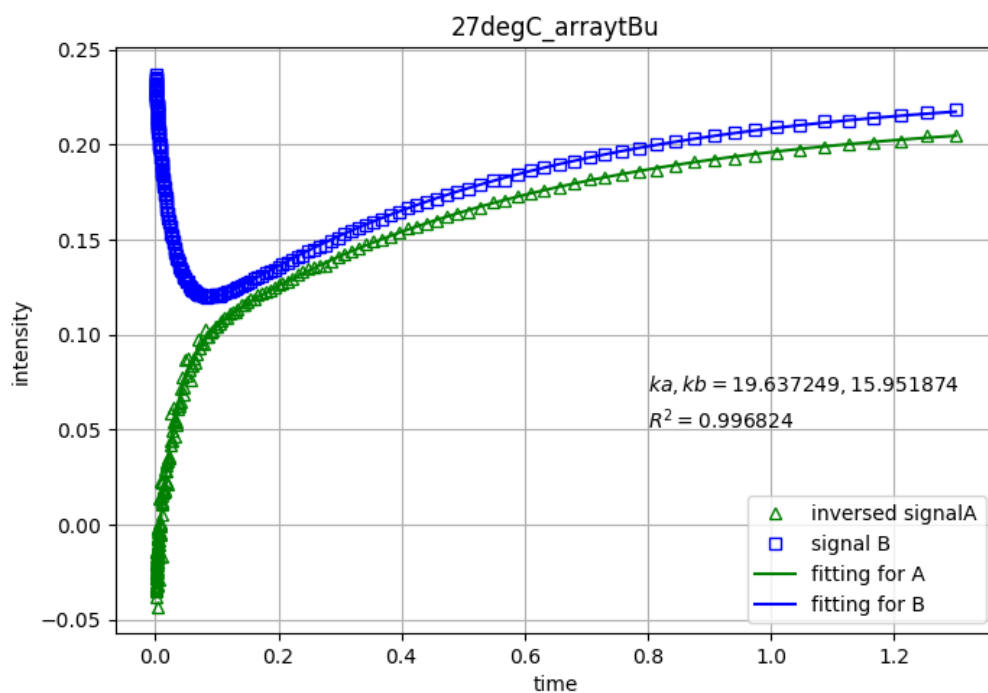


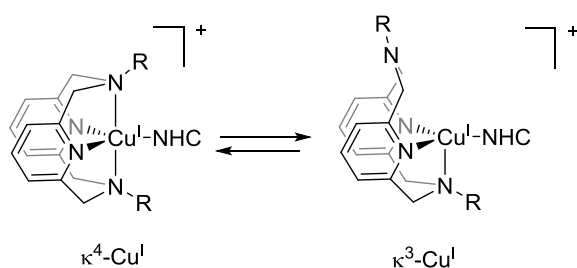
Figure S13. Experimental data and fitting of the intensity of signals **A** and **B** as a function of τ interval.

VI. Cyclic voltammetry

The cyclic voltammograms of complexes **Cu3-6** reflect the sterics-dependent conformational behavior of these complexes consistent with their solution NMR studies.

Complexes with less bulky N-Me and N-*n*-Pr substituents, which exist in a solution as a mixture of κ^4 and κ^3 -isomers, show one quasireversible wave corresponding to more easily oxidized κ^4 -isomer. Although the separation between forward and reverse peaks is somewhat larger than 59 mV, such behavior is typically assigned to only minor changes in R^N4 ligand conformation.^{8, 10} This is consistent with previous results showing that upon oxidation to Cu^{II} , R^N4 coordinates in a κ^4 -fashion, even for bulky *t*-Bu-substituted ligand.^{10b} The behavior does not change significantly when compared at slow and fast scan rates due to high fraction of κ^4 -isomer already present in the equilibrium mixture.

By contrast, CV's of more bulky complexes **Cu5** and **Cu6**, which are present in a solution predominantly as κ^3 -isomers according to NMR, show scan-rate dependent behavior. At high scan rates, higher potential oxidation wave is observed for a major κ^3 -isomer. The separation between forward and reverse peaks is 0.54 V, indicative of significant conformational changes in the ligand (κ^3 - to κ^4 -coordination in Cu^{II}).^{8, 10b} At lower scan rate, the rate of isomer interconversion (between κ^3 - Cu^I and κ^4 - Cu^I) is comparable to the cyclic voltammetry experiment timescale for **Cu5**, and a lower potential wave becomes observable for a minor, but more easily oxidized, κ^4 - Cu^I . At the same time, even at slow scan rates, κ^4 - Cu^I wave is not detected for *t*-Bu-substituted **Cu6**.



Scheme S9. Isomer interconversion in complexes **Cu3-6**.

Table S1. Electrochemical properties of **Cu3-6** (1 mM).^a

Complex	R	E_{pa1} (V vs. Fc)	E_{pc1} (V vs. Fc)	ΔE_p (mV) ^b
Cu3	Me	+0.05	-0.15	0.20
Cu4	<i>n</i> -Pr	+0.05	-0.14	0.19
Cu5	<i>i</i> -Pr	+0.21	+0.07	0.14
Cu6	<i>t</i> -Bu	+0.74	+0.20	0.54

^a 1 mM solution of complex in 0.1 M solution of nBu_4NPF_6 as a supporting electrolyte in CH_2Cl_2 at 23 °C, Pt disk electrode ($d = 1.6$ mm), all potentials were references vs. ferrocene. ^b The peak-to-peak separation ΔE_p was calculated as $E_{pa1} - E_{pc1}$.

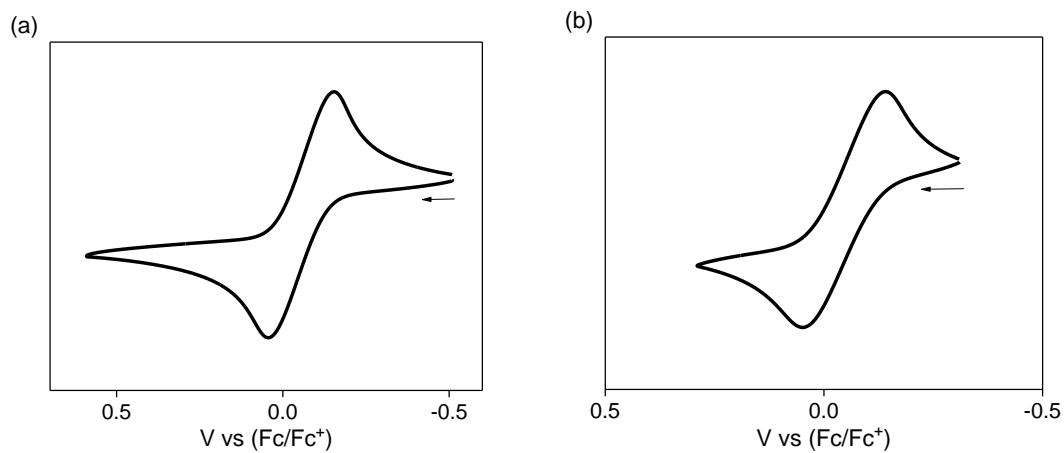


Figure S14. Cyclic voltammogram of (a) **Cu3** and (b) **Cu4** at scan rate of 0.1 V/s.

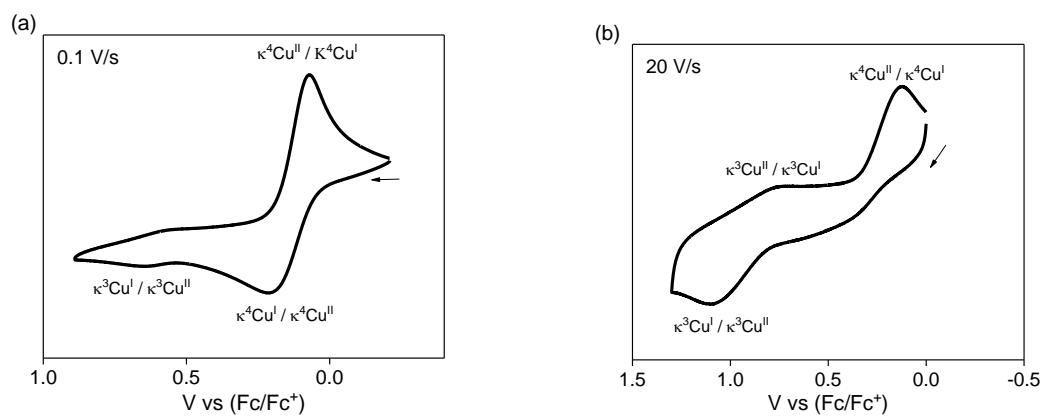


Figure S15. Cyclic voltammograms of **Cu5** at scan rates of: (a) 0.1 V/s and (b) 20 V/s.

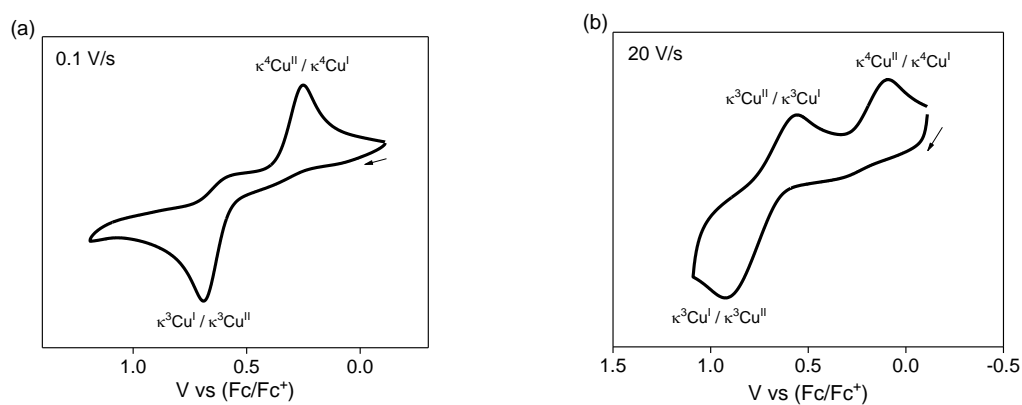


Figure S16. Cyclic voltammograms of **Cu6** at scan rate of (a) 0.1 V/s and (b) 20 V/s.

VII. Photophysical properties of complexes and polymer films

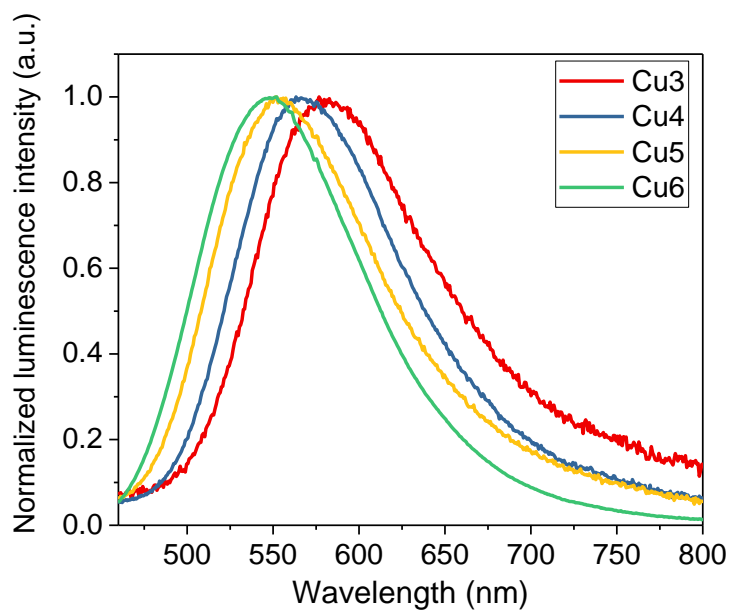


Figure S17. Emission spectra of **Cu3-6** in dichloromethane at 25 °C. Excitation at 380 nm.

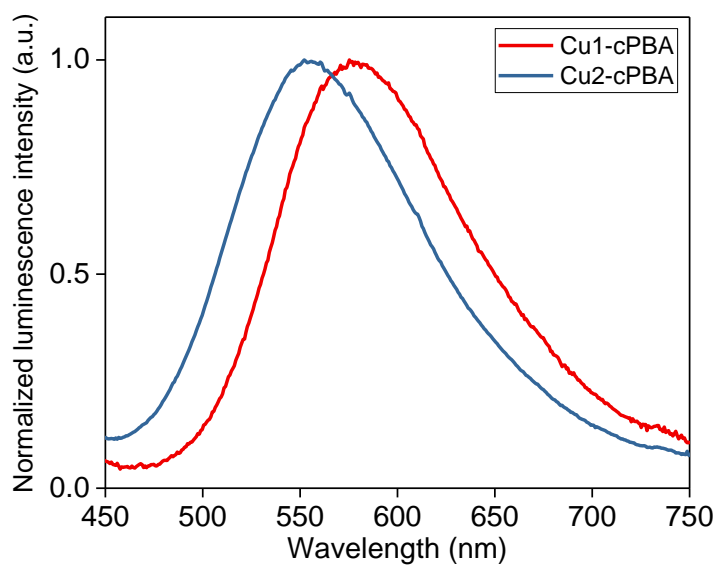


Figure S18. Emission spectra of **Cu1-cPBA** and **Cu2-cPBA** at 25 °C. Excitation at 380 nm.

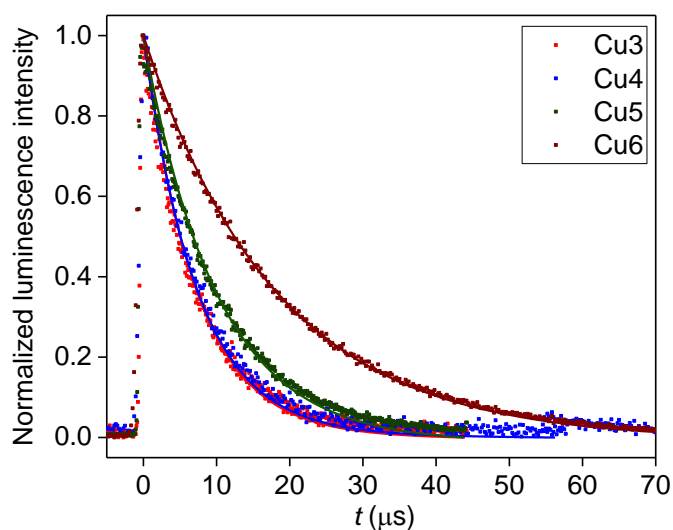


Figure S19. Normalized photoluminescence decay profile of **Cu3-6** in dichloromethane (5×10^{-5} M) at 25 °C. Excitation at 380 nm. Solid lines are fitting curves.

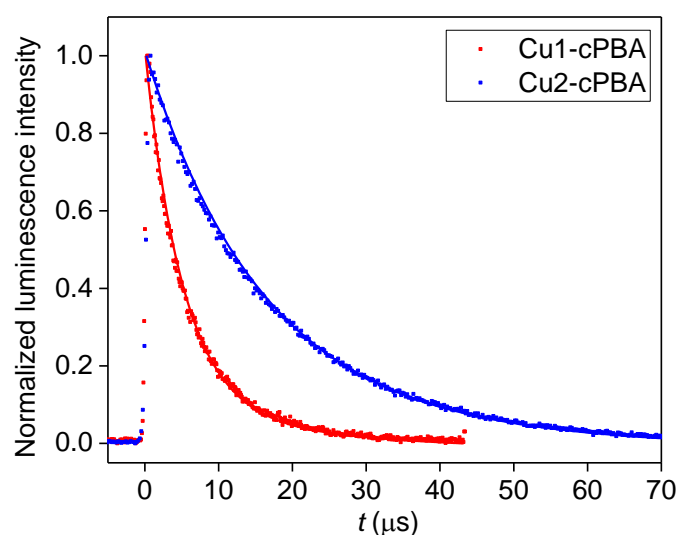


Figure S20. Normalized photoluminescence decay profile of **Cu1-cPBA** and **Cu2-cPBA** at 25 °C. Excitation at 380 nm. Solid lines are fitting curves.

Table S2. Photophysical properties of **Cu1-cPBA** and **Cu2-cPBA**.^a

Sample	λ_{\max} ^b (nm)	PLQY	τ (μ s) ^c	k_r^{-1} · 10 ⁻⁴ (s) ^d	k_{nr1} · 10 ⁻⁴ (s) ^e
Cu1-cPBA	584	0.075	7.17	1.05	12.9
Cu2-cPBA	560	0.27	17.4	1.55	4.20

^a All measurements were performed with excitation at 380 nm. ^b Emission maximum. ^c Emission lifetime at 298 K ^d Radiative decay rate constants were estimated as PLQY/ τ . ^e Non-radiative decay rate constants were calculated as $k_r \cdot (1 - \text{PLQY}) / \text{PLQY}$.

VIII. Photoluminescence intensity measurements in response to mechanical stress

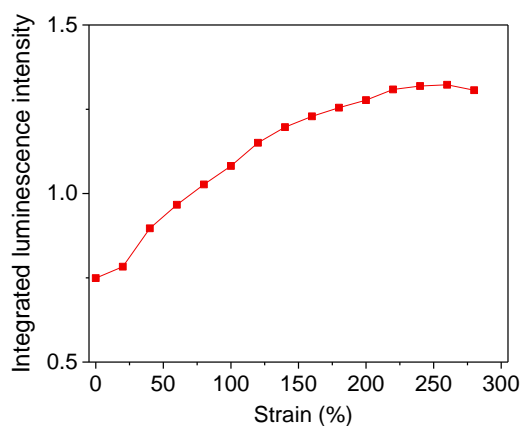


Figure S21. Plot of integrated photoluminescence intensity vs. strain of **Cu1-cPBA**.

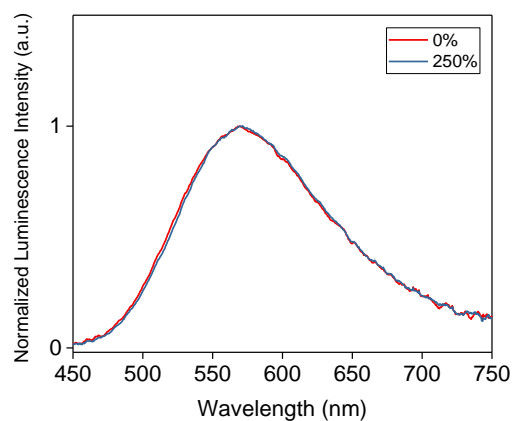


Figure S22. Normalized emission spectra of **Cu1-cPBA** at 0% and 250% of strain.

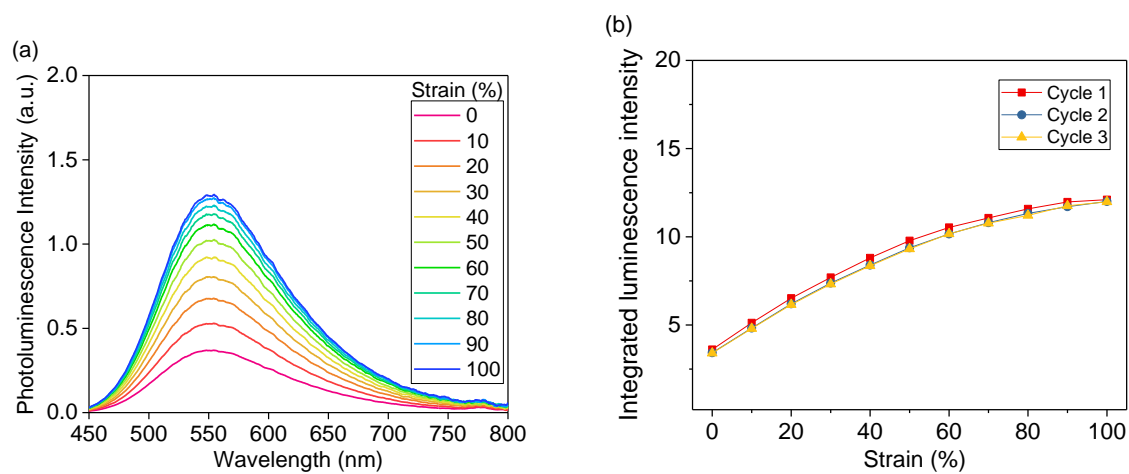


Figure S23. Change of photoluminescence intensity of **Cu2-cPBA** during stretching: (a) emission spectra at variable strain; (b) plot of integrated photoluminescence intensity vs. strain.

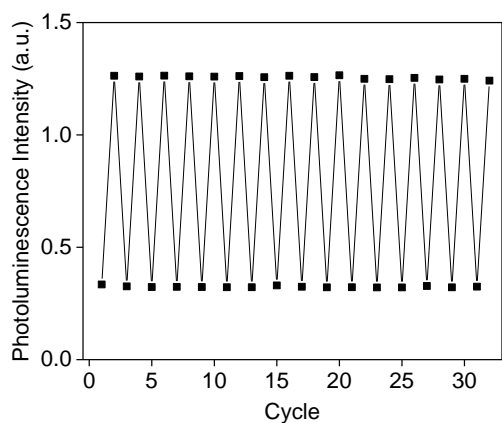


Figure S24. Photoluminescence intensity change of **Cu₂-cPBA** during repeated stretching (Strain range: 0-100%)

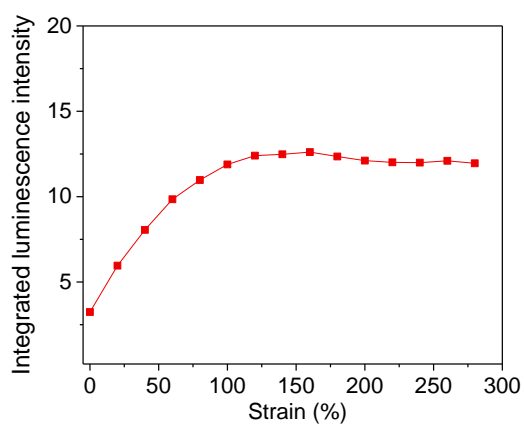


Figure S25. Plot of integrated photoluminescence intensity vs. strain of **Cu₂-cPBA**.

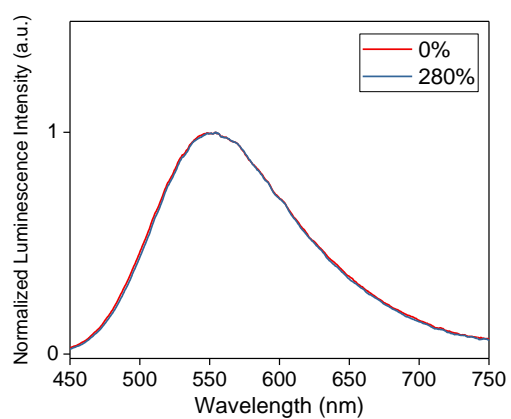


Figure S26. Normalized emission spectra of **Cu₂-cPBA** at 0% and 280% of strain.

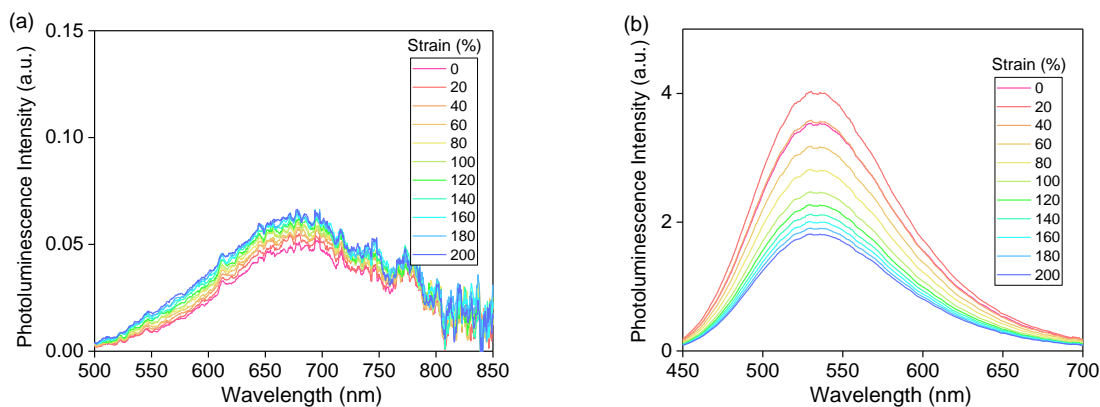


Figure S27. Emission spectra of the control experiments using mechanical mixtures of reference hexamethylene diacrylate-crosslinked poly(butyl acrylate) mixed with 1 wt% of (a) **Cu4** and (b) **Cu6** during stretching.

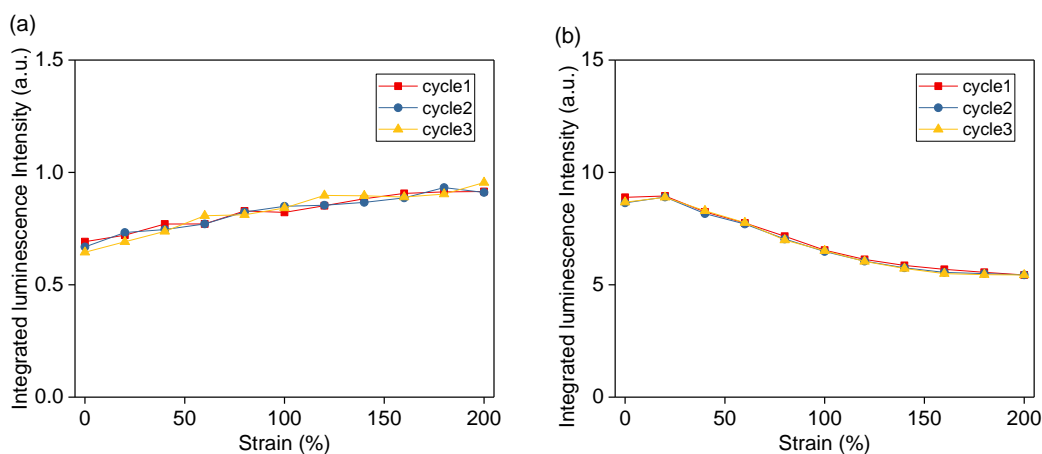


Figure S28. Plot of integrated photoluminescence intensity vs strain of the control experiments using mechanical mixture of reference hexamethylene diacrylate-crosslinked poly(butyl acrylate) and 1 wt% of (a) **Cu4** (b) **Cu6**. The films were tested three times.

The decrease observed in sample with incorporated **Cu6** can be explained by decreasing luminophore density on the film upon stretching. Although small increase of the PL intensity is observed for sample shown in (a), these changes are minor compared to **Cu1-cPBA** and **Cu2-cPBA**.

IX. Air stability

The films were placed on quartz dishes and kept in air under room light at ambient temperature. The samples were purged with a nitrogen gas for 30 min before measuring PLQY in integrating sphere. The PLQYs were measured under a nitrogen gas flow and was determined as an average of measurements for the three films.

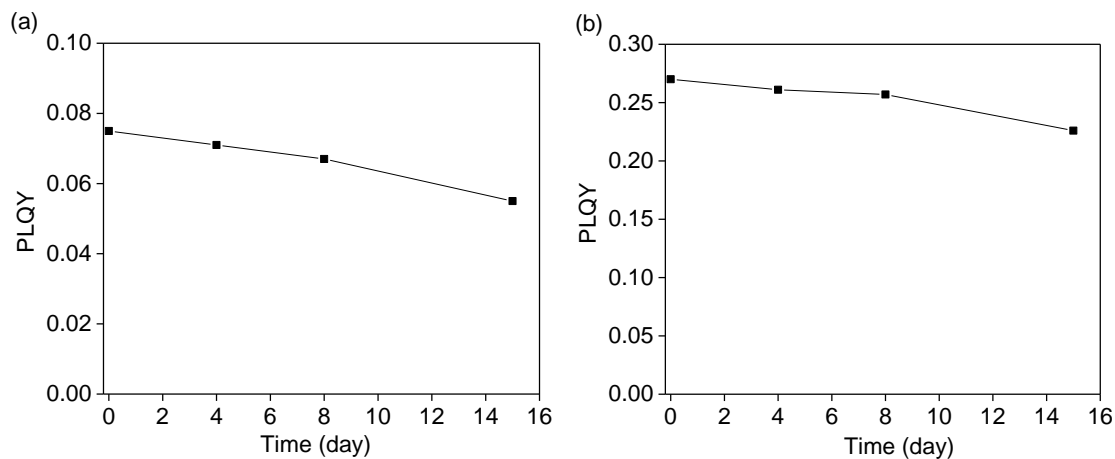


Figure S29. PLQY of (a) **Cu1-cPBA** and (b) **Cu2-cPBA** after exposing to air.

The air-saturated THF solutions of **Cu4** and **Cu6** in quartz cuvette were kept under at ambient temperature and UV/vis spectra were periodically recorded.

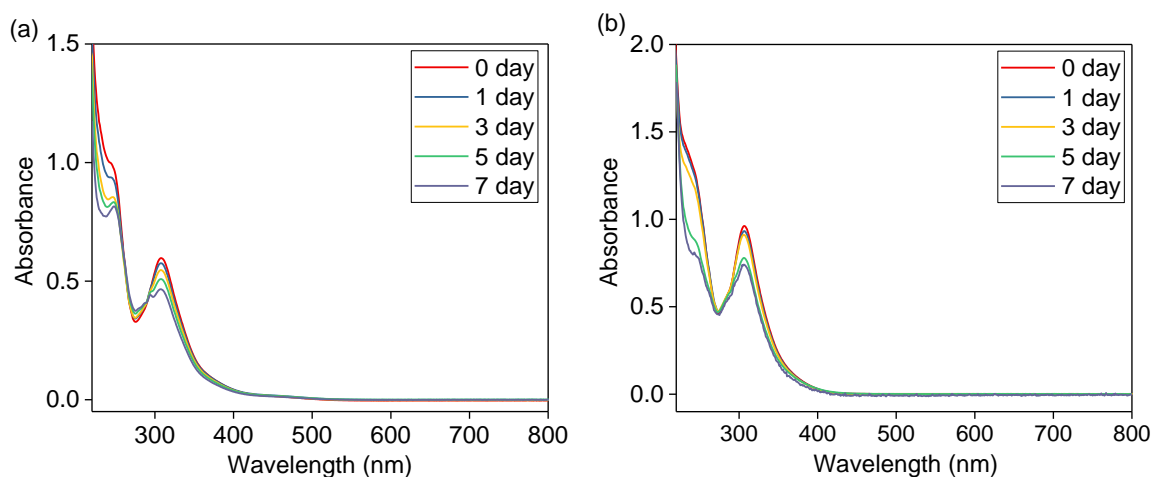


Figure S30. Time-dependent UV-vis absorption spectra of (a) **Cu4** and (b) **Cu6** in air-saturated THF.

X. Mechanical properties

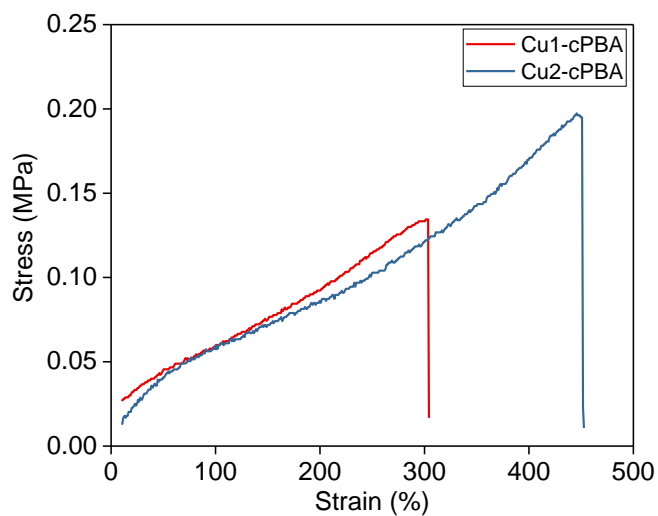


Figure S31. Representative Stress-Strain curve of **Cu1-cPBA** and **Cu2-cPBA**.

Table S3. Mechanical properties of **Cu1-cPBA** and **Cu2-cPBA**.

Sample	Stress at break [MPa]	Strain at break [%]
Cu1-cPBA	0.13 ± 0.017	323 ± 12
Cu2-cPBA	0.19 ± 0.022	476 ± 29

XI. DSC analysis

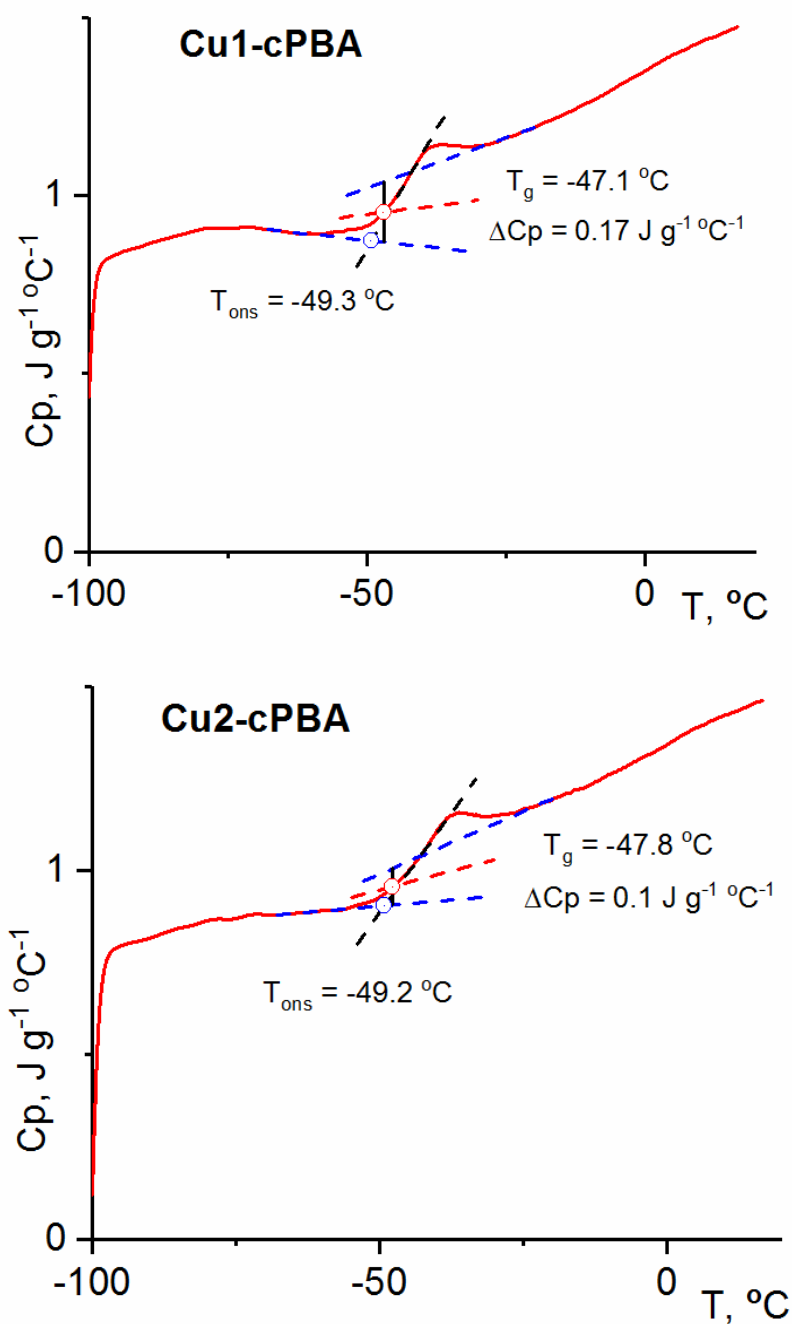


Figure S32. DSC curves of Cu1-cPBA and Cu2-cPBA.

XII. Imaging analysis

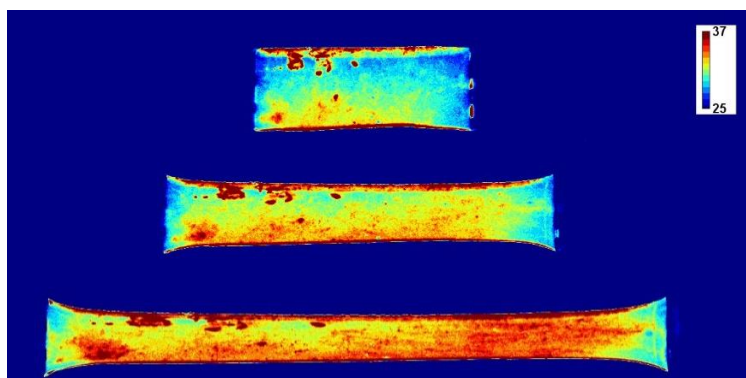


Figure S33. Imaging analysis of **Cu2-cPBA** at 0%, 100%, and 200% strain.

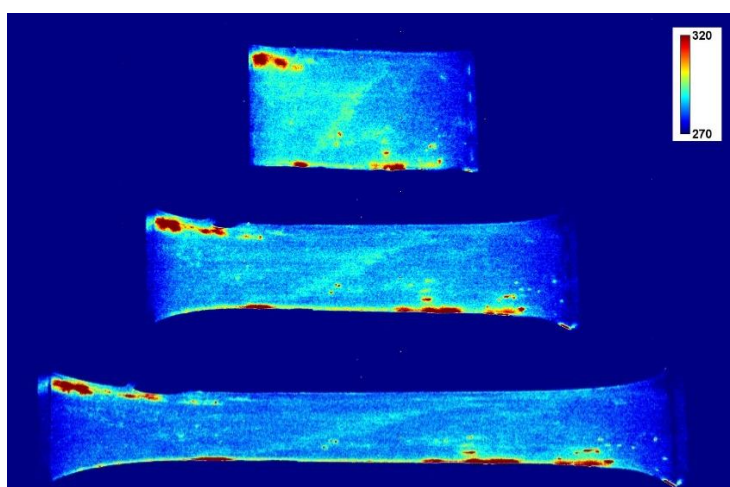


Figure S34. Imaging analysis of control experiment of a reference hexamethylene diacrylate-crosslinked **PBA** containing 1 wt% of **Cu4** at 0%, 100%, and 200% strain.

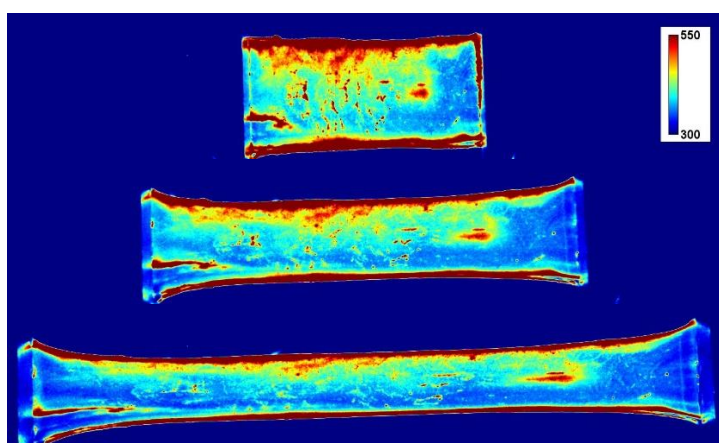


Figure S35. Imaging analysis of the control experiment of a reference hexamethylene diacrylate-crosslinked **PBA** containing 1 wt% of **Cu6** at 0%, 100%, and 200% of strain.

XIII. NMR spectra

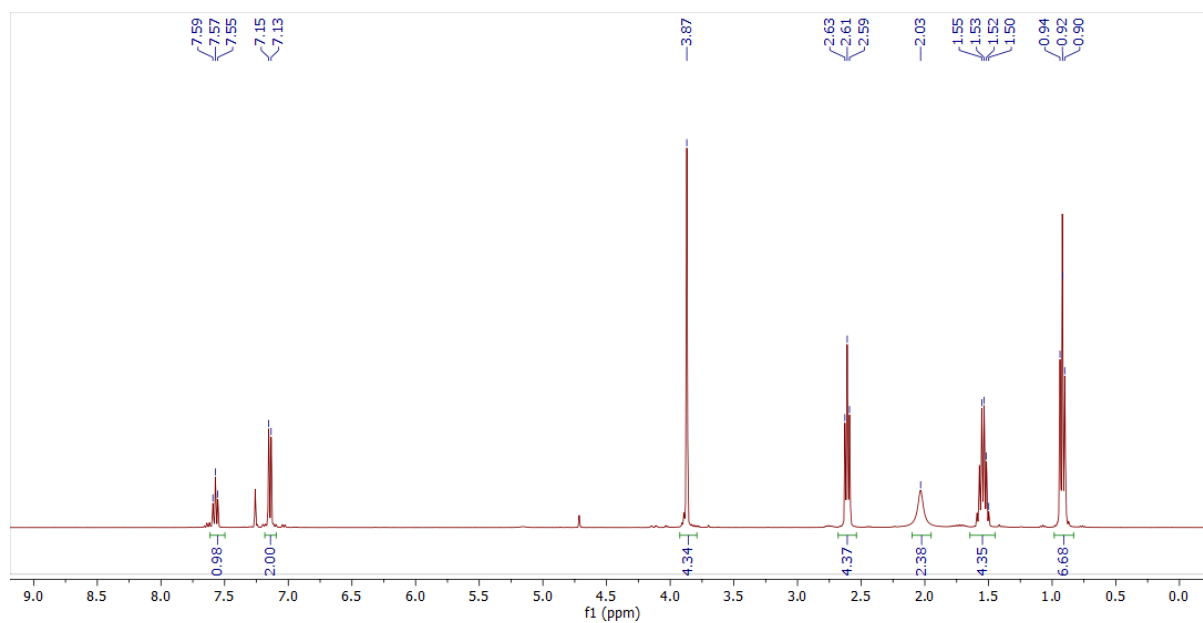


Figure S36. ¹H NMR spectrum of **2** in CDCl₃ at room temperature (400 MHz).

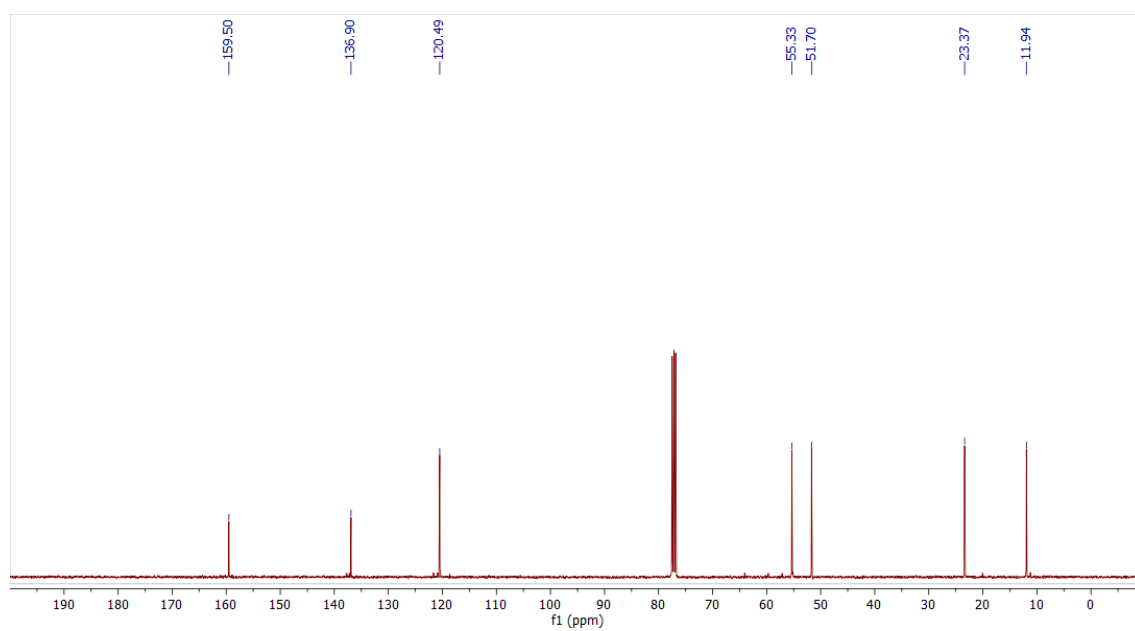


Figure S37. ¹³C NMR spectrum of **2** in CDCl₃ at room temperature (100 MHz).

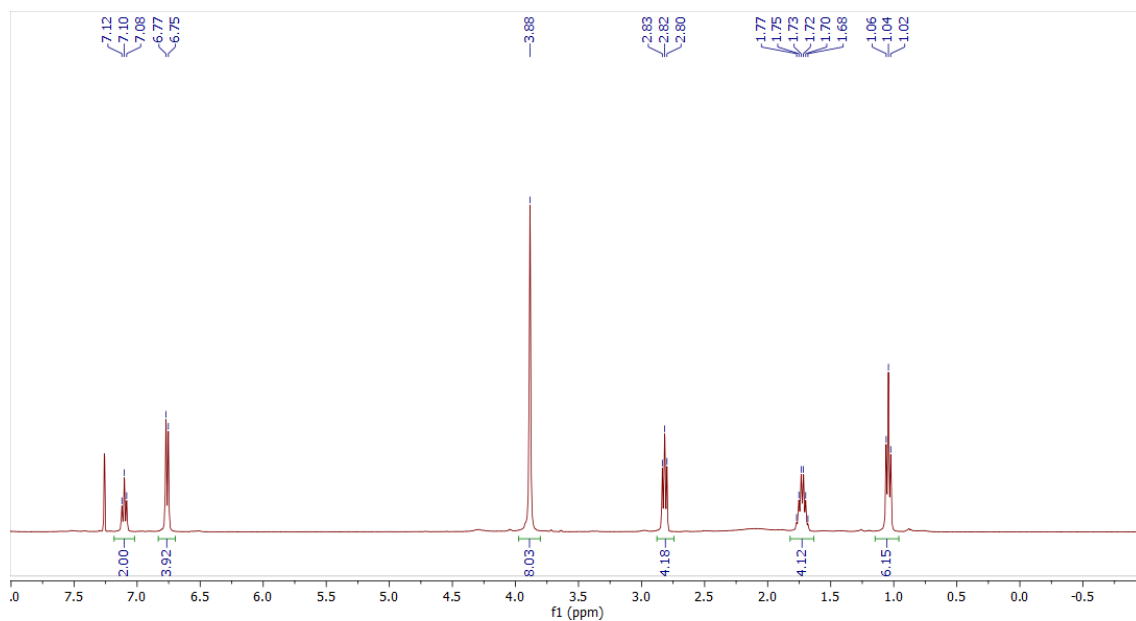


Figure S38. ^1H NMR spectrum of **3** in CDCl_3 at room temperature (400 MHz).

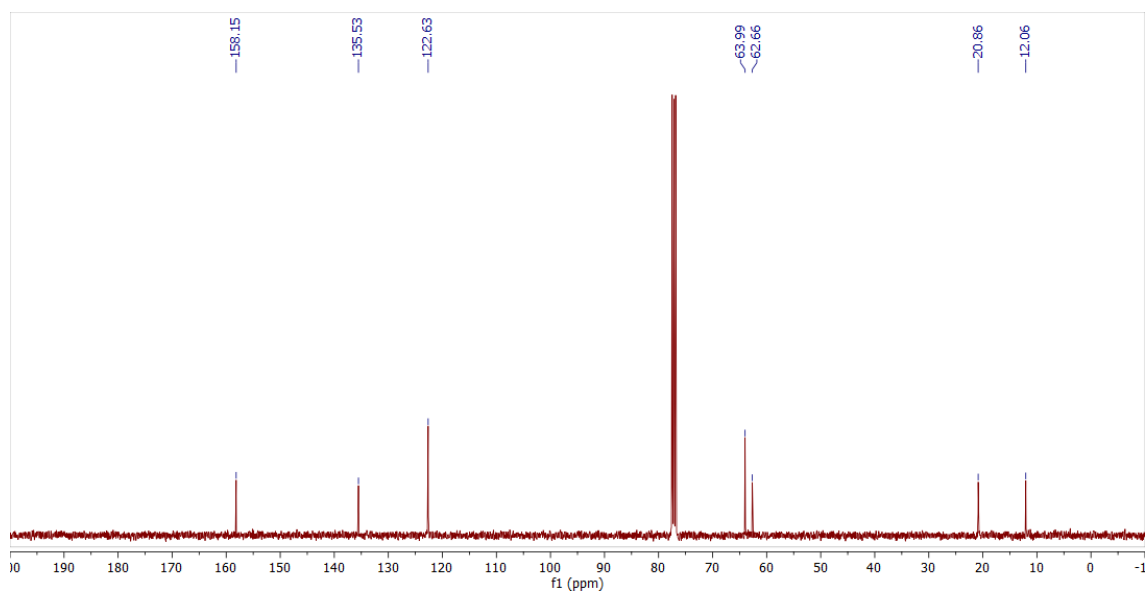


Figure S39. ^{13}C NMR spectrum of **3** in CDCl_3 at room temperature (100 MHz).

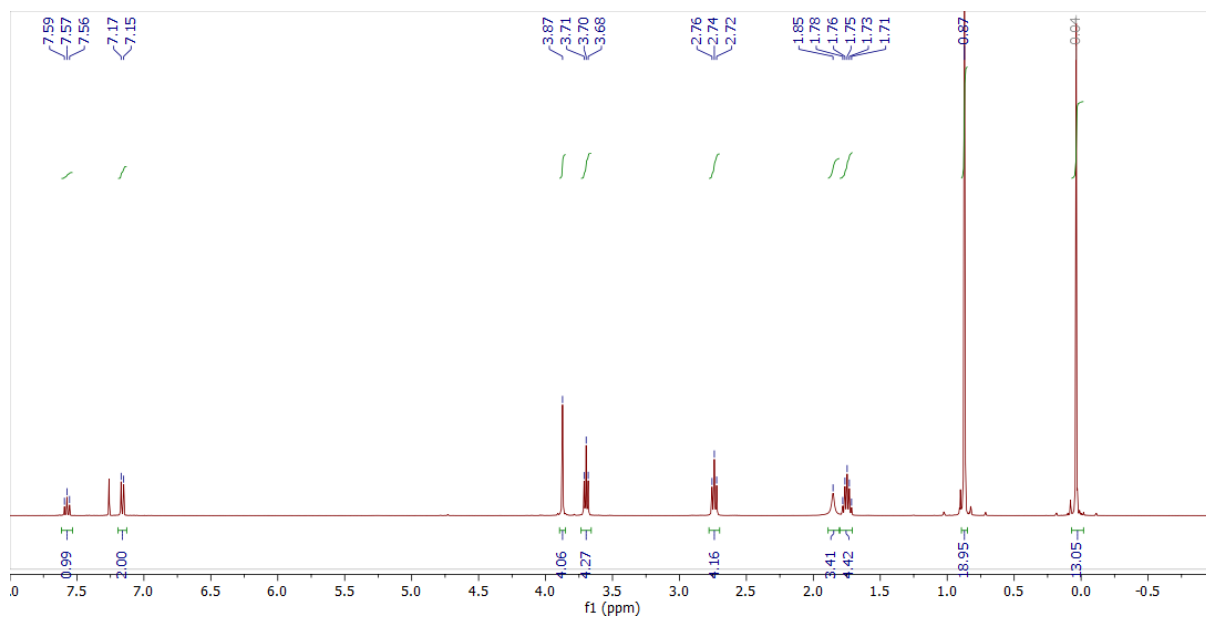


Figure S40. ^1H NMR spectrum of **4** in CDCl_3 at room temperature (400 MHz).

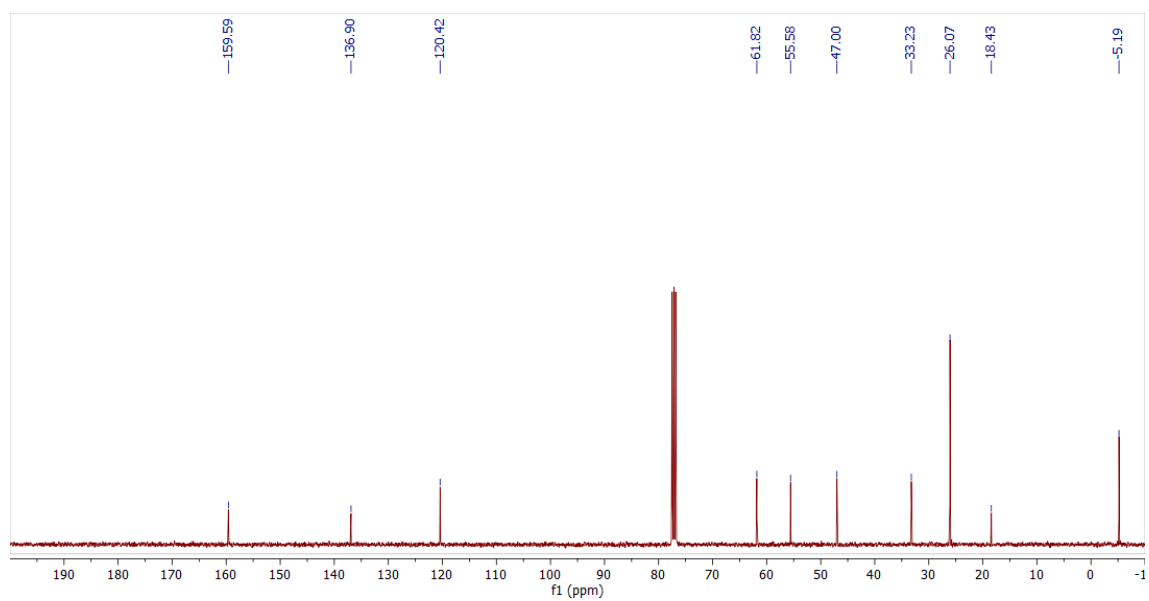


Figure S41. ^{13}C NMR spectrum of **4** in CDCl_3 at room temperature (100 MHz).

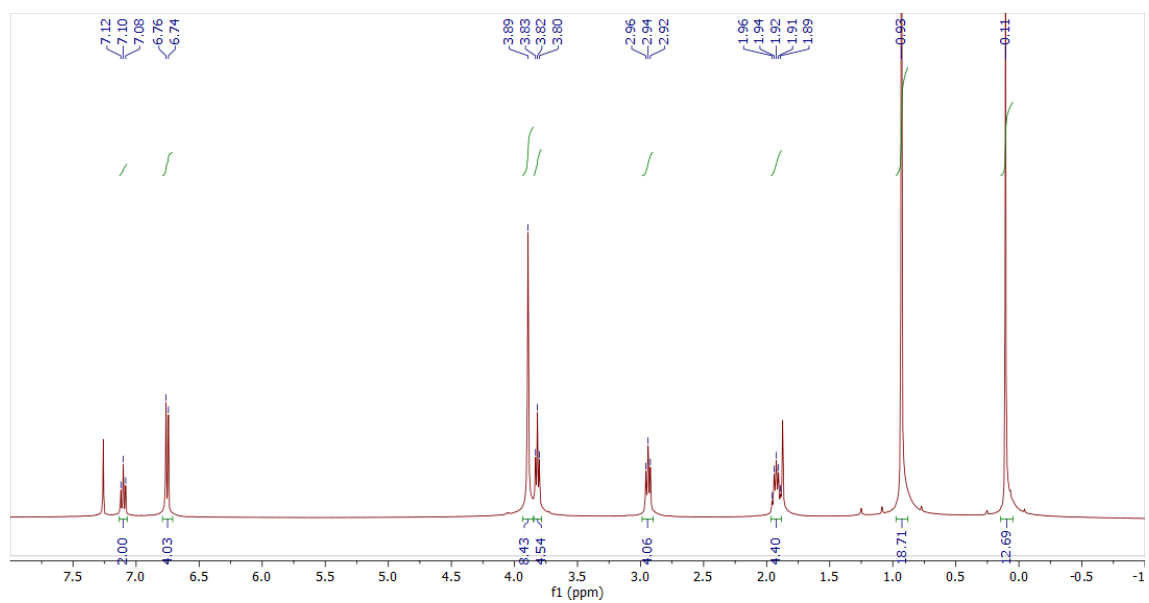


Figure S42. ^1H NMR spectrum of **5** in CDCl_3 at room temperature (400 MHz).

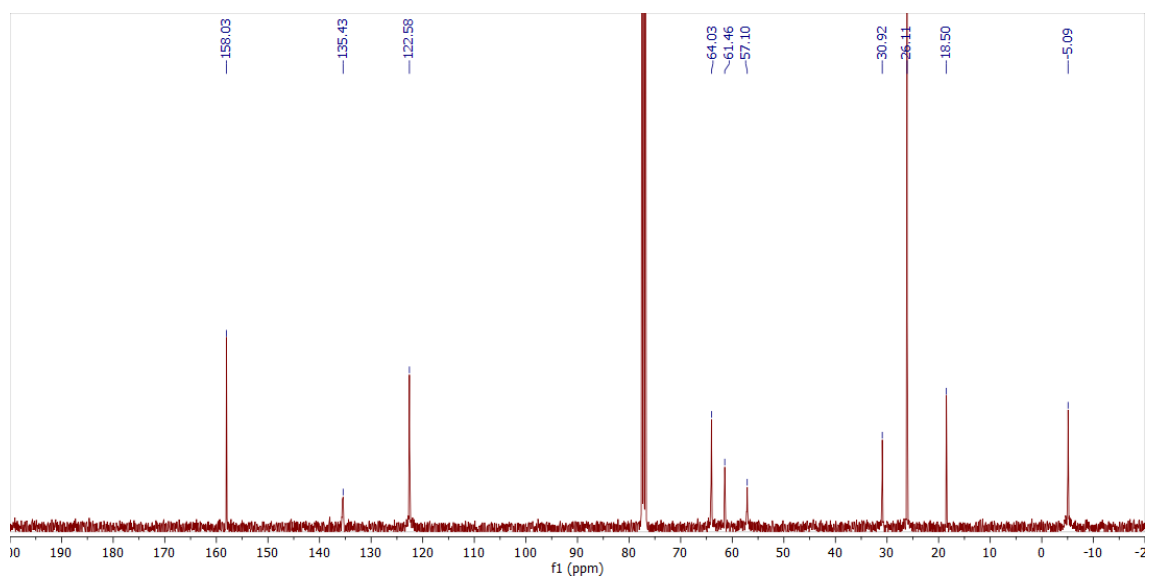


Figure S43. ^{13}C NMR spectrum of **5** in CDCl_3 at room temperature (100 MHz).

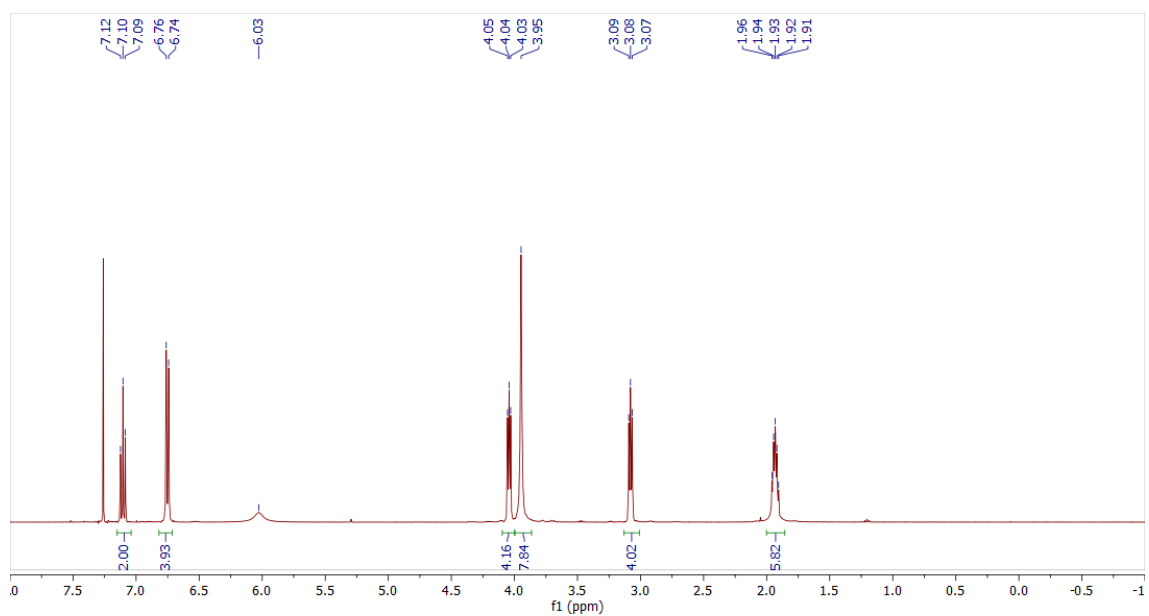


Figure S44. ^1H NMR spectrum of **6** in CDCl_3 at room temperature (400 MHz).

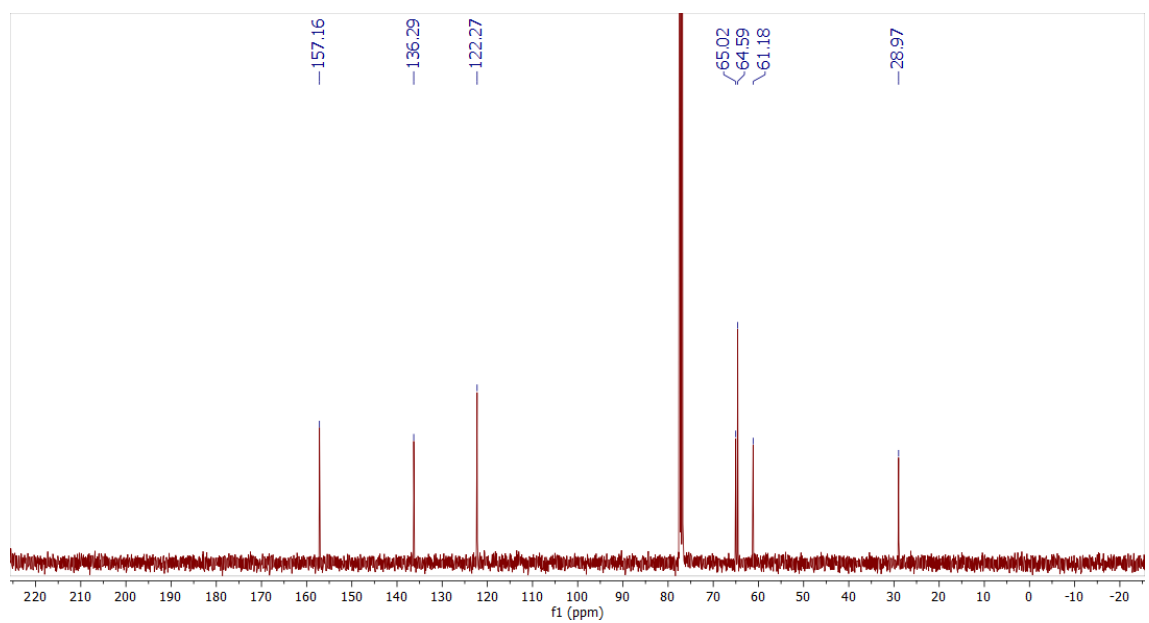


Figure S45. ^{13}C NMR spectrum of **6** in CDCl_3 at room temperature (100 MHz).

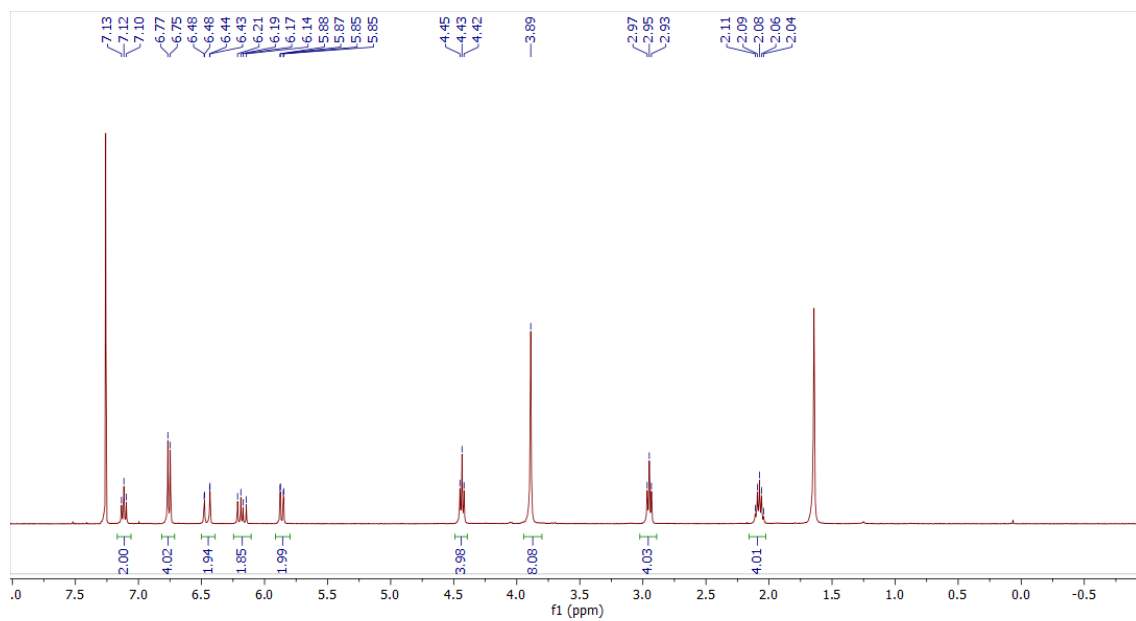


Figure S46. ^1H NMR spectrum of **L1** in CDCl_3 at room temperature (400 MHz).

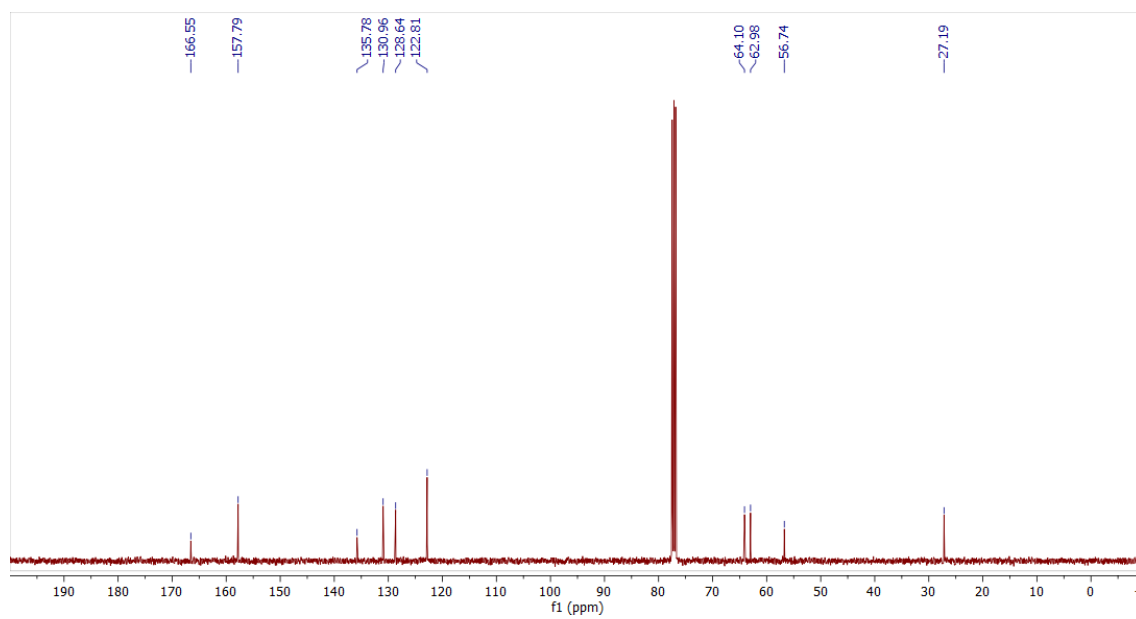


Figure S47. ^{13}C NMR spectrum of **L1** in CDCl_3 at room temperature (100 MHz).

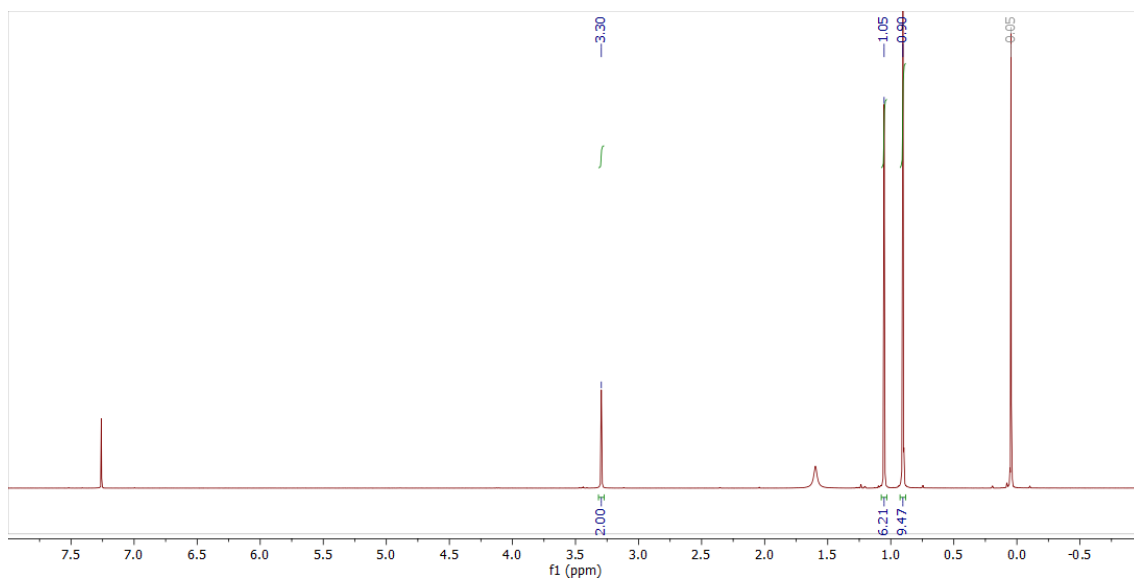


Figure S48. ^1H NMR spectrum of **7** in CDCl_3 at room temperature (400 MHz).

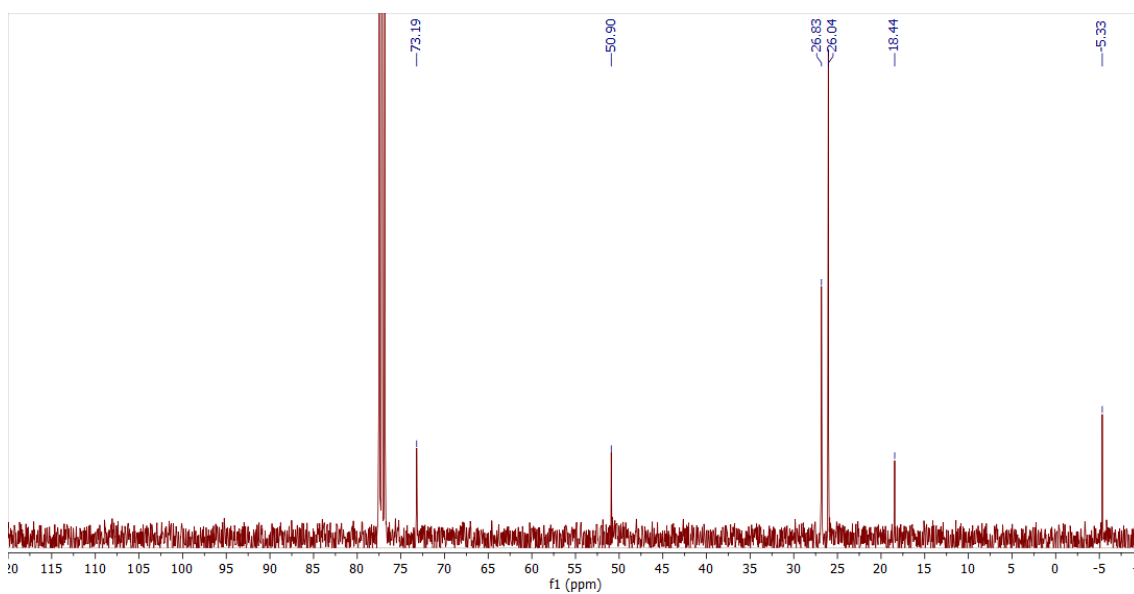


Figure 49. ^{13}C NMR spectrum of **7** in CDCl_3 at room temperature (100 MHz).

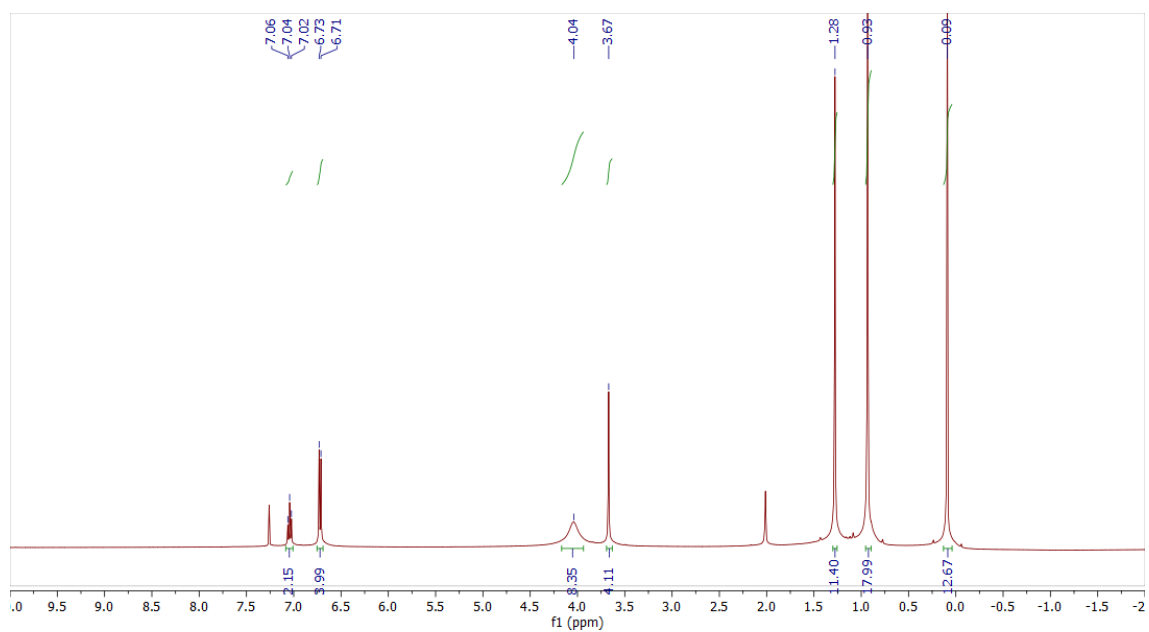


Figure S50. ^1H NMR spectrum of **8** in CDCl_3 at room temperature (400 MHz).

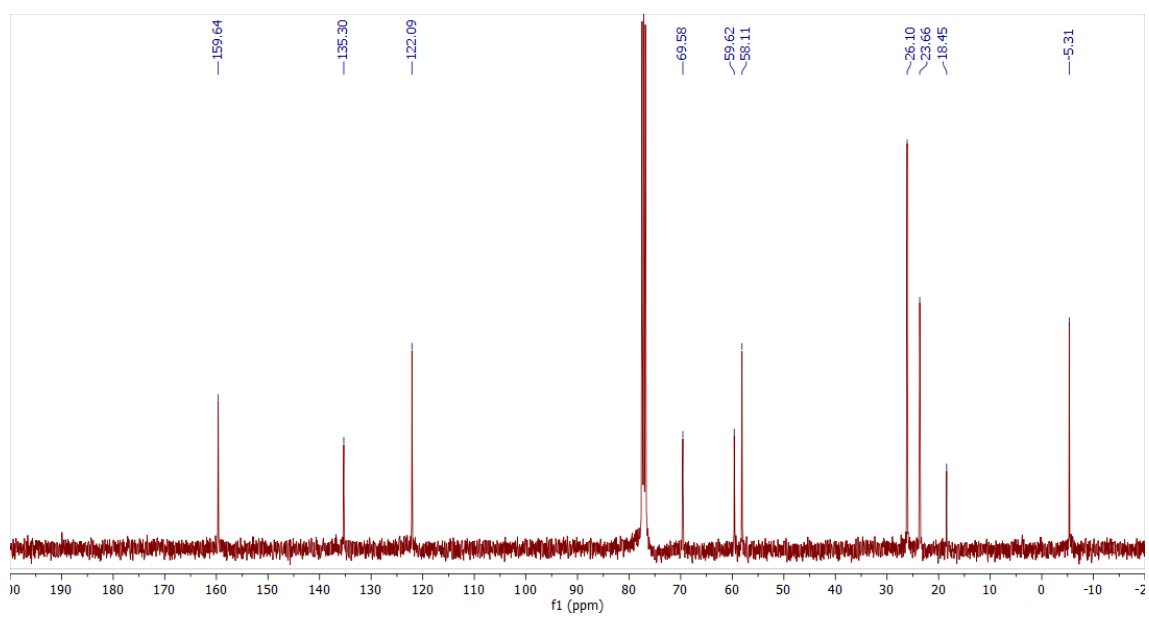


Figure S51. ^{13}C NMR spectrum of **8** in CDCl_3 at room temperature (100 MHz).

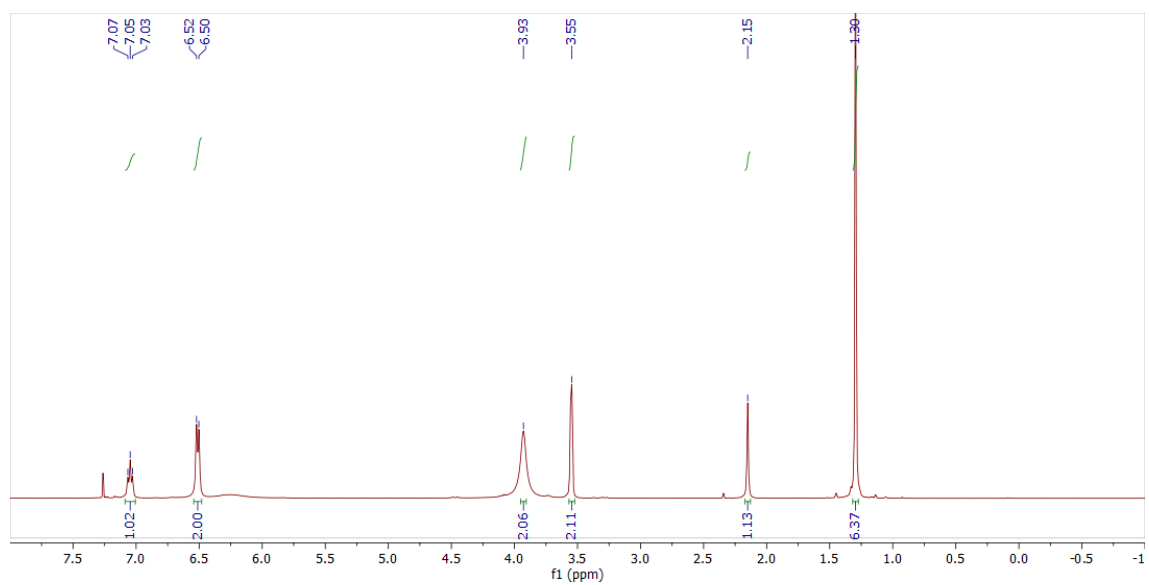


Figure S52. ^1H NMR spectrum of **9** in CDCl_3 at room temperature (400 MHz).

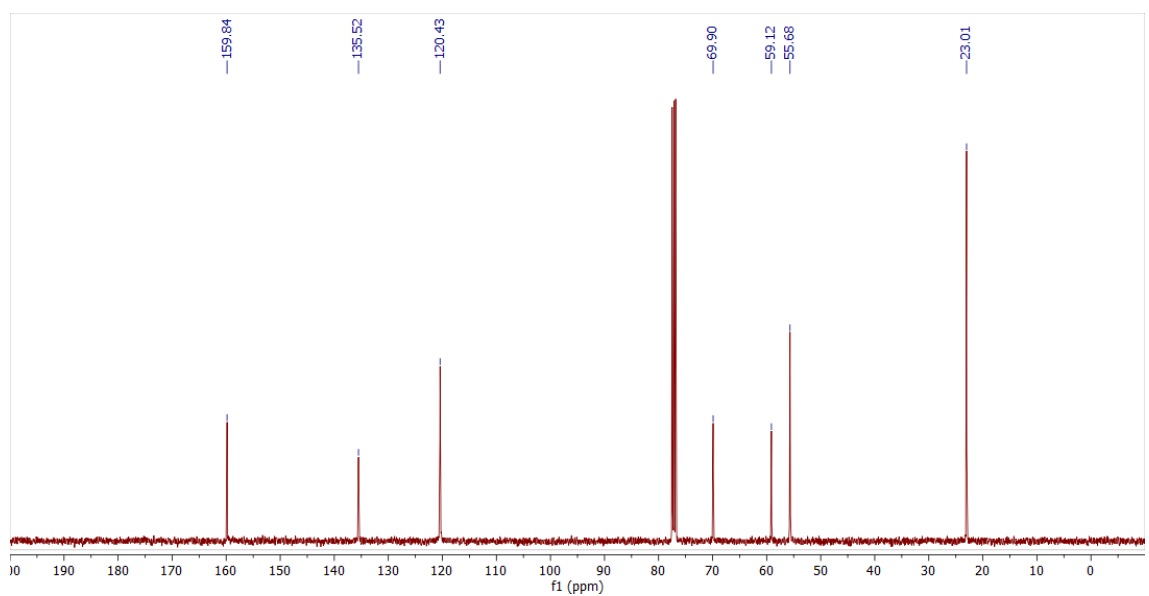


Figure S53. ^{13}C NMR spectrum of **9** in CDCl_3 at room temperature (100 MHz).

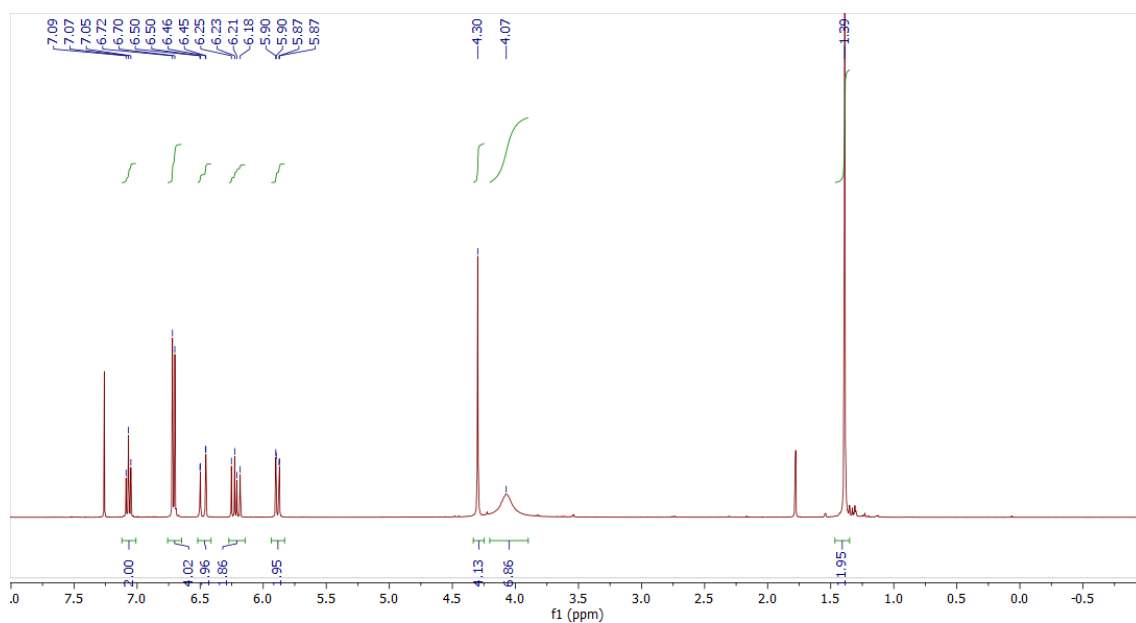


Figure S54. ^1H NMR spectrum of **L2** in CDCl_3 at room temperature (400 MHz).

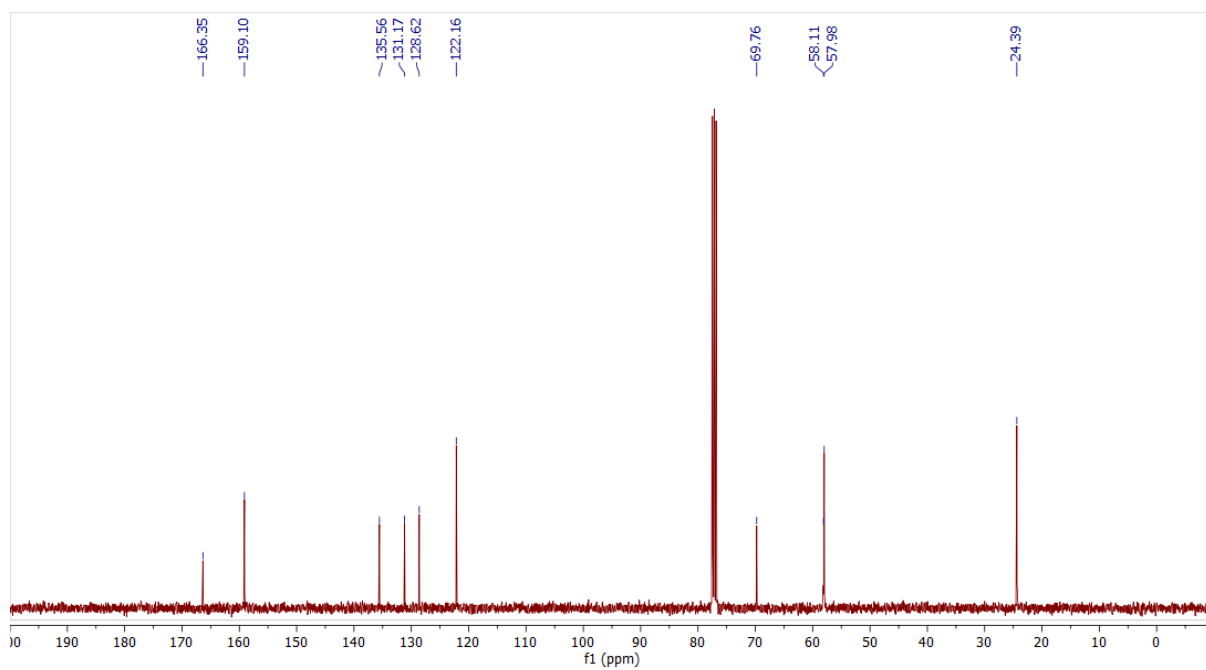


Figure S55. ^{13}C NMR spectrum of **L2** in CDCl_3 at room temperature (100 MHz).

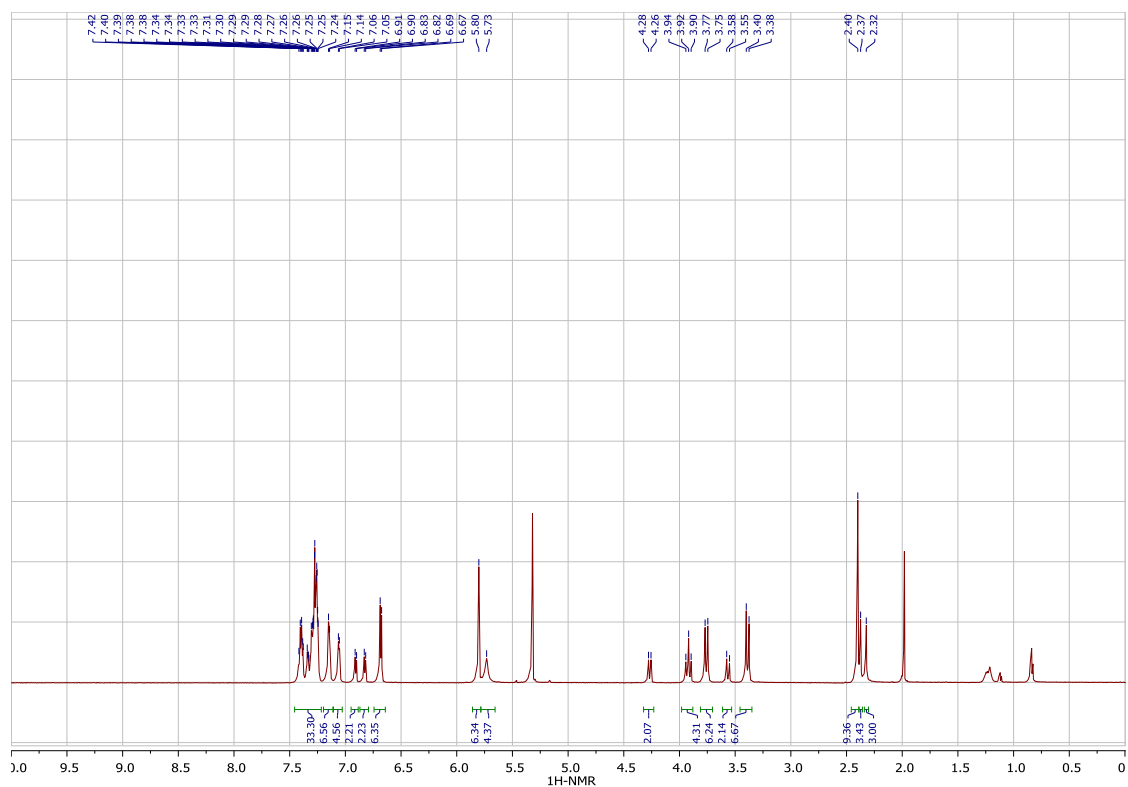


Figure S56. ^1H NMR spectrum of **Cu3** in CD_2Cl_2 at $-30\text{ }^\circ\text{C}$ (600 MHz).

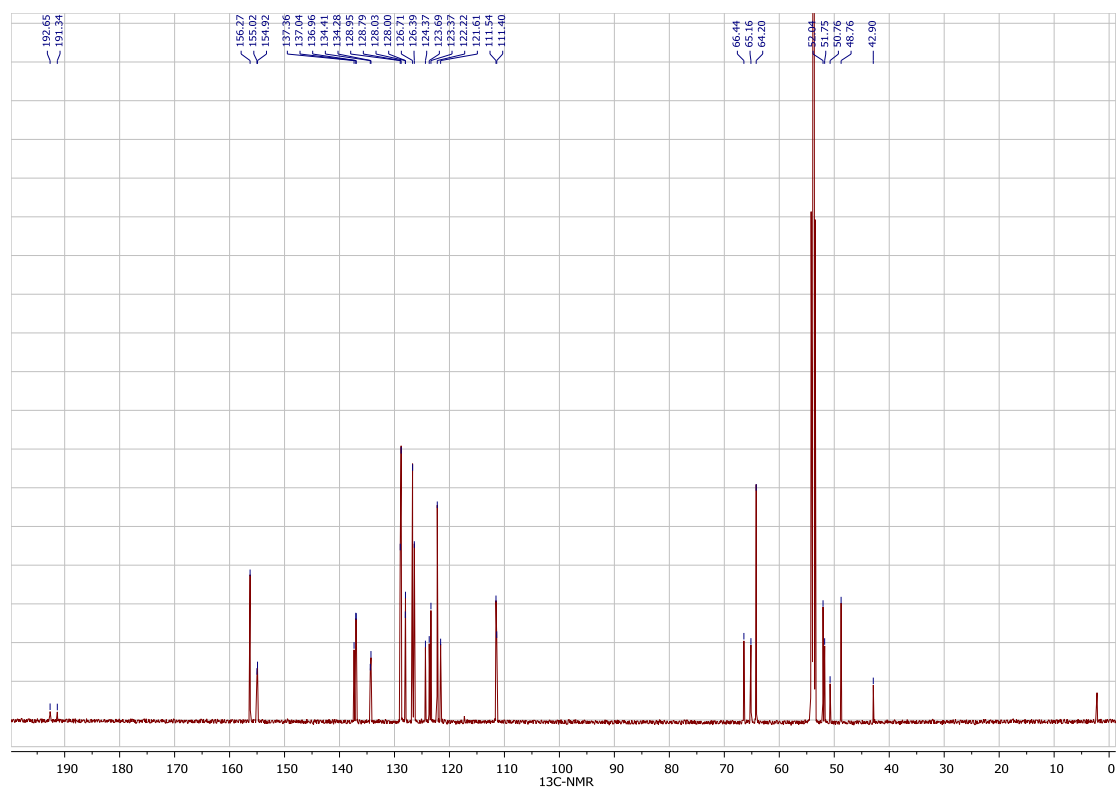


Figure S57. ^{13}C NMR spectrum of **Cu3** in CD_2Cl_2 at $-30\text{ }^\circ\text{C}$ (150 MHz).

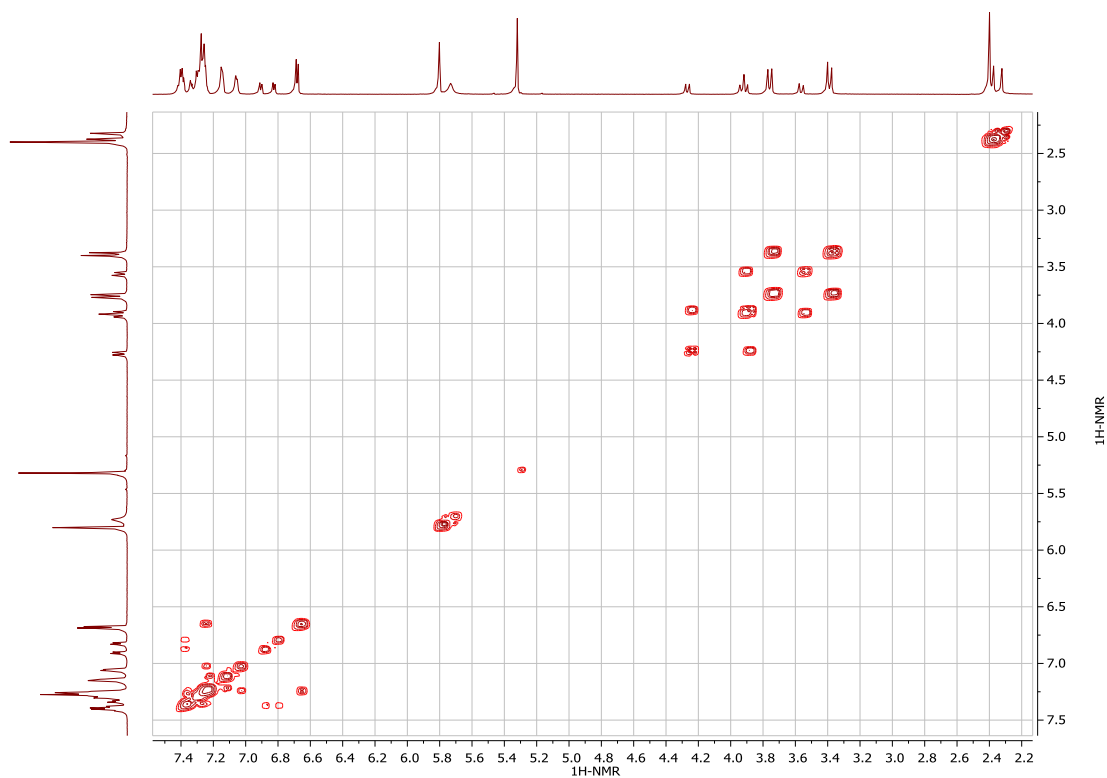


Figure S58. ^1H - ^1H COSY spectrum of **Cu3** in CD_2Cl_2 at $-30\text{ }^\circ\text{C}$.

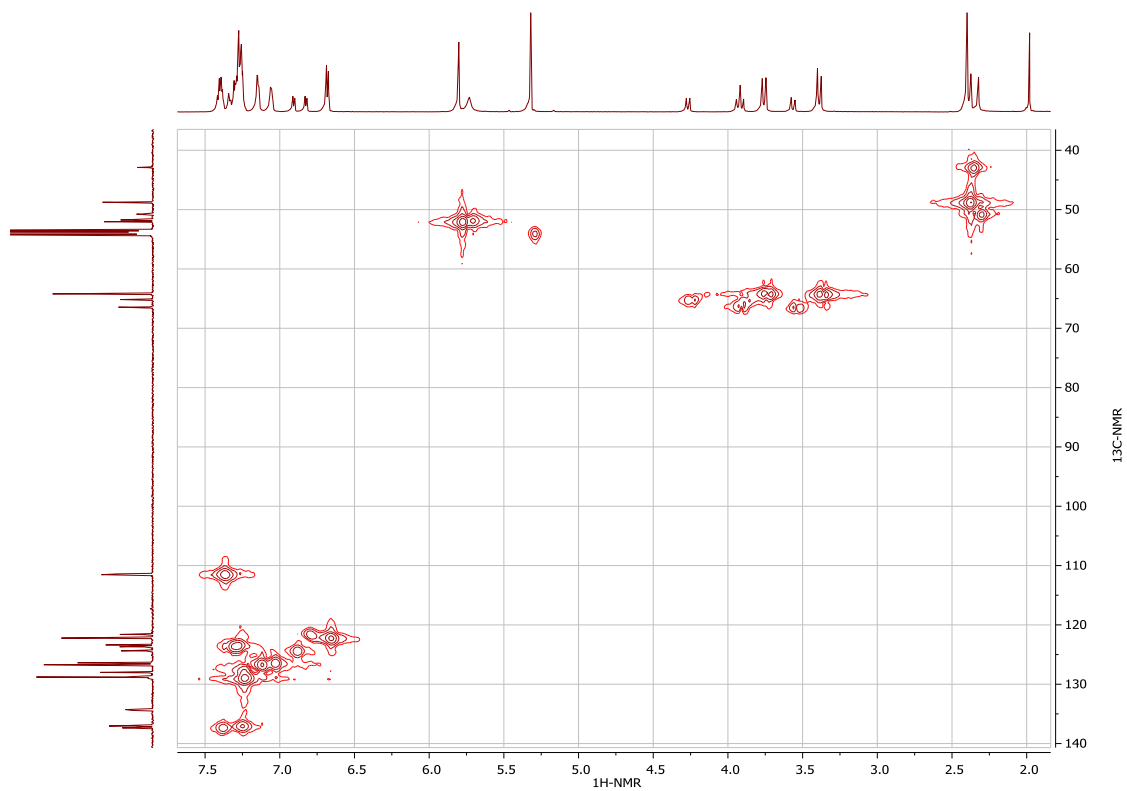


Figure S59. ^1H - ^{13}C HMQC spectrum of **Cu3** in CD_2Cl_2 at $-30\text{ }^\circ\text{C}$.

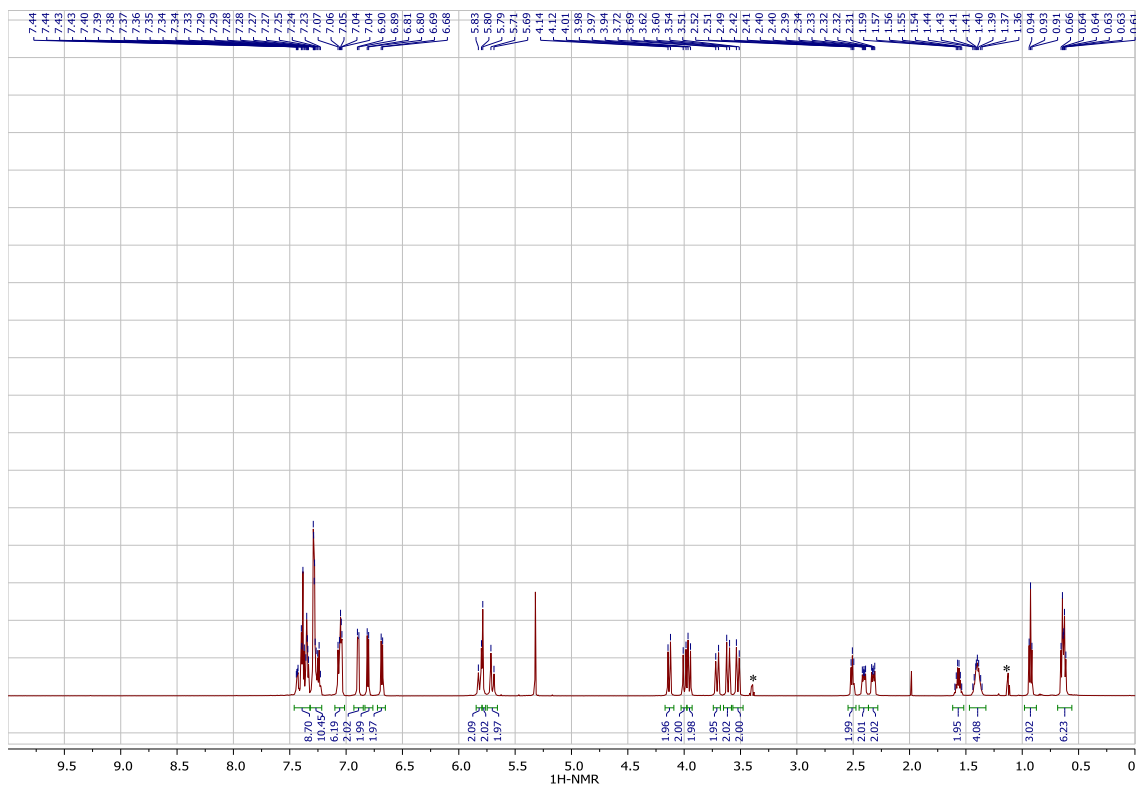


Figure S60. ^1H NMR spectrum of **Cu4** in CD_2Cl_2 at $-30\text{ }^\circ\text{C}$. Diethyl ether peaks are denoted with an asterisk. (600 MHz).

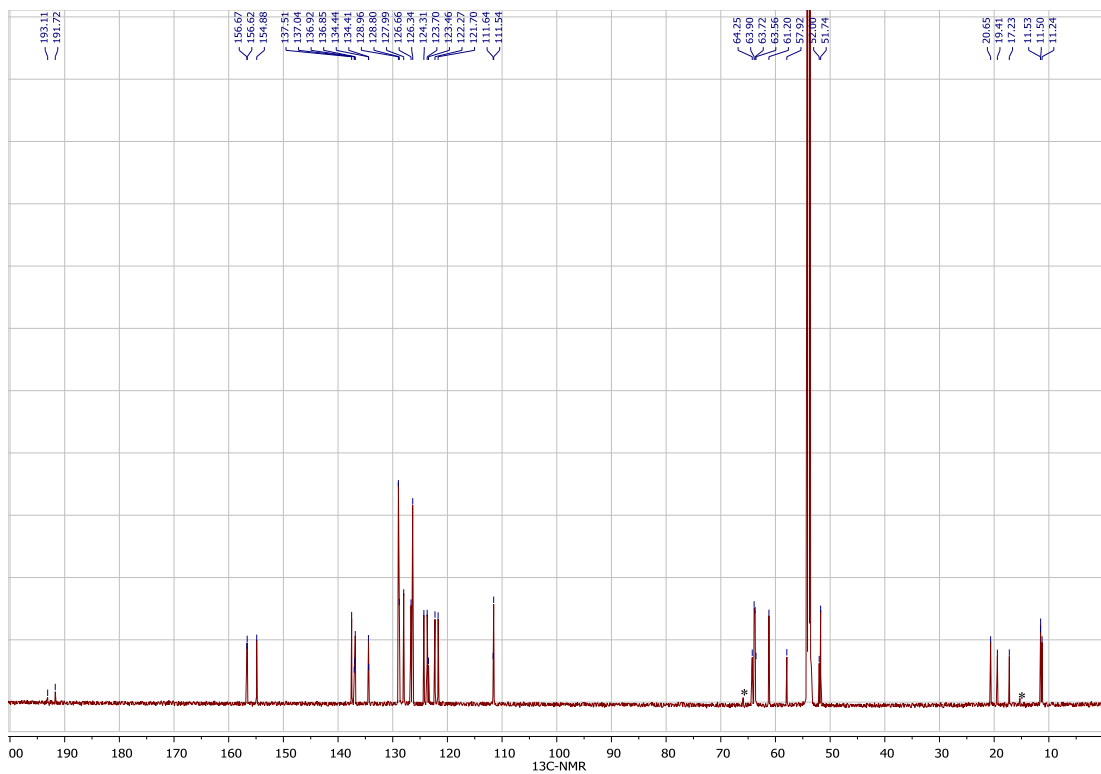


Figure S61. ^{13}C NMR spectrum of **Cu4** in CD_2Cl_2 at $-30\text{ }^\circ\text{C}$. Diethyl ether peaks are denoted with asterick. (150 MHz).

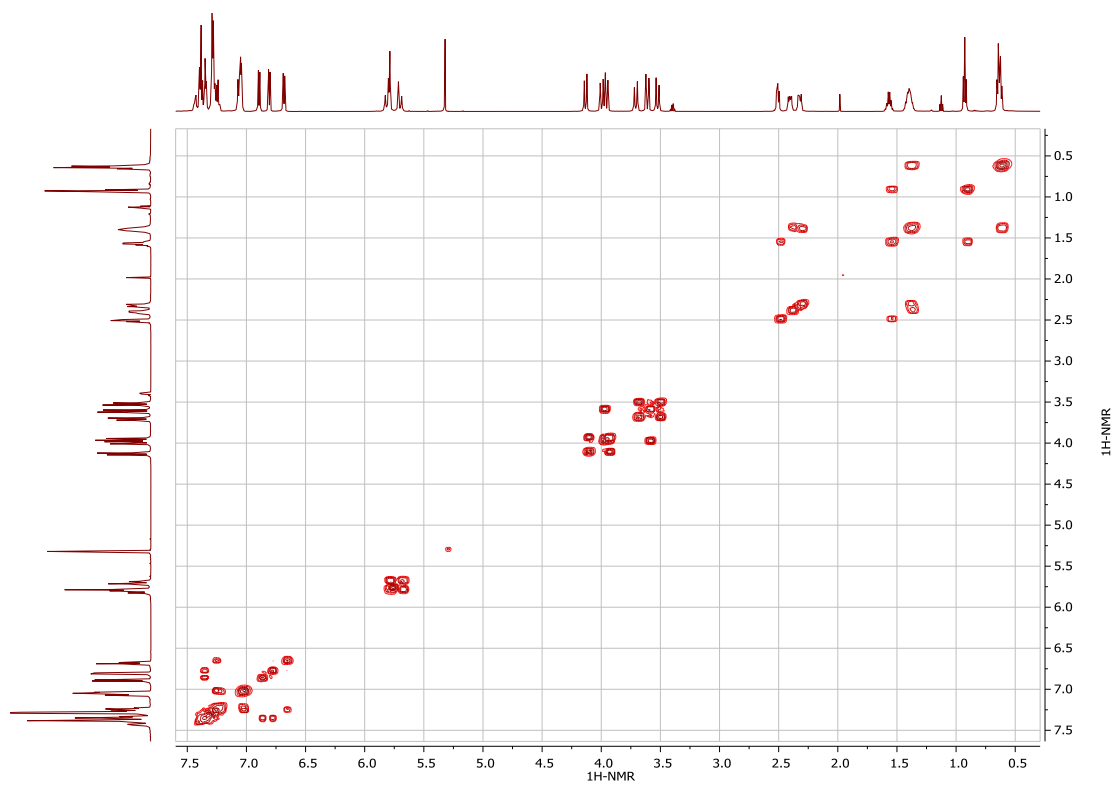


Figure S62. ^1H - ^1H COSY spectrum of **Cu4** in CD_2Cl_2 at $-30\text{ }^\circ\text{C}$.



Figure S63. ^1H - ^{13}C HMQC spectrum of **Cu4** in CD_2Cl_2 at $-30\text{ }^\circ\text{C}$.

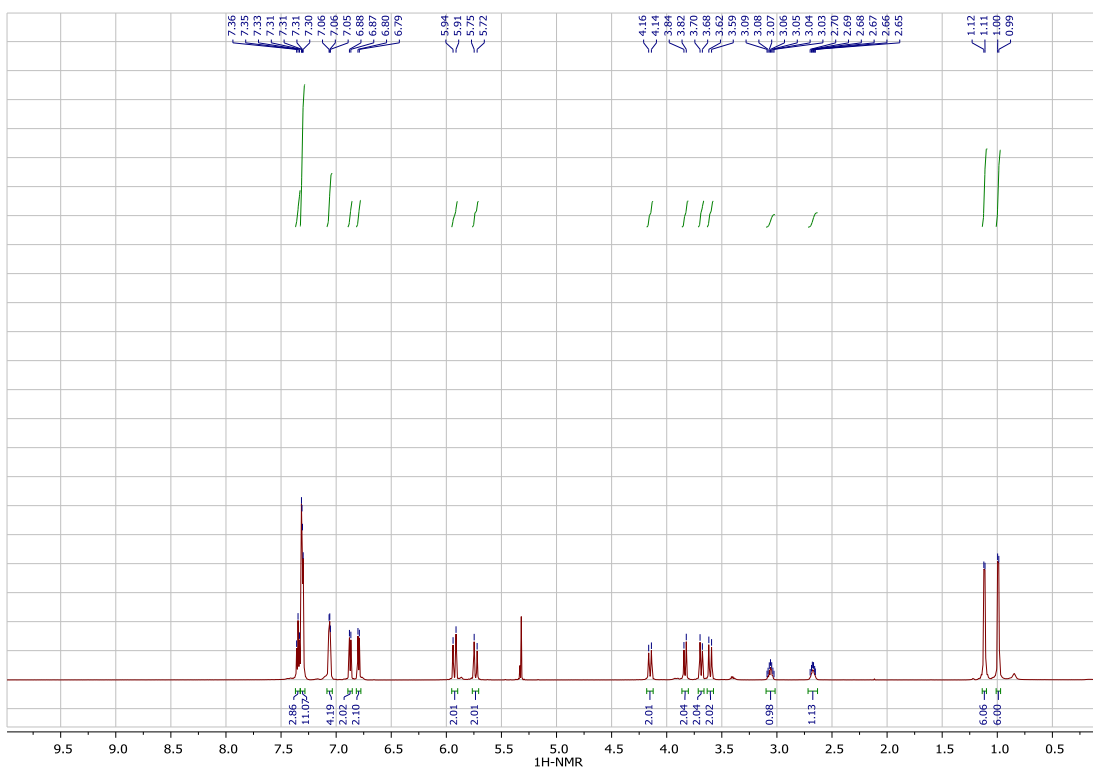


Figure S64. ^1H NMR spectrum of **Cu5** in CD_2Cl_2 at $-30\text{ }^\circ\text{C}$. (600 MHz).

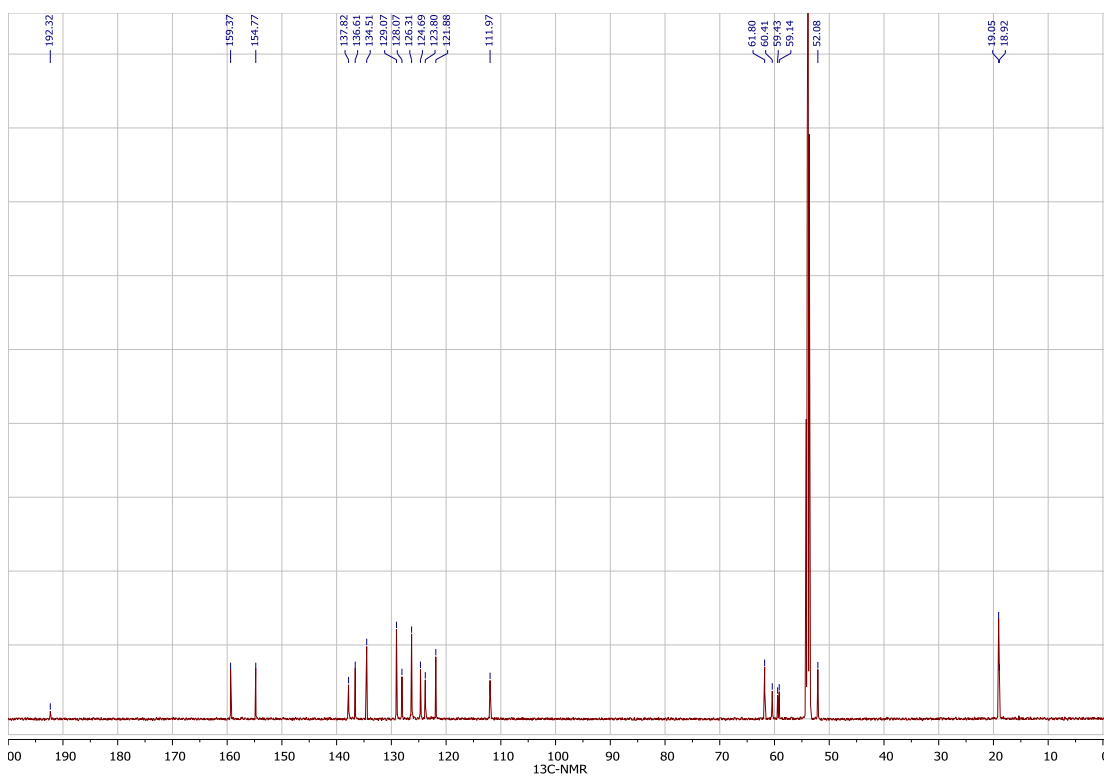


Figure S65. ^{13}C NMR spectrum of **Cu5** in CD_2Cl_2 at $-30\text{ }^\circ\text{C}$. (150 MHz).

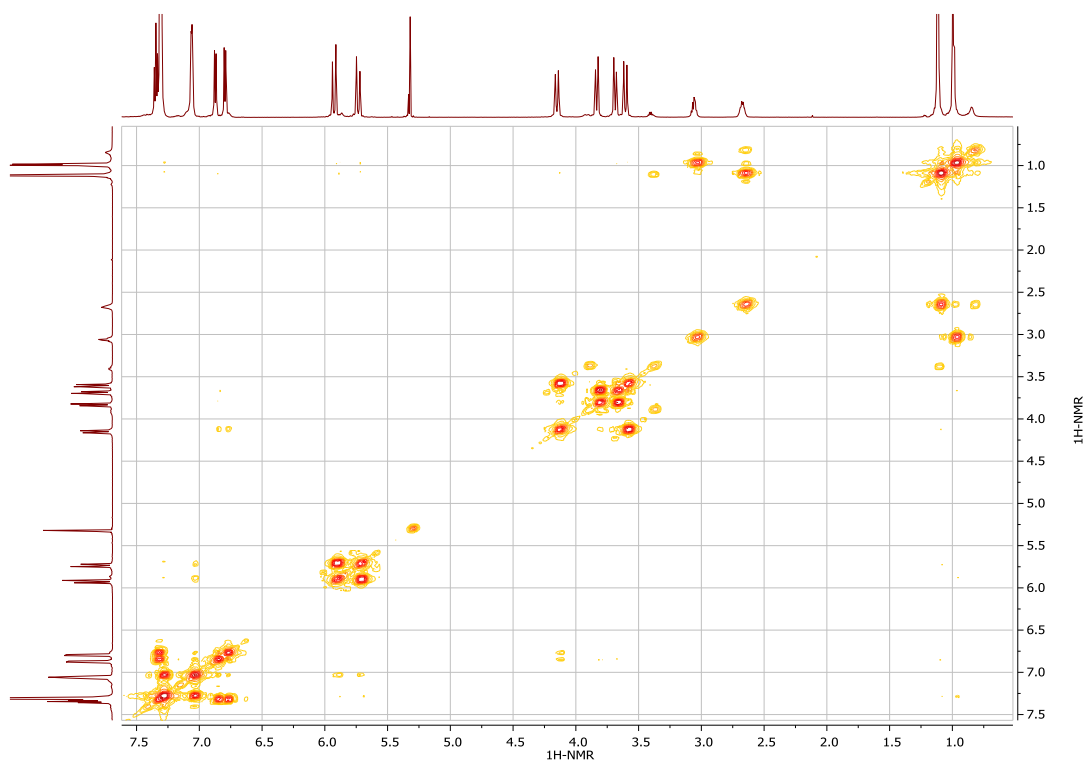


Figure S66. ^1H - ^1H COSY spectrum of **Cu5** in CD_2Cl_2 at $-30\text{ }^\circ\text{C}$.

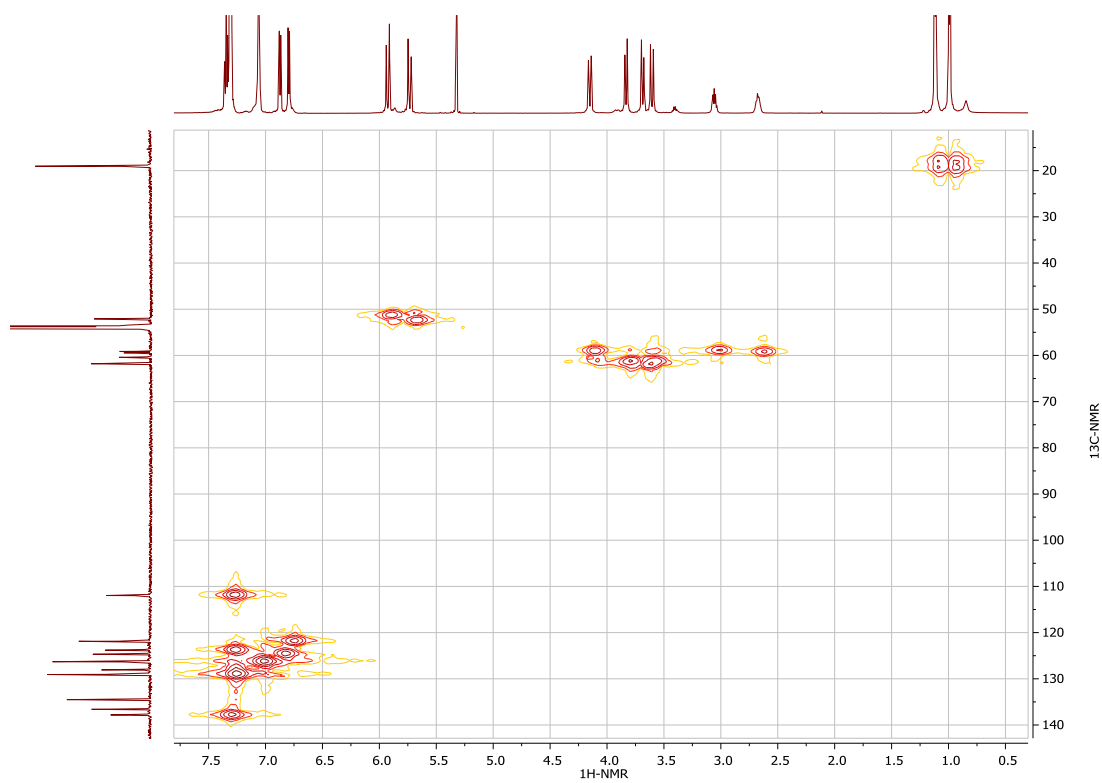


Figure S67. ^1H - ^{13}C HMQC spectrum of **Cu5** in CD_2Cl_2 at $-30\text{ }^\circ\text{C}$.

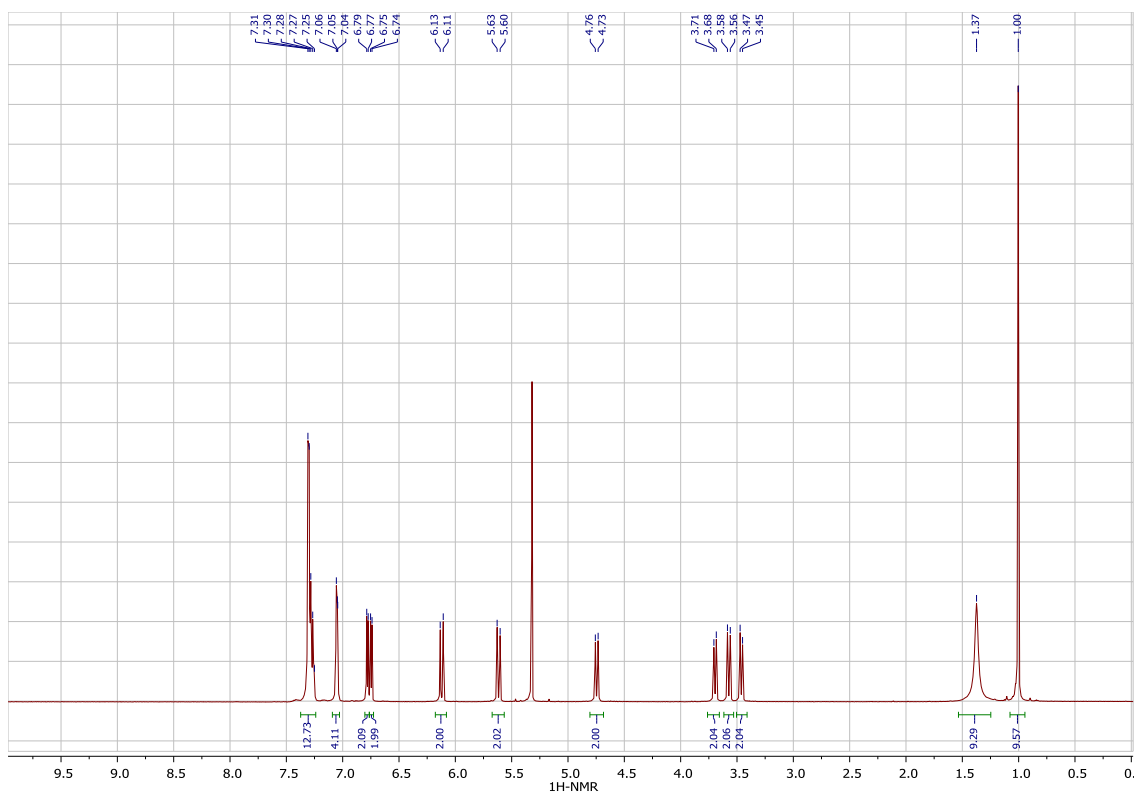


Figure S68. ^1H NMR spectrum of **Cu6** in CD_2Cl_2 at 20 °C. (600 MHz).

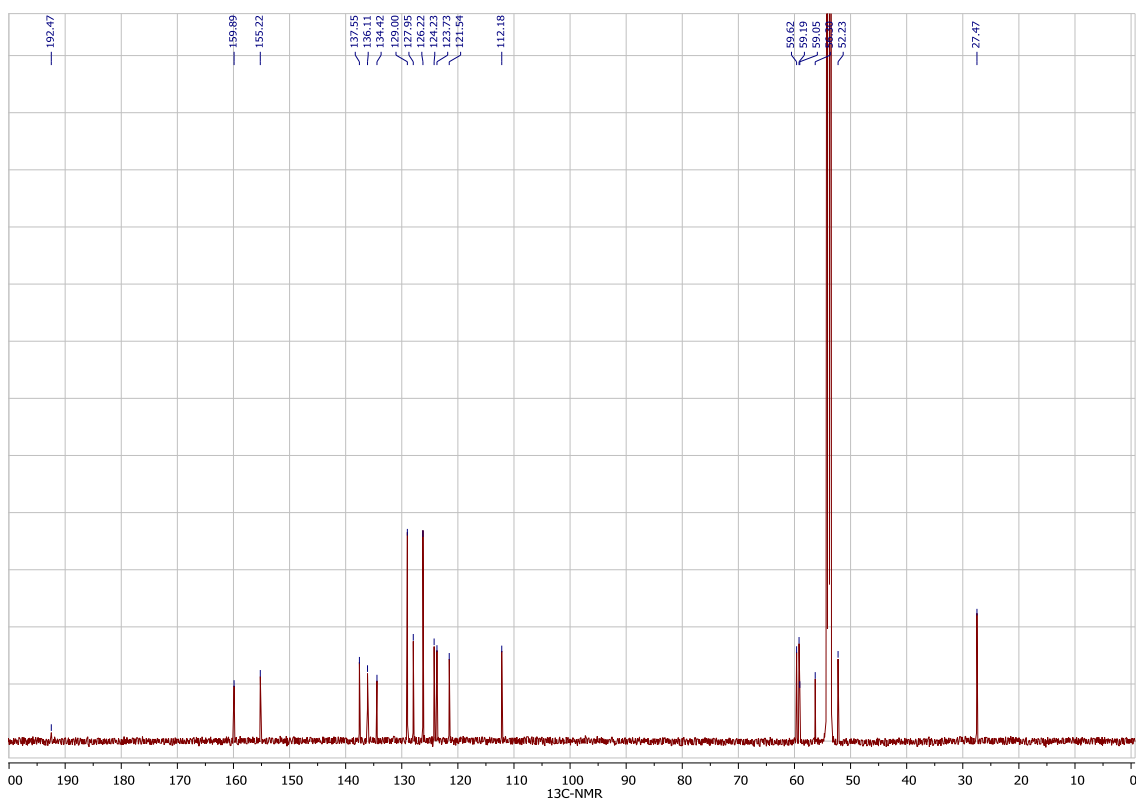


Figure S69. ^{13}C NMR spectrum of **Cu6** in CD_2Cl_2 at 20 °C. (150 MHz).

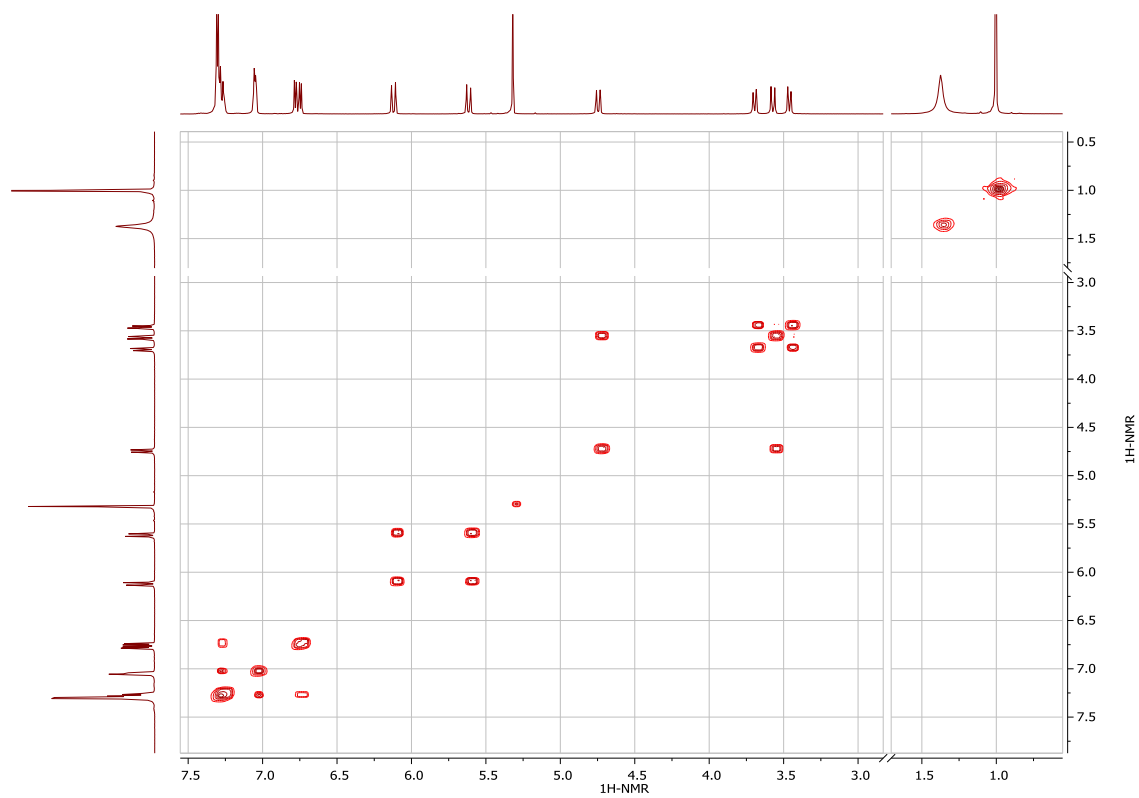


Figure S70. ^1H - ^1H COSY spectrum of **Cu6** in CD_2Cl_2 at 20 °C.

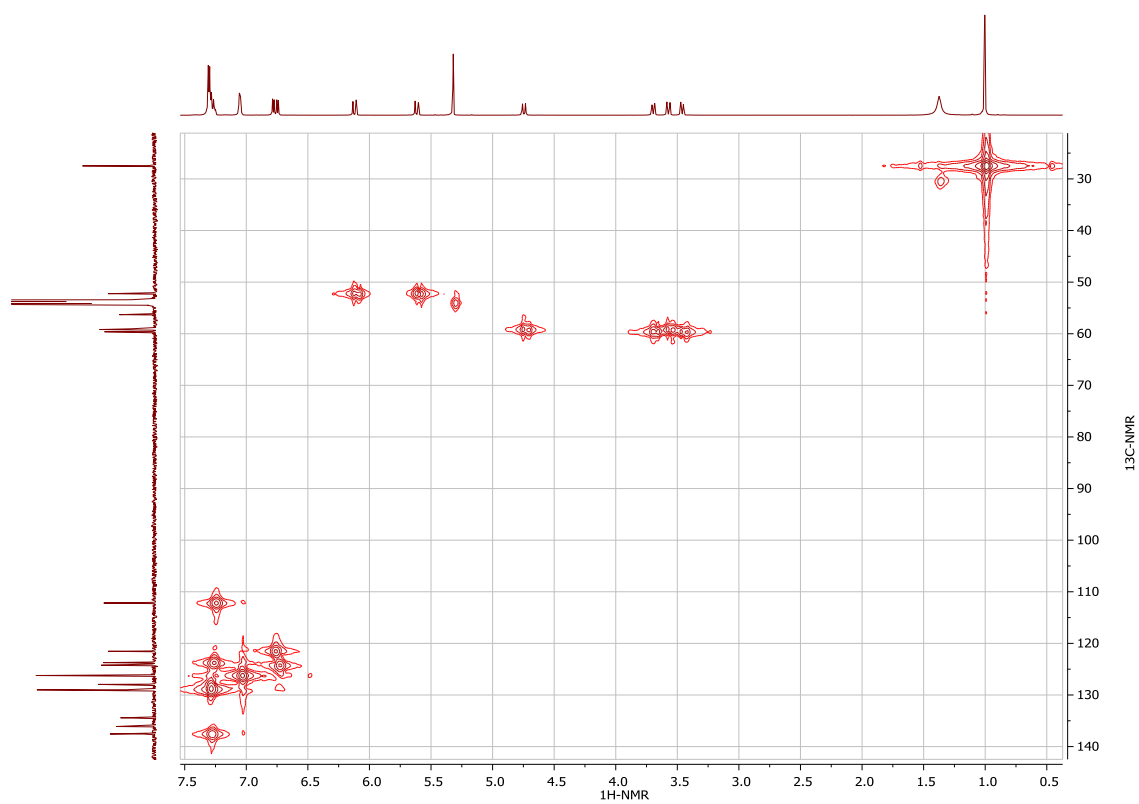


Figure S71. ^1H - ^{13}C HMQC spectrum of **Cu6** in CD_2Cl_2 at 20 °C.

XIV. X-ray structure determination details

The X-ray diffraction data for the single crystals were collected on a Rigaku XtaLab PRO instrument (κ -goniometer) with a PILATUS3 R 200K hybrid pixel array detector using MoK α (0.71073 Å) radiation monochromated by means of multilayer optics. The performance mode of a MicroMaxTM-003 microfocus sealed X-ray tube was 50 kV, 0.60 mA. The diffractometer was equipped with a Rigaku GN2 system for low temperature experiments. Suitable crystals of appropriate dimensions were mounted on loops in random orientations. Preliminary unit cell parameters were determined with three sets of a total of 10 narrow frame scans. The data were collected according to recommended strategies in an ω -scan mode. Final cell constants were determined by global refinement of reflections from the complete data sets using the Lattice wizard module. Images were indexed and integrated with “smart” background evaluation using the *CrysAlis^{Pro}* data reduction package (1.171.39.46, Rigaku Oxford Diffraction, 2018). Analysis of the integrated data did not show any decay. Data were corrected for systematic errors and absorption using the ABSPACK module: Numerical absorption correction based on Gaussian integration over a multifaceted crystal model and empirical absorption correction based on spherical harmonics according to the point group symmetry using equivalent reflections. The GRAL module and the ASSIGN SPACEGROUP routine of the *WinGX* suite were used for analysis of systematic absences and space group determination. The structures were solved by the direct methods using *SHELXT*-2018/2¹¹ and refined by the full-matrix least-squares on F^2 using *SHELXL*-2018/3,¹² which uses a model of atomic scattering based on spherical atoms. Calculations were mainly performed using the *WinGX*-2018.3 suite of programs.¹³ Non-hydrogen atoms were refined anisotropically. The positions of the hydrogen atoms of methyl groups were found using a rotating group refinement with idealized tetrahedral angles. The hydrogen atoms were inserted at the calculated positions and refined as riding atoms. The disorder, if present, was resolved using free variables and reasonable restraints on geometry and anisotropic displacement parameters. The structure of complex **Cu6** was refined as a 2-component twin with the fractional volume contribution of 0.4476(81) for the minor component; the twin law was (1.00 0.00 0.00, 0.00 -1.00 0.00, 0.00 0.00 -1.00). All the compounds studied have no unusual bond lengths and angles. Absolute structure of complexes **Cu5** and **Cu6** was determined on the basis of the Flack parameter.¹⁴

The τ_4' parameters¹⁵ for tetracoordinate Cu centers in the studied complexes are 0.57 (**Cu3**), 0.63 (**Cu4**), 0.62 (**Cu5**), and 0.63 (**Cu6**) indicative of a noticeable distortion from the ideal tetrahedral geometry where τ_4' value equal to 1 is expected. In all the complexes, the pyridinophane ligands adopt a *syn*-boat-chair conformation. An important feature of the studied crystalline complexes is the tight placement of the aromatic units within the pyridinophane ligands that may enable the intramolecular π - π interaction between these pyridine rings: centroid-centroid distance of 3.3094(6) Å (**Cu3**), 3.5510(6) Å (**Cu4**), 3.6498(18) Å (**Cu5**), and 3.3392(12) Å (**Cu6**); angle of 25.34(4)° (**Cu3**), 36.31(4)° (**Cu4**), 41.81(10)° (**Cu5**), and 27.55(7)° (**Cu6**); shift distance of 0.8091(15) Å (**Cu3**), 1.0034(18) Å (**Cu4**), 1.328(5) Å (**Cu5**), and 0.765(3) Å (**Cu6**). Additionally, compound **Cu3** demonstrates the intermolecular π - π interactions between pyridine Py(2) rings {symmetry operation: $2-x, 1-y, -z$; centroid-centroid distance of 3.6567(9) Å, angle of 0.000(8)°, and shift distance of 1.5262(17) Å} and between aromatic moieties C(1-7)N(5-6) {symmetry operation: $1-x, 1-y, -z$; centroid-centroid distance of 3.9430(7) Å, angle of 0.000(7)°, and shift distance of 2.0872(12) Å}. The intermolecular π - π interaction between phenyl C(52-57) and pyridine Py(2) rings was found in the crystal structure of **Cu4**: symmetry operation: $x+1, y, z$; centroid-centroid distance of 3.8736(6) Å, angle of 18.15(4)°, and shift distance of 1.1666(17) Å. The intermolecular π - π interaction between aromatic C(2-7) and pyridine Py(1) rings can be found in the crystal structure of **Cu5**: symmetry operation: $x, 1-y, z-0.5$; centroid-centroid distance of 3.7156(18) Å, angle of 13.45(11)°, and shift distance of 1.189(5) Å. Notably, no intermolecular π - π interactions were found in the case of complex **Cu6**. Structures of the cationic part of the investigated complexes in the crystalline phase and accepted partial numbering are presented as ORTEP diagrams in Figures S73-S76.

Deposition numbers 1903712, 1903713, 1937851, and 1937852 contain the supplementary crystallographic data of complexes **Cu4**, **Cu6**, **Cu3**, and **Cu5**, respectively, for this paper. These data are provided free of charge by the joint Cambridge Crystallographic Data Centre and Fachinformationszentrum Karlsruhe Access Structures service www.ccdc.cam.ac.uk/structures.

Crystallographic data for **Cu3**.

C₃₇H₃₈CuN₆¹⁺F₆P¹⁻, yellow prism (0.363 × 0.250 × 0.162 mm³), formula weight 775.24; monoclinic, $P2_1/c$ (No. 14), $a = 15.83319(17)$ Å, $b = 17.71151(19)$ Å, $c = 12.63601(15)$ Å, $\beta = 97.3523(10)^\circ$, $V = 3514.38(7)$ Å³, $Z = 4$, $Z' = 1$, $T = 93(2)$ K, $d_{calc} = 1.465$ g cm⁻³, $\mu(\text{MoK}\alpha) = 0.736$ mm⁻¹, $F(000) = 1600$;

$T_{\max/\min} = 1.000/0.401$; 130963 reflections were collected ($2.260^\circ \leq \theta \leq 33.508^\circ$, index ranges: $-24 \leq h \leq 23$ $-27 \leq k \leq 27$, $-19 \leq l \leq 18$), 13162 of which were unique, $R_{\text{int}} = 0.0465$, $R_\sigma = 0.0218$; completeness to θ of 25.242° 99.9 %. The refinement of 542 parameters with 334 restraints converged to $R_1 = 0.0331$ and $wR_2 = 0.0797$ for 11810 reflections with $I > 2\sigma(I)$ and $R_1 = 0.0376$ and $wR_2 = 0.0813$ for all data with $S = 1.033$ and residual electron density, $\rho_{\max/\min} = 0.527$ and $-0.363 e \text{ \AA}^{-3}$. The crystals were grown by vapor diffusion of diethyl ether into a DCM solution at r.t.

Crystallographic data for Cu4.

$\text{C}_{41}\text{H}_{46}\text{CuN}_6^{1+} \text{F}_6\text{P}^{1-}$, yellow prism ($0.443 \times 0.347 \times 0.294 \text{ mm}^3$), formula weight 831.35; triclinic, $P\bar{1}$ (No. 2), $a = 11.36657(18) \text{ \AA}$, $b = 11.3830(2) \text{ \AA}$, $c = 17.2143(2) \text{ \AA}$, $\alpha = 76.7608(13)^\circ$, $\beta = 71.4730(12)^\circ$, $\gamma = 64.7231(17)^\circ$, $V = 1898.30(6) \text{ \AA}^3$, $Z = 2$, $Z' = 1$, $T = 93(2) \text{ K}$, $d_{\text{calc}} = 1.454 \text{ g cm}^{-3}$, $\mu(\text{MoK}\alpha) = 0.687 \text{ mm}^{-1}$, $F(000) = 864$; $T_{\max/\min} = 1.000/0.188$; 83923 reflections were collected ($2.046^\circ \leq \theta \leq 32.415^\circ$, index ranges: $-16 \leq h \leq 16$ $-17 \leq k \leq 16$, $-25 \leq l \leq 25$), 12578 of which were unique, $R_{\text{int}} = 0.0444$, $R_\sigma = 0.0271$; completeness to θ of 25.242° 99.8 %. The refinement of 498 parameters with no restraints converged to $R_1 = 0.0318$ and $wR_2 = 0.0827$ for 11453 reflections with $I > 2\sigma(I)$ and $R_1 = 0.0357$ and $wR_2 = 0.0843$ for all data with $S = 1.027$ and residual electron density, $\rho_{\max/\min} = 0.543$ and $-0.522 e \text{ \AA}^{-3}$. The crystals were grown by vapor diffusion of diethyl ether into a DCM solution at r.t.

Crystallographic data for Cu5.

$\text{C}_{41}\text{H}_{46}\text{CuN}_6^{1+} \text{F}_6\text{P}^{1-}$, yellow prism ($0.180 \times 0.086 \times 0.062 \text{ mm}^3$), formula weight 831.35; monoclinic, Cc (No. 9), $a = 10.8787(2) \text{ \AA}$, $b = 19.7204(4) \text{ \AA}$, $c = 18.0429(4) \text{ \AA}$, $\beta = 94.732(2)^\circ$, $V = 3857.57(14) \text{ \AA}^3$, $Z = 4$, $Z' = 1$, $T = 100(2) \text{ K}$, $d_{\text{calc}} = 1.431 \text{ g cm}^{-3}$, $\mu(\text{MoK}\alpha) = 0.676 \text{ mm}^{-1}$, $F(000) = 1728$; $T_{\max/\min} = 0.688/0.141$; 32877 reflections were collected ($2.356^\circ \leq \theta \leq 29.930^\circ$, index ranges: $-15 \leq h \leq 14$ $-27 \leq k \leq 27$, $-23 \leq l \leq 24$), 9480 of which were unique, $R_{\text{int}} = 0.0338$, $R_\sigma = 0.0299$; completeness to θ of 25.242° 99.9 %. The refinement of 564 parameters with 371 restraints converged to $R_1 = 0.0407$ and $wR_2 = 0.1069$ for 9149 reflections with $I > 2\sigma(I)$ and $R_1 = 0.0421$ and $wR_2 = 0.1079$ for all data with $S = 1.083$ and residual electron density, $\rho_{\max/\min} = 0.472$ and $-0.501 e \text{ \AA}^{-3}$. Flack parameter $x = 0.010(9)$ by classical fit to all intensities. Flack parameter $x = 0.004(11)$ determined using 4041 selected quotients by Parsons' method. The crystals were grown by vapor diffusion of diethyl ether into a DCM solution at r.t.

Crystallographic data for Cu6.

$\text{C}_{43}\text{H}_{50}\text{CuN}_6^{1+} \text{F}_6\text{P}^{1-}$, yellow prism ($0.236 \times 0.118 \times 0.052 \text{ mm}^3$), formula weight 859.40; orthorhombic, $Pca2_1$ (No. 29), $a = 20.03506(17) \text{ \AA}$, $b = 13.30252(12) \text{ \AA}$, $c = 15.03486(14) \text{ \AA}$, $V = 4007.05(6) \text{ \AA}^3$, $Z = 4$, $Z' = 1$, $T = 93(2) \text{ K}$, $d_{\text{calc}} = 1.425 \text{ g cm}^{-3}$, $\mu(\text{MoK}\alpha) = 0.653 \text{ mm}^{-1}$, $F(000) = 1792$; $T_{\max/\min} = 1.000/0.441$; 172675 reflections were collected ($1.838^\circ \leq \theta \leq 32.426^\circ$, index ranges: $-28 \leq h \leq 30$, $-19 \leq k \leq 19$, $-21 \leq l \leq 22$), 13516 of which were unique, $R_{\text{int}} = 0.0438$, $R_\sigma = 0.0206$; completeness to θ of 25.242° 100 %. The refinement of 521 parameters with 1 restraint converged to $R_1 = 0.0392$ and $wR_2 = 0.1009$ for 13018 reflections with $I > 2\sigma(I)$ and $R_1 = 0.0406$ and $wR_2 = 0.1018$ for all data with $S = 1.094$ and residual electron density, $\rho_{\max/\min} = 0.516$ and $-0.722 e \text{ \AA}^{-3}$. Flack parameter $x = -0.009(70)$ by classical fit to all intensities. Flack parameter $x = 0.018(11)$ determined using 5904 selected quotients by Parsons' method. The crystals were grown by vapor diffusion of diethyl ether into a DCM solution at r.t.

Summary of XRD data for complexes **Cu3-6** are shown in Figure S72 and individual ORTEP plots are given in Figures S73-S76.

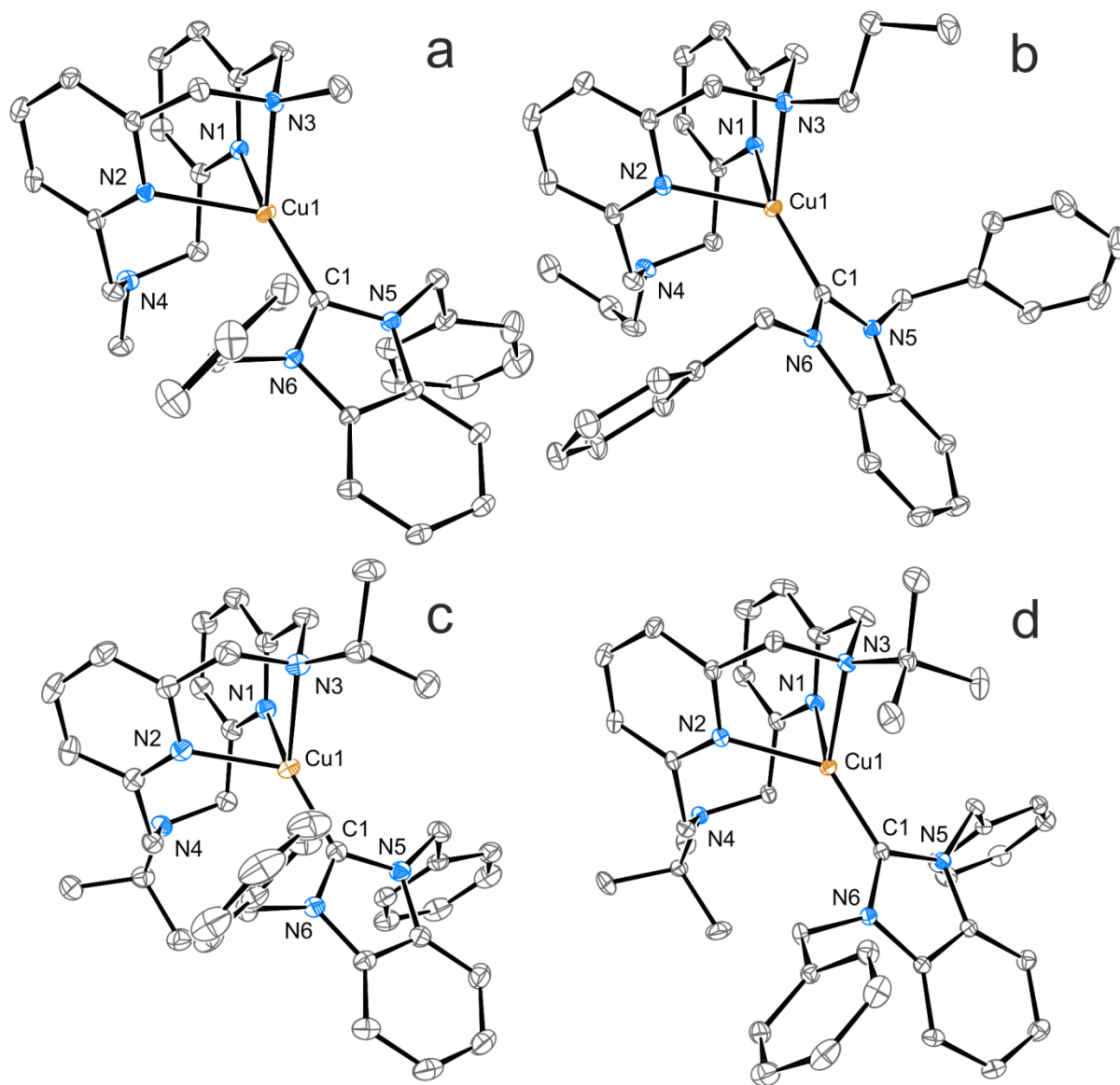


Figure S72. ORTEP of the cationic parts of complexes **Cu1** (a), **Cu2** (b), **Cu3** (c), and **Cu4** (d) at 50 % probability level according to single crystal XRD data. Hexafluorophosphate anions, hydrogen atoms, and, in the case of **Cu1**, the minor disordered component are omitted for clarity. Selected interatomic distances [Å] for **Cu1**: Cu1–N1 2.1098(9), Cu1–N2 2.1952(9), Cu1–N3 2.1677(9), Cu1–C1 1.9002(10); **Cu2**: Cu1–N1 2.1164(9), Cu1–N2 2.1109(9), Cu1–N3 2.1628(9), Cu1–C1 1.8922(10); for **Cu3**: Cu1–N1 2.096(3), Cu1–N2 2.130(3), Cu1–N3 2.217(3), Cu1–C1 1.900(3); for **Cu4** [Å]: Cu1–N1 2.1539(17), Cu1–N2 2.1144(17), Cu1–N3 2.1852(17), Cu1–C1 1.8977(19).

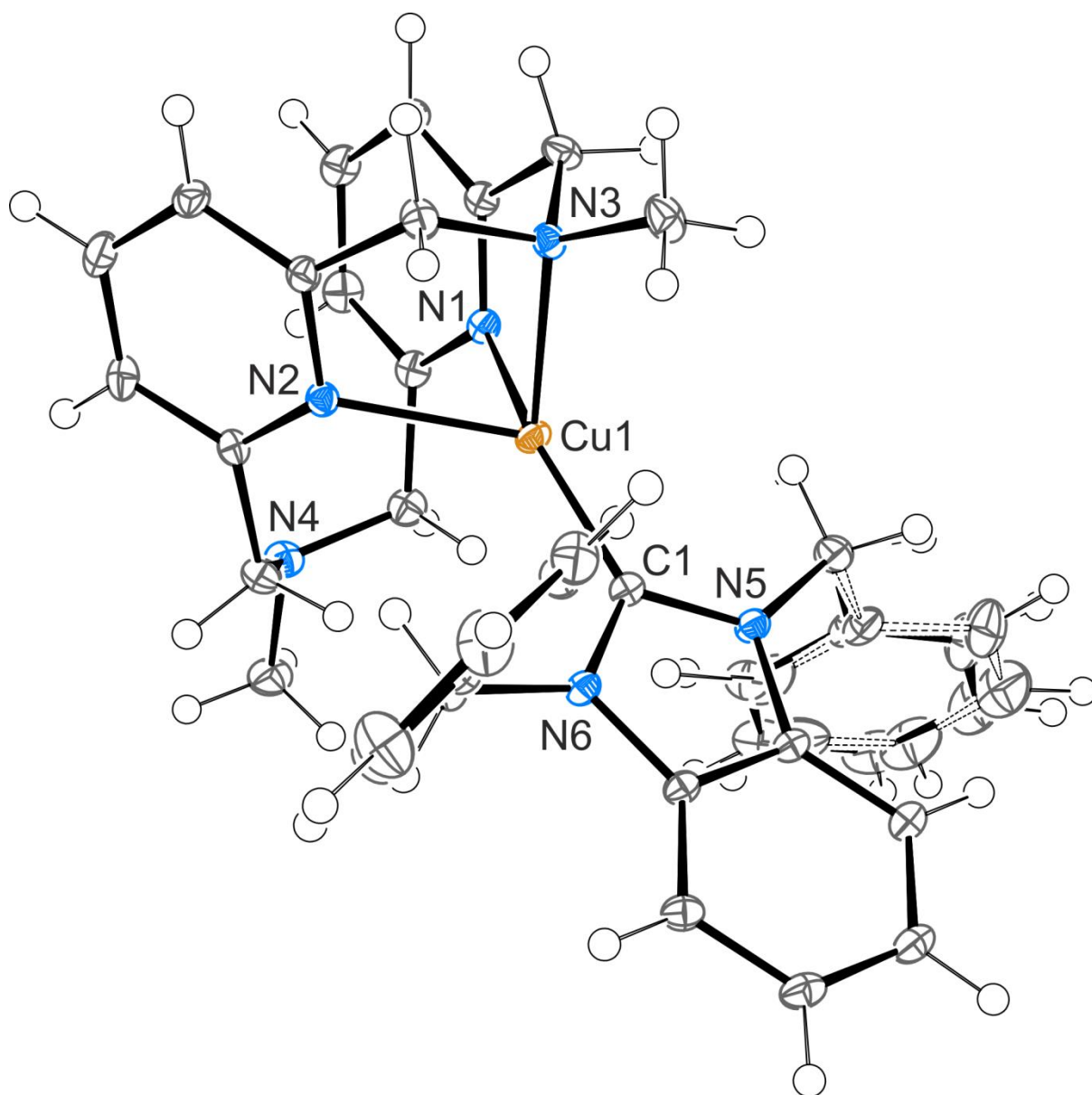


Figure S73. ORTEP diagram showing 50 % probability anisotropic displacement ellipsoids of non-hydrogen atoms for compound **Cu3** according to single crystal X-ray diffraction data. The hexafluorophosphate anion is omitted for clarity. The second disordered component is shown by dashed lines. Selected interatomic distances [\AA]: Cu1–N1 2.1098(9), Cu1–N2 2.1952(9), Cu1–N3 2.1677(9), Cu1–C1 1.9002(10).

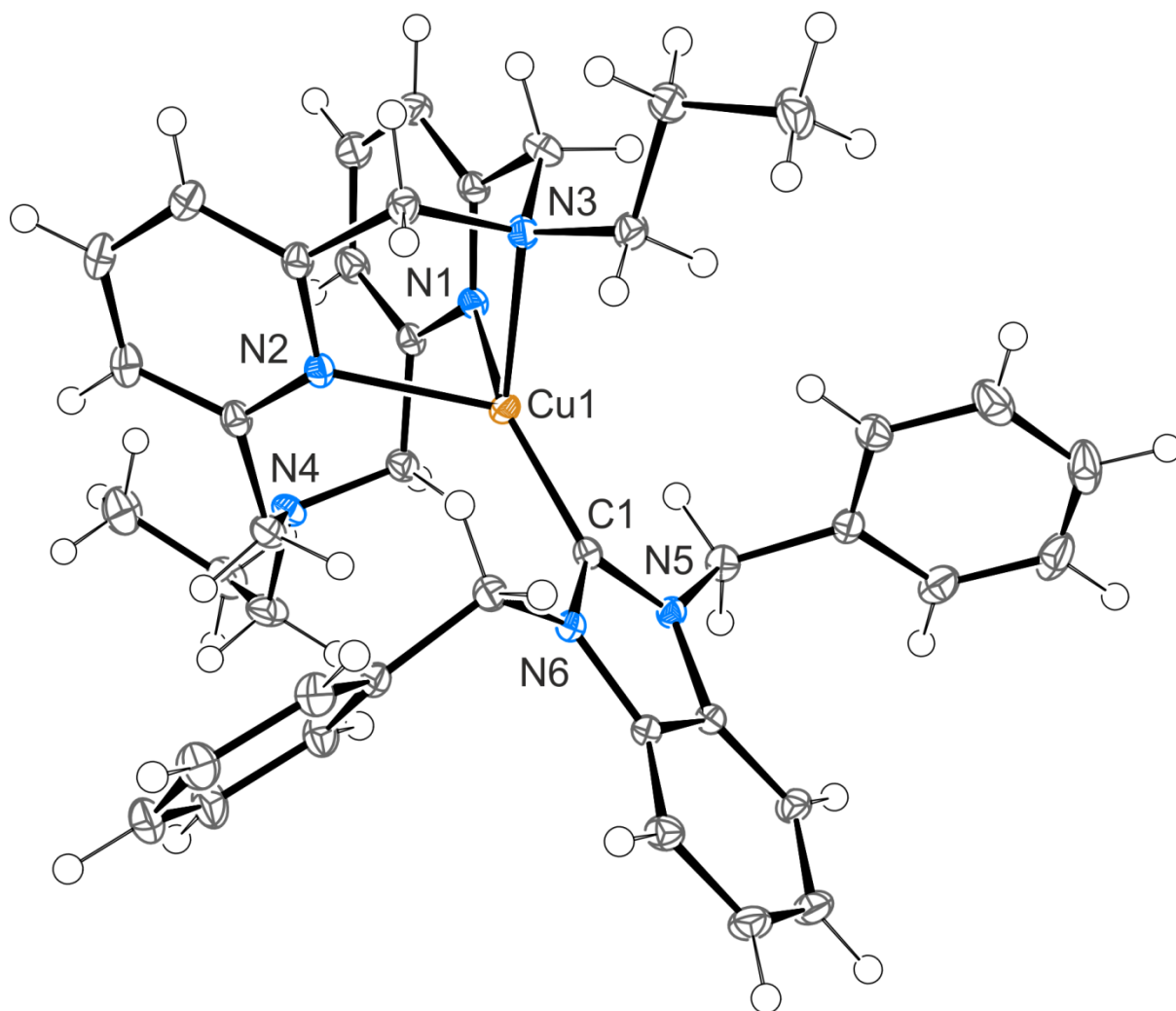


Figure 74. ORTEP diagram showing 50 % probability anisotropic displacement ellipsoids of non-hydrogen atoms for compound **Cu4** according to single crystal X-ray diffraction data. The hexafluorophosphate anion is omitted for clarity. Selected interatomic distances [Å]: Cu1–N1 2.1164(9), Cu1–N2 2.1109(9), Cu1–N3 2.1628(9), Cu1–C1 1.8922(10).

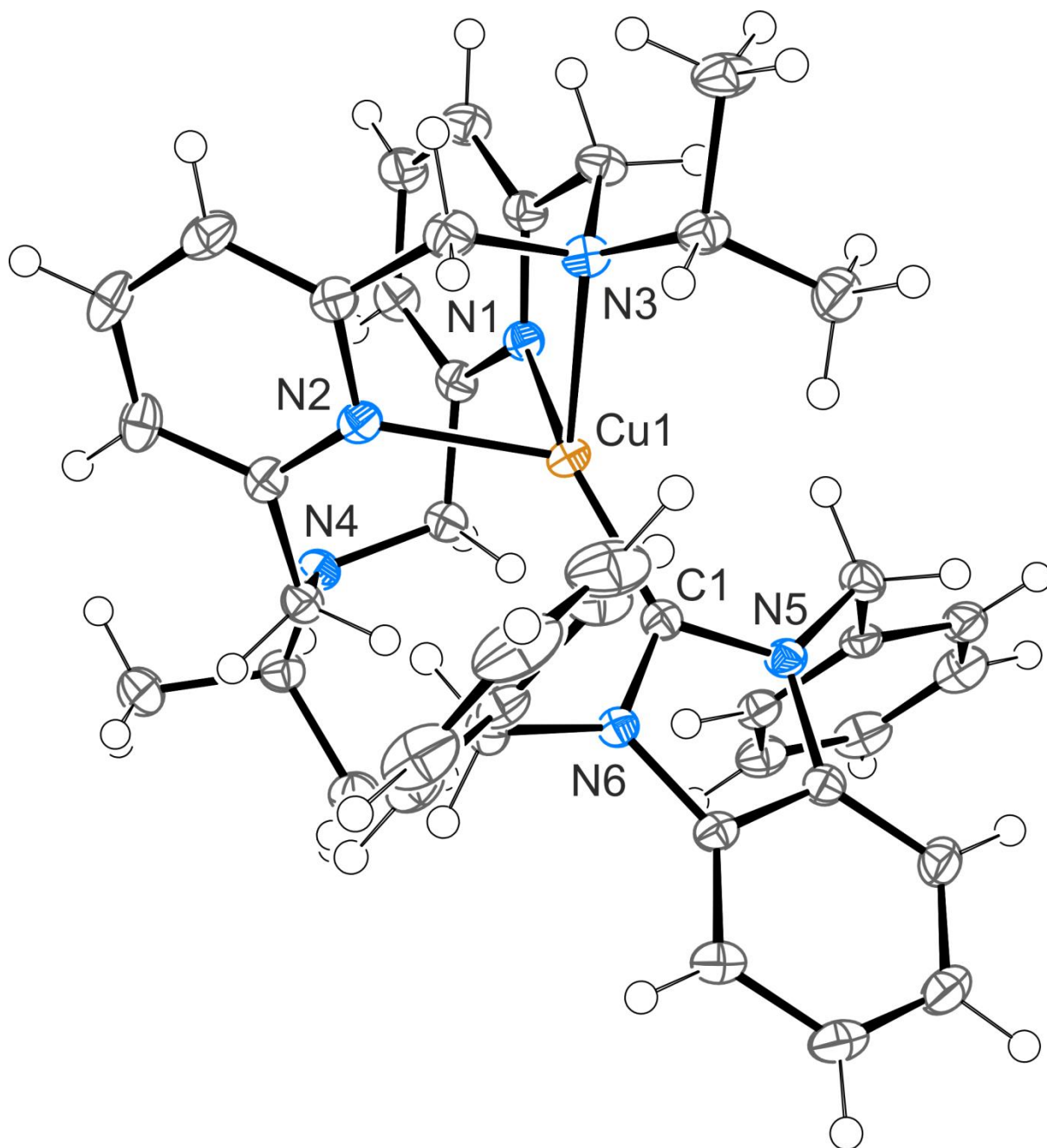


Figure S75. ORTEP diagram showing 50 % probability anisotropic displacement ellipsoids of non-hydrogen atoms for compound **Cu5** according to single crystal X-ray diffraction data. The hexafluorophosphate anion is omitted for clarity. Selected interatomic distances [Å]: Cu1–N1 2.096(3), Cu1–N2 2.130(3), Cu1–N3 2.217(3), Cu1–C1 1.900(3).

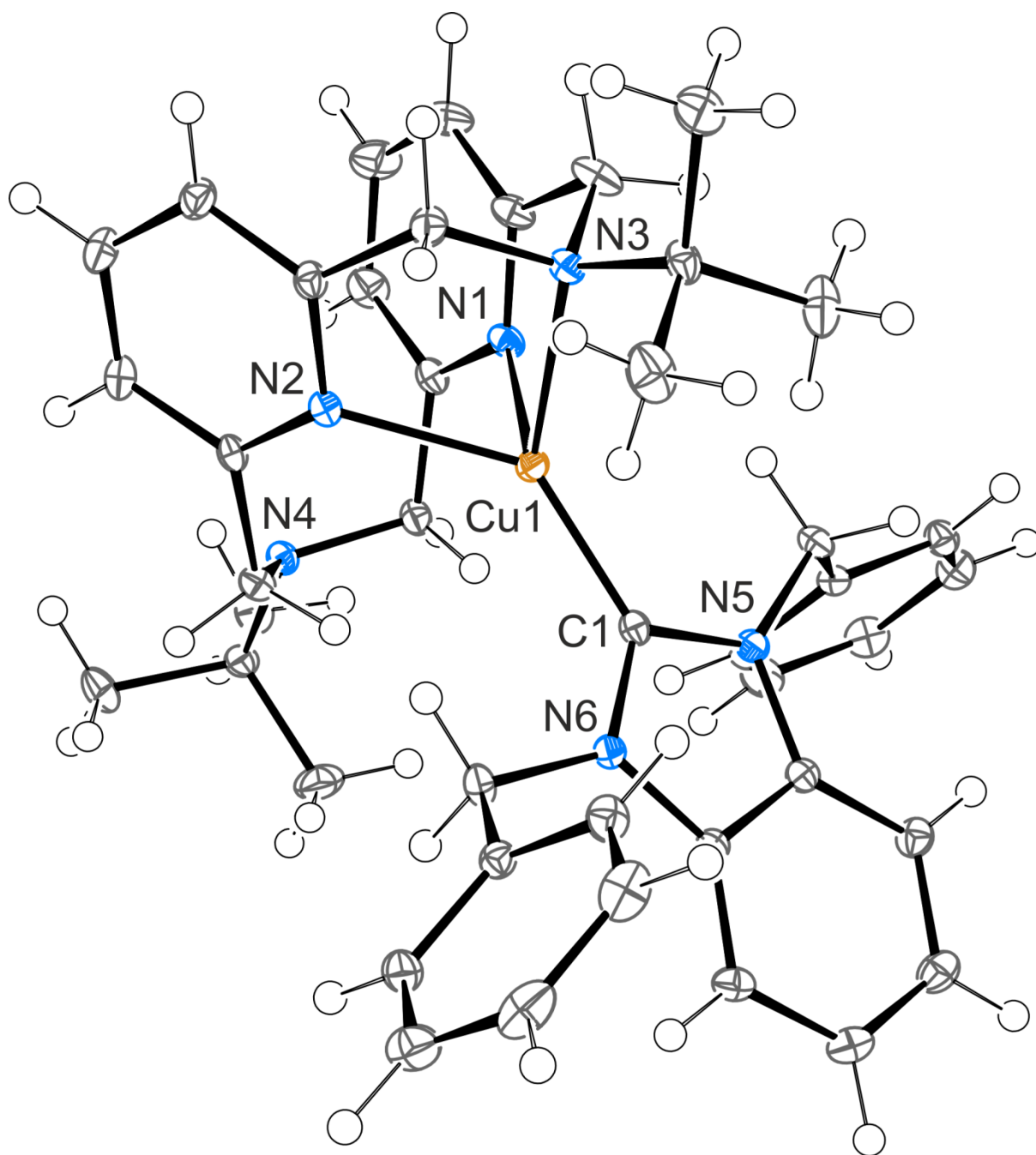


Figure S76. ORTEP diagram showing 50 % probability anisotropic displacement ellipsoids of non-hydrogen atoms for compound **Cu6** according to single crystal X-ray diffraction data. The hexafluorophosphate anion is omitted for clarity. Selected interatomic distances [Å]: Cu1–N1 2.1539(17), Cu1–N2 2.1144(17), Cu1–N3 2.1852(17), Cu1–C1 1.8977(19).

XV. References

1. N. T. Coogan, M. A. Chimes, J. Raftery, P. Mocilac and M. A. Denecke, *J. Org. Chem.*, 2015, **80**, 8684-8693.
2. E. van de Winckel, R. J. Schneider, A. de la Escosura and T. Torres, *Chem. Eur. J.*, 2015, **21**, 18551-18556.
3. F. Tang, F. Qu, J. R. Khusnutdinova, N. P. Rath and L. M. Mirica, *Dalton Trans.*, 2012, **41**, 14046-14050.
4. Z.-Y. L. Chi-Ming Che, Kwok-Yin Wong, Chung-Kwong Poon, Thomas C. W. Mak, Shie-Ming Peng, *Polyhedron*, 1994, **13**, 771-776.
5. N. I. S. Korotkikh, V. S.; Kiselev, A. V; Glinyayana, N. V; Marichev, K. A.; Pekhtereva, T. M.; Dudarenko, G. V; Bumagin, N. A.; Shvaika, O. P., *Chem. Heterocycl. Compd.*, 2012, **47**, 1551-1560.
6. Z. Zhong, B. J. Postnikova, R. E. Hanes, V. M. Lynch and E. V. Anslyn, *Chem. Eur. J.*, 2005, **11**, 2385-2394.
7. C. C. E. Musonda, C. D; Boyle, G. A., *Patent WO 2013072903 A1*, 2013.
8. P. H. Patil, G. A. Filonenko, S. Lapointe, R. R. Fayzullin and J. R. Khusnutdinova, *Inorg. Chem.*, 2018, **57**, 10009-10027.
9. J. R. Alger and J. H. Prestegard, *J. Magn. Reson.*, 1977, **27**, 137-141.
10. (a) J. R. Khusnutdinova, N. P. Rath and L. M. Mirica, *Inorg. Chem.*, 2014, **53**, 13112-13129; (b) J. R. Khusnutdinova, J. Luo, N. P. Rath and L. M. Mirica, *Inorg. Chem.*, 2013, **52**, 3920-3932.
11. G. M. Sheldrick, *Acta Crystallogr. Sect. A: Found. Crystallogr.*, 2015, **71**, 3-8.
12. G. M. Sheldrick, *Acta Crystallogr. Sect. C: Cryst. Struct. Commun.*, 2015, **71**, 3-8.
13. L. J. Farrugia, *J. Appl. Crystallogr.*, 2012, **45**, 849-854.
14. S. Parsons, H. D. Flack and T. Wagner, *Acta Crystallogr. Sect. B: Struct. Sci.*, 2013, **69**, 249-259.
15. A. Okuniewski, D. Rosiak, J. Chojnacki and B. Becker, *Polyhedron*, 2015, **90**, 47-57.